ENGINEERING MULTIFUNCTIONAL NUCLEIC ACID PROBES/NANOMATERIALS FOR CANCER STUDIES

By

YANRONG WU

A DISSERTATION PRESENTED TO THE GRADUATE SCHOOL
OF THE UNIVERSITY OF FLORIDA IN PARTIAL FULFILLMENT
OF THE REQUIREMENTS FOR THE DEGREE OF
DOCTOR OF PHILOSOPHY

UNIVERSITY OF FLORIDA

2009

To my parents and my husband, Jianguo Mei

ACKNOWLEDGMENTS

I am deeply indebted to a long list of people, without whom this dissertation would not be possible. First, I want to express my gratitude to my research advisor, Dr. Weihong Tan. I thank Dr. Tan for offering me a lot of freedom and support to pursue my research interests. Without his advice and suggestions, my projects would not have been accomplished successfully. Under his guidance, I have kept challenging myself to be a better scientist and become more mature.

I also thank Dr. Richard A. Yost, Dr. Kirk S. Schanze, Dr. Gail E. Fanucci and Dr. Christopher Batich for being my committee members. I greatly appreciate their advice, helpful discussion, encouragement and assistance during the past years.

This dissertation work has received valuable help from a group of people in different research areas. I am very thankful to Dr. Gail Fanucci, Dr. Rolf Renne, Dr. Dietmann W. Siemann, Dr. Glenn A. Walter, Dr. Art Edison and Dr. Leonid Moroz for their insightful suggestions about my research projects. I greatly appreciate Dr. David Powell, Dr. Jodie Johnson, Dr. Hong Yu, Li Tan and Basri Gulbakan for their helpful discussions about mass spectrometry. I would like to thank Dr. Yiider Tseng and his student Pei-hsu Wu for interesting comments and assistance in the particle bombardment project. I am especially grateful to Mr. Mike Ruler for providing me unconditional help with the microinjection technique. I would like to thank Dr. Chaoyong James Yang and Hui Lin for helping me start my very first research project. I would like to thank Dr. Joseph Phillips, Dalia Lopez Colon, Tao Chen and Lu Peng for providing me kind help to film a video for the carbon nanotube project. I thank Dr. Zunyi Yang for his critical comments and helpful discussion about ion exchange HPLC and radioisotope test. I thank Jianguo Mei and Dr. Ruowen Wang for offering me organic synthesis help. I thank Meghan B. O'Donoghue for assistance in several techniques and interesting discussion, Dr. Jinlin Yan for gold nanoparticle synthesis assistance, Dr. Ye Xu and Rahul R. Kamath for flow

microfluidic channel preparation help, Kwame Sefah for experimental help, and Jennifer Meekel for writing suggestions. I am thankful to Li Bo and Patrick Colon for their research assistance and nice friendship.

The Tan research group is a big family. I am very thankful for helpful discussion and kind encouragements from Dr. Colin Medley, Dr. Joshua Smith, Dr. Prabodhika Mallikaratchy, Dr. Lin Wang, Dr. Dihua Shangguan and Dr. Lisa Hilliard. I would also like to thank the following family members for creating my unforgettable memories in beautiful Gainesville and their nice and special friendship: Dr. Kathryn Williams, Dr. Xiaoling Zhang, Dr. Xiaolan Chen, Dr. Huanghao Yang, Dr. Ronghua Yang, Dr. Huimin Li, Dr. Tianfu Liu, Dr. Julia Xiaojun Zhao, Dr. Charles Lofton, Dr. Gang Yao, Dr. Tmothy Drake, Dr. Marie Vicens, Dr. Alina Munteanu, Dr. Shelly John, Dr. Hong Wang, Dr. Zhiwen Tang, Dr. Yufen Huang, Dr. Carmen Maria Estevez , Dr. Haipeng Liu, Dr. Wenjun Zhao, Dr. Zeyu Xiao, Dr. Karen Martinez, Dr. Hui Chen, Dr. Youngmi Sohn, Dr. Kelong Wang, Dr. Liu Yang, Dr. Shukoor Ibrahim, Dr. Quan Yuan, Parag Parekh, Kwame Sefah, Dosung Sohn, Huaizhi Kang, Meng Ling, Yan Chen, Pinpin Sheng, Jennifer Martin, Zhi Zhu, Hui Wang, Suwussa Bamrungsap, Dimitri Simaeys Van , Elizabeth Jimenez, Xiangling Xiong, Guizhi Zhu, Mingxu You, Jin Huang, Tahir Bayrac, Pu Ying, Eunjung Lee, Sewon Bae, Michael Donovan, Michael Mavros and Yunfei Zhang.

I am deeply indebted to my parents for their unconditional love, and my elder sister for taking care of my parents for me during the past years.

I am extremely grateful to my husband, Jianguo Mei, for always being there for me as my wonderful friend, helpful colleague and supportive spouse. Without his love, patience, encouragement and assistance, I could not reach this far. The marriage with him is my biggest achievement during my past years in the USA.

TABLE OF CONTENTS

page

LIST OF TABLES

LIST OF FIGURES

LIST OF ABBREVIATIONS

VEGF	Vascular Endothelial Growth Factor
AMD	Age-related Macular Degeneration
CABG	Coronary Artery Bypass Grafting
NF-κB	Nuclear Factor kappa B
AML	Acute Myeloid Leukemia
FIX	Factor IX
PCI	Percutaneous Coronary Intervention
TMA	Thrombotic Microangiopathies
TTP	Thrombotic Thrombocytopenic Purpura
CEA	Carotid Endarterectomy
PDGF-B	Platelet-Derived Growth Factor-B
MCP-1	Monocyte Chemotactic Protein-1
SDF-1	Stromal Cell-Derived Factor-1

Abstract of Dissertation Presented to the Graduate School
of the University of Florida in Partial Fulfillment of the
Requirements for the Degree of Doctor of Philosophy

ENGINEERING MULTIFUNCTIONAL NUCLEIC ACID PROBES/NANOMATERIALS FOR CANCER STUDIES

By

Yanrong Wu

December 2009

Chair: Weihong Tan
Major: Chemistry

Essential cancer research studies include diagnosis of early-stage cancer and elucidation of the disease processes, with the hope of finding efficient anti-cancer therapy systems. Among the various types of molecular tools, multifunctional nucleic acid probes serve versatile roles via rational selection and construction processes (e.g., use as sensors, catalytic enzymes, drugs, and aptamers). My doctoral research has focused exclusively on the sensor and aptamer functions, in particular the engineering of multifunctional nucleic acid probes or nanomaterials for detection and analysis of cancer cells.

My most recent work has involved the construction of an aptamer-micelle as an efficient detection and delivery vehicle toward cancer cells. An aptamer, which can specifically bind to a broad spectrum of targets, including small molecules, proteins, and even disease cells, is a single-stranded DNA or RNA molecule isolated from combinational libraries by a process termed SELEX (Systematic Evolution of Ligands by Exponential enrichment). The Tan research group has developed a whole-cell-SELEX strategy to generate a panel of aptamers for specific diseased cells without any prior knowledge about the target molecules. Although aptamers have shown great promise in molecular recognition toward specific cancer cells, the relatively weak binding affinities of some aptamers at physiological temperatures has hampered cell targeting

and applications to targeted therapy. To solve this problem, an aptamer-micelle strategy was implemented by attaching lipid tails onto the ends of low-affinity aptamers. This resulted in several beneficial and innovative properties, such as greatly enhanced binding ability, extremely low dissociation rates, additional internalization pathways, as well as sensitive and rapid cancer detection.

Cancer originates from mutations in human genes and genetic alterations which cause molecular changes to cell structure that ultimately result in morphological and physiological abnormalities. Consequentially, my research has also focused on designing molecular sensors to detect such changes via intracellular mRNA monitoring. The monitoring of oncogene expression or spatial localization allows cellular events and disease pathogenesis to be more accurately understood. Besides serving as genetic information housekeepers, nucleic acids can also be built into various sensors based on Watson-Crick base-pairing and diverse signal transduction mechanisms. However, the complex nature of living cells poses challenges to the design of such sensors by the susceptibility of nucleic acids to enzyme digestion and inefficient self-delivery into the cells. Two methods were tested to address these limitations: introduction of locked nucleic acid bases into the sensor design and modification of sensors with single-walled carbon nanotubes. These two methodologies have yielded robust probes, thus permitting more reliable intracellular gene studies at the single-cell level.

Results of my doctoral research demonstrate that multifunctional nucleic acids can be utilized as key building blocks to fulfill the various goals in cancer research.

CHAPTER 1
INTRODUCTION

Cancer remains the second leading cause of death in the United States [1], allthough the survival rate for many types of cancer has improved in recent years. The 2003 World Cancer Report's prediction that cancer rates may increase by 50% to 15 million new cases in the year 2020 has compelled scientists in many areas to become involved in cancer research. Essential cancer research includes diagnosis of early-stage cancer and elucidation of the disease processes, with the hope of finding efficient anti-cancer therapy systems.

In an attempt to create molecular tools for the above-mentioned major cancer research areas, this doctoral research was undertaken to utilize nucleic acid as the key component to construct various probes. This dissertation has focused on the construction of nanomaterials based on nucleic acid aptamers evolved from the whole-cell-SELEX methodology for cancer detection with potential promise in targeted therapy, as well as two types of molecular probe designs for intracellular gene monitoring.

In order to set the foundation of these objectives, the following sections will review some critical properties of nucleic acids and their applications in cancer diagnosis, cancer therapy and cancer intracellular biomolecular study. Additional key subjects involved in this dissertation will be introduced separately: structure and chemical synthesis of nucleic acids, locked nucleic acids, nucleic acid aptamers, micelles, flow cytometric analysis of aptamer binding ability with cells, and fluorescence measurement for signal transduction. Finally, a summary of the overall scope of this dissertation will be outlined.

Nucleic Acids for Cancer Research

Completion of the human genome project has revolutionized fundamental understanding of biological processes. Increasing emphasis on molecular level understanding of biological

organisms has allowed certain diseases to be redefined in terms of their underlying molecular characteristics. It is well accepted that cancer originates from mutations of genes, either inherited from parent(s) or genetically influenced, with resulting changes in cell morphology and physiology [2]. To decipher the underlying cancer processes and facilitate cancer diagnosis with the promise of efficient cancer treatment, nucleic acid has become an ideal building block for its widespread utilization in bioanalytical and biomedical research fields. The popularity of nucleic acid mainly results from its specific recognition ability toward a wide spectrum of targets, including another piece of nucleic acids, small molecules, proteins or even diseased cells. Additionally, the automated oligonucleotide synthesis and easy modification make nucleic acids attractive molecular tools with which to work.

Properties of Nucleic Acids

To appreciate their applications in cancer research, the biological functions of nucleic acids and their structural properties must be understood.

As described in the central dogma of molecular biology, every life form develops from hundreds of thousands of types of cells. Inside one single cell, an equal amount of proteins carry out all our daily functions. To synthesize those proteins, an enormous amount of information is required to assemble peptides piece-by-piece based on exact instructions. This information, detailing every single protein's specific structure, is stored in an array of biomolecules called nucleic acids. Nucleic acids carry genetic information from parent cell to daughter cell; therefore, genetic traits can be passed along to offspring. These unique genetic traits provide an intrinsic avenue to understand life; and therefore represent attractive targets for cancer research.

Since it contains the essence of genetic material, the significance of nucleic acid is greatly enhanced by an understanding of its intrinsic structures. Nucleic acids are largely divided into two groups, deoxyribonucleic acid (DNA) and ribonucleic acid (RNA), of which share the same

general structures. Nucleic acids can be regarded as the polymerization product of nucleotides. As presented in Figure 1-1, the monomer unit, or nucleotide, consists of three components: the sugar ring, phosphate group and a nucleotide base. In the famous DNA double helix structure (shown in Figure 1-2) proposed by James D. Watson and Francis Crick in 1953 [3], the outer layer of the helix is the helix backbone made by the sugar and phosphate groups. Because of the presence of phosphate groups, nucleic acid is highly negatively charged. In contrast, nitrogenous bases are paired and preserved inside the helix. Although only four types of different nucleotide bases can occur in a nucleic acid, each nucleic acid contains millions of bases bonded to it. The order in which these nucleotides appear is the genetic code for a certain proteins. In other words, nucleotide bases serve as a genetic alphabet by which the structure of each protein is encoded.

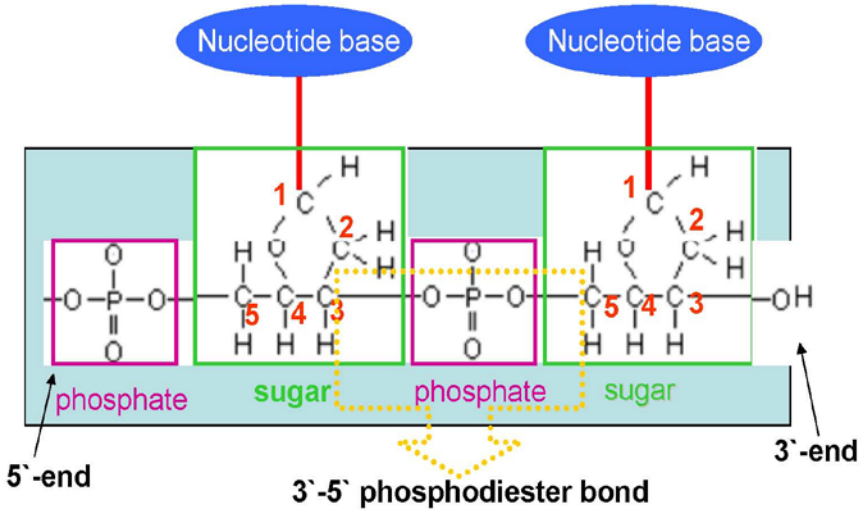

Figure 1-1. General structure of nucleic acids.

The structures of the nucleotide bases, shown in Figure 1-2, enable their roles as the informational molecules. The hydrogen atoms of amino groups provide hydrogen bond donors, whereas the carboxyl oxygens and ring nitrogens provide hydrogen bond acceptors. The different positions of hydrogen bonds give the bases their unique structural identities; that is adenine can specifically hydrogen bond to thymine (in DNA or uracil in RNA) and cytosine can specifically

hydrogen bond to guanine, a process which allow them to serve as the genetic information. Since the aromatic rings are rigid planar molecules, the bases can stack within the helix. This stacking helps protect the chemical identity of the bases as well as improve thermal stability of the helix.

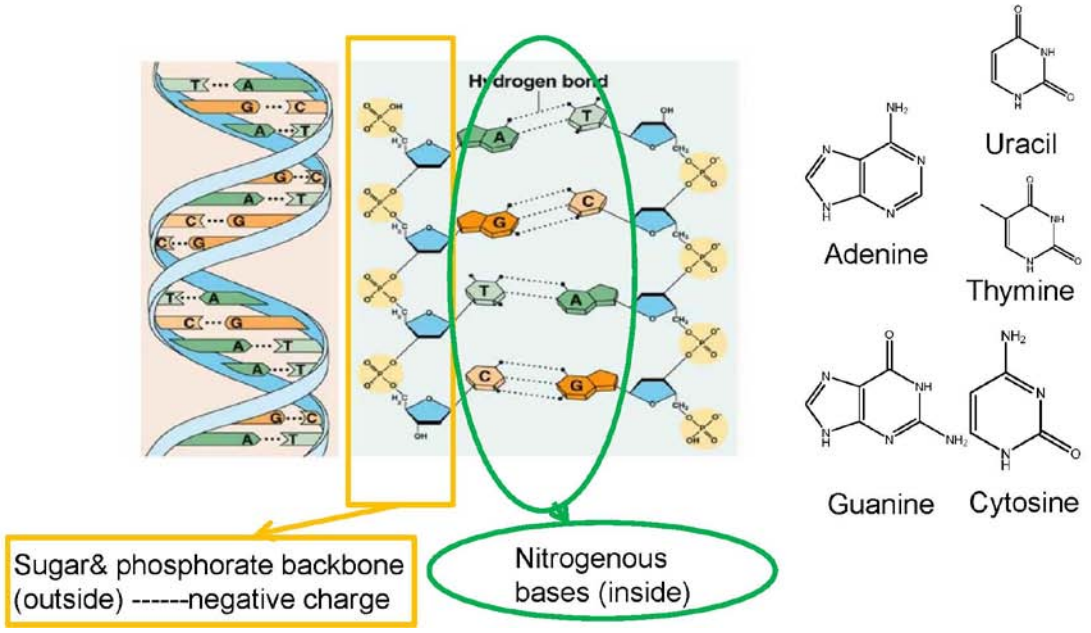

Figure 1-2. DNA double helix structure and nitrogeneous bases.

However, it is the very structure of nucleic acid that, paradoxically, defines the challenge it confronts in cancer research. For example, RNase H cleaves RNA only at sites where the 2' position of the sugar ring is not modified (2'-OH) [4]; therefore, blocking the 2' cleavage site becomes a popular way to achieve good biostable bases. Locked nucleic acid, which will be introduced later, is one such example. Additionally, nucleic acids are polar. However, the cell membrane is composed of a lipid bilayer structure with a hydrophilic head outside and a hydrophobic tail inside, which prevents polar solutes, such as nucleic acid, from diffusing across the membrane. Moreover, phospholipid, which have a negative charge, form the major component of cell membranes. Therefore, this negatively charged cell membrane creates an extra barrier to the same negatively charged nucleic acid molecules to move through it. Thus, an

additional challenge is how to design the efficient delivery of nucleic acids to and through the cell membrane.

Multifunctional nucleic acids

There are three main reasons why nucleic acids are believed to play multifunctional roles. First, automated synthesis allows easy incorporation of molecules with various functional groups into a nucleic acid sequence. For example, if a fluorescence dye molecule is bonded, the nucleic acid can function as a detection probe to determine its analyte. Also, by introducing cytotoxic drug molecules, the corresponding nucleic acid can act as a delivery vehicle towards its specific target. Moreover, with conjugated functional groups, nucleic acids can self-assemble into a certain nanostructure or be conjugated onto some nanomaterials to achieve unique properties. Second, nucleic acids have great capability for selective recognition against a wide range of targets, including other nucleic acid molecules by specific base pairings, small molecules, proteins, or even whole diseased cells. Nucleic acids which can recognize non-nucleic acid targets are termed aptamers, which will be detailed in the following section. Third, as found recently, nucleic acids not only play a main role in storing genetic information, but also perform several other functions. For instance, small RNAs and microRNAs regulate gene activitity [5,6]; DNA with nonmethylated CpG sequences exert an immunostimulating effect [7,8]; and ribozymes and deoxyribozymes can have interesting enzymatic catalytic functions [9,10]. Thus, molecular engineering of multifunctional nucleic acids sparks numerous applications in biological studies, especially cancer research. In the following section, three major applications of nucleic acids in cancer research (cancer detection, cancer therapy and intracellular biomolecular study) will be briefly reviewed.

Nucleic Acids for Cancer Detection

The survival rate of any form of cancer depends on how early and what stage it is detected. Thus, the highest survival rates correlate to the earliest stages of detection. For example, colon cancer is one of the most curable cancers when detected in the early stages. Based on the data from the National Cancer Institute, the overall survival rate for colon cancer in the United States is as high as 93% at stage 1 and 85% at stage 2A, but it will dramatically drop to 8% at stage 4 [11].

Several methods are currently utilized for cancer detection, including biopsy, magnetic resonance imaging (MRI), polymerase chain reaction (PCR), microarray and immunological assays. Biopsy is typically used as a diagnostic method to histologically identify whether a previously detected tumor, lesion, or other abnormal tissue is cancerous. However, it is an invasive method with potential damage, especially when it is targeting brain tissue. MRI, as a noninvasive method, has been shown to be useful for staging cancers and deciding on treatment avenues, but it is considered too costly for routine detection.

The increasing emphasis on molecular level understanding of bio-organisms, especially with the completion of the human genome, has allowed diseases to be re-defined in terms of underlying molecular level abnormalities rather than pathological differences. Cancers are known to originate from mutations of human genes; therefore, biomarker gene detection and profiling has become one of the most popular ways to correlate the unique molecular signature of tumors for identifying subsets of patients and tailoring treatment regimes to achieve more personalized medical therapies. Gene expression microarray and PCR are two commonly used techniques to analyze biological differences between tumors that account for variations in morphology and clinical behaviors. Microarray provides a powerful tool for massive parallel analysis of the RNA/DNA expression level of thousands of genes. The genomic gains or losses

can be analyzed for complete genomes in a single experiment, thus creating new opportunities for deciphering distinct chromosomal changes in the development of cancer [12,13]. Using microarrays, investigators have developed gene expression-based classifications for many malignancies, such as lymphoma [14], leukemia [15], breast [16] and lung carcinoma [17]. These molecular classifications are clinically significant, because they correlate tumor characteristics with patient outcome and explain the variability seen in the natural course of certain tumors with the same anatomic diagnosis [14-17]. Besides microarray, PCR-based methods have proven to be highly sensitive diagnostic techniques for cellular recognition. However, amplification of gene products has been reported to have variable sensitivities, which can lead to false positive or false negative results [18].

Besides DNA/RNA, the protein itself can be a cancer biomarker. Traditional methods are immunological assays, such as enzyme-linked immunoabsorbant assays (ELISA) and immunophenotyping by flow cytometry. These techniques largely rely on the selectivity of antibodies and can be limited by tedious production, instability and difficult modification of the antibodies. Fortunately, the discovery of aptamer selection in 1990 [19,20], especially the proposed whole-cell-SELEX strategy [21], has brought an antibody mimic in the form of a nucleic acid aptamer into the research field of protein expression-based cancer diagnosis. Aptamers have rivaled antibodies in various cancer research, including cancer diagnosis, as a result of various merits, such as stability, the speed of probe discovery, and the ease and reproducibility of their synthesis and modification [22-24].

Many examples have demonstrated how aptamers can be effective substitutes for antibodies. One such example is an aptamer-based new diagnosis technique, so-called enzyme-linked oligonucleotide assay (ELONA) developed in 1996, which compete with traditional

antibody based ELISA [25]. In this ELONA method, the capture reagent remains a monoclonal antibody, while the detection antibody is replaced with a fluorescein-tagged hVEGF-binding aptamer. Measures of precision, accuracy, interference, and specificity showed that this aptamer-based assay was equivalent to a typical sandwich ELISA assay. Later on, the aptamer was also shown to be a surrogate for the capture antibody [26]. In addition, aptamers, as recognition elements substituting for antibodies, are widely applied in flow cytometry [27], microscope studies [28], microarrays [29], and biosensors [30].

Aptamers can also be superior to antibodies in some cases. As mentioned above, even within the same categories, multiple subsets of cancer with different clinical outcomes exist. Apart from gene profiling as a means of exploring differences at the molecular level, protein profiling can also help delineate unique fingerprints of tumor cells, especially considering the fact that it is the protein, not the gene, which eventually executes the cellular activities. The systematic production of a panel of antibodies for molecular profiling of cancer cells with unknown biomarkers has proved to be very difficult. Cell-based selection of aptamers, however, is able to generate multiple molecular probes for cancer cell identification and subcategorization [31-34]. Six aptamers, which were originally selected against two types of leukemia cells respectively, produced distinct binding patterns for different tumor cells. The differential binding of these aptamers among the T-ALL patient samples showed the ability of aptamers to distinguish molecular differences among patients with the same diagnosis by current technology [35].

Ready synthesis and easy site-specific chemical modification of nucleic acid aptamers facilitate the integration of aptamer chemistry and nanotechnology into cancer research, including cancer detection. Some cancer cells, especially those in the early stages of disease,

may have a low density of biomarker target on the cell surface available for recognition. Therefore, to enhance the binding affinity and amplify the signal, multivalent binding, instead of single aptamer binding, is usually considered to be an effective approach. Owing to the large surface area and variable sizes, nanomaterials are particularly advantageous as multivalent ligand scaffolds. For example, one single Au-Ag nanorod (NR) 12 nm × 56 nm in size can incorporate up to 80 fluorophore-labeled sgc8 aptamers on the surface, leading to a 26-fold higher affinity and over 300-fold higher fluorescence signal [36]. Additionally, by virtue of the significant color change of gold nanoparticles resulting from overlapped surface plasmon resonances when they are in close promixity, a colorimetric assay for sensitive cancer cell detection was developed using aptamers conjugated with 50 nm gold nanoparticles [37]. This assay allows 1000 target cells to be readily detected by the naked eye.

Detection of cancer in the body fluids usually requires an enrichment step since the malignant cells are present at very low abundance in the body fluids. To meet this need, a novel aptamer-based two-nanoparticle assay was developed for the rapid collection and detection of leukemia cells from complex mixtures including whole blood samples [38]. In this assay, aptamer-modified iron oxide-doped silica nanoparticles provide enhanced extraction capability, while fluorescent dye-doped silica nanoparticles offer amplified signal intensity. Compared to immunophenotype and PCR methods, which usually take hours to complete, this assay was relatively fast (less than 1 hour). Furthermore, to realize the enrichment in the flow system and meet the potential goal for online targeted biological analysis, an aptamer-modified microfluidic device was developed to capture rare cells from a large amount of background cells without any need for sample pretreatment [39]. Even though antibody-coated microfluidic devices have been demonstrated for cancer cell enrichment [40], this aptamer-based microfluidic device is

envisioned to be a more manageable system because DNA-based devices can be stored for a long period of time and can be easily handled in clinical settings.

Nucleic Acids for Cancer Therapy

The application of nucleic acids in cancer therapy largely involves cancer gene therapy and anti-cancer treatment modalities.

Most cancers are characterized by abnormal gene expression. Modulation of these abnormal genes, either by initiating or silencing gene expression, appears to be a rational approach to cancer therapy. Since the first human *in vivo* gene transfer study in 1989 [41], over 900 clinical trials involving gene transfer have been approved by regulatory bodies worldwide [42,43]. Given the complex nature of cancer, many therapeutic strategies have been developed for cancer treatment. These strategies can be categorized into two main avenues: immunological and molecular [44].

Cancer is immunogenic in nature; therefore, it can be targeted on the immunological level. Boosting the immune response against cancerous cells is usually achieved via genes encoding for immune stimulating molecules, such as cytokines [45]. Intensive research has focused on transfection with the interleukin-12 (IL-12) gene, which was demonstrated to play an important role in the induction of cellular immune responses. Complete tumor regression in rat animal models was observed in hepatocellular carcinoma and a denocarcinoma after successful IL-12 gene transfection in the cancer cells [46,47].

As an alternative approach, molecular targeted gene therapy aims to efficiently upregulate or downregulate the genes involved in the development of cancerous cell [44].Two main gene groups are oncogenes and tumor suppressor genes. Tumor repressor genes are growth inhibiting; however, the growth-suppressive function is generally lost with mutation. Thus, introducing wild-type tumor suppressor genes to the cancer cells is one of the most widely used methods in

cancer treatment [48]. Besides suppressing cancer development and progression, wild-type p53 further confers chemo-sensitivity and radio-sensitivity upon tumor cells [49]. The combination of an adenovirus-carrying wild-type p53 gene (Ad-p53) and chemotherapy (Cisplatin) [50] or radiation [51] was reported to have promising clinical outcomes. Ad-p53 has been commercialized by Introgen Therapeutics, Inc. and has been approved as an orphan drug by the U.S. Food and Drug Administration. It is the first successfully approved tumor suppressor gene therapy [52].

On the other hand, oligonucleotides, which bind and subsequently inhibit oncogenes (i.e., anti-oncogenes), can also be utilized in cancer therapy. Of the strategies available, the anti-mRNA gene silencing approach has attracted much attention [53]. This strategy includes three types of agents: (1) single-stranded antisense oligonucleotides through Watson-Crick base pairing to inhibit the translation step of the protein synthesis [54]; (2) catalytically active oligonucleotides, such as ribozymes, and DNAzymes that possess inherent RNA cleaving activity [55] and (3) small interfering RNA (siRNA) molecules that induce RNA interference (RNAi) [5].

As mentioned above, the structure of nucleic acid is antithetic to the properties of the cell membrane, thereby reducing the efficiency of nucleic acid's self-delivery into the cell. To remedy this shortcoming, the use of viral or nonviral vectors or micro-/nano-particles is required [56]. In this concept, the therapeutic gene is either encapsulated inside the vehicle or complexed onto cationic particles which pass through the cell membrane barrier.

Besides modulating gene activity, nucleic acid can also modulate the activity of proteins. This type of nucleic acid is again the province of aptamers. The concept that nucleic acid ligands could modulate the activity of proteins emerged from basic science studies of viruses and early

work in the field of gene therapy [57]. The observation that viruses use RNA ligands for their ends suggested that RNA ligands might also be useful for therapeutic purposes. After two groundbreaking studies [19,20], several RNA aptamers and, subsequently, some DNA aptamers were identified as therapeutic agents. Currently, several aptamers are now being evaluated in clinical trials, which are detailed in Table 1-1. Table 1-2 is provided to to help understand the differences between DNA and RNA aptamers.

Despite being discovered less than two decades ago, an aptamer-based drug known as Macugen® (or pegaptanib) has already received U.S. FDA approval for the treatment of age-related macular degeneration [58,59].Among various therapeutic DNA aptamer agents, G-rich quadruplex-forming oligonucleotides particularly stand out. Nuclease susceptibility and inefficient cellular uptake have proved to be universal hurdles in the development of therapeutic oligonucleotides. However, G-rich quadruplex-forming oligonucleotides have demonstrated outstanding biostability and cellular uptake.

Some aptamers were never developed from SELEX, but have earned that name because of their activities arising from binding to protein targets via shape-specific recognition. This type of aptamer is also coined as decoy. One of successful DNA aptamer is AS1411, formally AGRO 100, the first nucleic acid-based aptamer tested for cancer treatment in humans, was subjected to phase II studies for the treatment of AML in 2007 and renal cell carcinoma in 2008 [60]. To explain the tumor-selectivity of AS1411, the proposed binding target, nucleolin, was reported to be selectively expressed in cancer cells compared to normal cells; therefore, AS1411 can specifically target cancer cells [61]. More recently, AS1411 has served as a template for the synthesis of stable PbS and FeO nanocrystals, while retaining selective recognition and

therapeutic targeting to cancer cells with 3-4 times enhanced efficacy in proliferation reduction of MCF-7 breast cancer cells compared with DNA aptamers without nanocrystals [62].

Table 1-1. Aptamers in the clinical pipeline (summarized from corresponding developer company websites)

Aptamer candidate	Target/indication	Developer	Clinical phase	Type
Macugen (pegaptanib)	VEGF/AMD	Eyetech(Cedar Knolls, JN, USA)	FDA approved	RNA
Edifoligide(E2F decoy)	E2F/CABG surgery	Anesiva (formerly Corgentech, San Francisco, CA, USA)	No better than placebo in Phase III	RNA
Avrina(NF-κB decoy)	NF-κB/eczema	Anesiva (formerly Corgentech, San Francisco, CA, USA)	Phase III	ds DNA
AS1411	Nucleolin/anticancer (AML, renal cell carcinoma)	Antisoma (Lodon, UK)	Phase II	DNA
REG1	FIX/arterial thrombosis	Regado Biosciences (Durham, NC, USA)	Phase II	RNA
REG2	FIX/venous thrombosis	Regado Biosciences (Durham, NC, USA)	Phase I	RNA
ARC 1779 (TMA/TTP)	Vwf/TMA, TTP, CEA	Archemix (Cambridge, MA, USA)	Phase II	DNA/RNA
ARC183	Thrombin/ anticoagulation	Archemix (Cambridge, MA, USA)	Phase I completed, not in development	DNA
NU172 (ARC2172)	Thrombin/anticoagulation (PCI, CABG)	Nuvelo/Archemix (San Carlos, CA/Cambridge, MA, USA)	Commence a Phase II study	DNA
E10030	PDGF-B/wet AMD	Ophthotech (Princeton, NJ, USA)	Phase I	DNA
ARC1905	C5/ wet and dry AMD	Ophthotech (Princeton, NJ, USA)	Phase I	RNA
NOX-E36	MCP-1/ chronic inflammation	NOXXON (Berlin, Germany)	Phase I	L-RNA
NOX-E12	SDF-1/autologous stem cell transplantation	NOXXON (Berlin, Germany)	Commence a phase I study	L-RNA

Table 1-2. Comparison between DNA and RNA aptamers

Properties	DNA aptamer	RNA aptamer
Degradation susceptibility	Moderate	High
Easy synthesis and modification	Yes	No
Directly used in *in vivo*	Possible	No
Storage	Easy	Hard
Steps in one SELEX cycle	Moderate	Long
Cost of SELEX procedure	Moderate	High
Cost of bulk production	Moderate	High
Applied to whole cell-SELEX	Yes	No
Diversity of 3D structure and functionality	Moderate	High
Possibility to be expressed by cell	No	Yes
Binding affinity	Comparable	Comparable
Immunogenicity and toxicity	Not observed	Not observed

Another type of emerging application of nucleic acids in anti-cancer therapy results from the utility of nucleic acid aptamers as targeting ligands for diseased cells. This means that aptamers function only as recognition ligands to cancer cells. This is especially significant in relation to the whole-cell-SELEX strategy proposed by the Tan group in 2006 [31]. Since that time, the group has generated a pool of DNA aptamers for various types of cancer cells, including lymphocytic leukemia, myeloid leukemia, liver cancer, small cell lung cancer and non-small cell lung cancer [32-35,63,64]. Additionally, using a similar strategy, DNA aptamers for stem cells [65] and live bacteria cells [66] have been developed in other laboratories over the past year.

DNA aptamers can be easily conjugated with therapeutic molecules and applied to targeted drug delivery by virtue of the aptamer's excellent targeting ability. For instance, covalent linkage of the anti-tumor drug doxorubicin (Dox) to aptamer sgc8c can kill the target CCRF-CEM (T-cell acute lymphoblastic leukemia (T-ALL)) cells, yet with minimal toxicity towards nontarget cells [67]. The results demonstrated that the sgc8c–Dox conjugate possesses many of the properties of the sgc8c aptamer, including high binding affinity and the capability to be

efficiently internalized to endosomes by target cells. Moreover, the adopted conjugation method allows an acid-labile linkage connecting the sgc8c–Dox conjugate, to be cleaved inside the acidic endosome. This further facilitates released Dox for rapid transport to the nucleus to interrupt the growth of target cells. It is noteworthy that nonspecific uptake of membrane-permeable Dox to non-target cell lines could also be inhibited by linking the drug with the aptamer. With a growing numbers of selected aptamers, we foresee that this drug-aptamer conjugation strategy will have broad implications for targeted drug delivery. Additionally, aptamers have been reported to delivery phototherapeutic drugs [68,69] and lysosomal enzymes [70] to the target cells in a selective manner.

More recently, aptamers have begun to find applications at the interface of nanotechnology and medicine in the form of aptamer-nanoparticle conjugates. On one hand, the high surface areas of nanoparticles offer excellent platforms for multiple aptamer conjugation. On the other hand, empty interiors render excellent places to house high amounts of drug molecules for enhanced loading efficiency. Research progress in the integration of RNA aptamers with nanotechnology (e.g., PSMA aptamer integrated with PLGA nanoparticles) has been summarized in a recent review [71]. Thus, only DNA aptamer-nanoparticle conjugates for cancer treatment will be examined here.

Nanoparticles can be utilized as a platform for the immobilization of multiple aptamers to generate a multivalent nanoconjugate. For example, we once constructed an aptamer nanoconjugate using Au-Ag nanorods (NRs) [36,72]. These aptamer-NR conjugates were then used as effective therapeutic agents for targeted photothermal cancer cell destruction [72]. Either in a mixed-cell suspension or in a solid tumor, target cells are severely damaged when exposed to near-infrared laser light with specific intensity and duration. Another interesting vehicle

constructed recently is a viral capsid DNA-aptamer conjugate [73]. By a chemoselective oxidative coupling reaction, up to 60 sgc8c aptamer strands can be attached to each viral capsid. However, since this system has been tested only with a strong binder, sgc8c, it remains unknown whether this nanomaterial can enhance the binding affinity of low-affinity aptamers. The utility of its interior for loading anti-cancer drugs is under investigation.

In addition to enhanced binding affinity, hollow nanoparticles are envisioned to be beneficial for efficient drug loading. Among various drug delivery systems, the liposome-based system is one of the most established technologies, particularly due to its well-documented low cytotoxicity. Although a number of liposome-based systems have been approved by the U.S. Food and Drug Administration for clinical use [74], it was not until early this year that the successful application of aptamers with a liposome delivery system was first published by Lu group [75]. Tests in culture cells yielded promising results. Four days after cells were exposed to the drug delivery system, 59.5 percent of the cancer cells had died, while less than 12 percent of cancer cells treated with cisplatin alone had died. AS1411, a therapeutic aptamer described above, was their adopted aptamer. Even though it was reported to be directly cytotoxic toward [61], only its cancer recognition ability was utilized for this aptamer-liposome system since much lower aptamer concentration was used. Under experimental conditions, it was claimed that the aptamer-liposomes containing no cisplatin showed no noticeable cell death, with a viability of about 97.8% at day 4. Even more interesting, simply by adding a piece of complementary DNA (cDNA) to this G-quadruplex aptamer as the antidote, the aptamer's targeting capability was reversed and, as a result, drug delivery was terminated.

Although studies have been ongoing for less than two decades, the results obtained for aptamers, combined with intrinsic properties and diversified selection protocols, have been

promising, particularly in the field of anti-cancer therapy. The emerging integration of aptamers and nanotechnology is envisioned to open up a huge potential for numerous clinical applications. A this time, the potential of aptamers as targeting ligands for both disease diagnosis and treatment is yet to be fully appreciated, but the new aptamer selection protocols, especially whole-cell-SELEX, which can generate ligands to distinguish diseased from normal cells without prior knowledge of target molecules, is expected to produce more versatile target-specific molecules. The availability of new aptamers will further stimulate new diagnostic and therapeutic nanotechnologies in the near future. Meanwhile, we should collectively realize that aptamer research, compared with antibody studies, is still in its infancy. Nonetheless, aptamers have already met several challenges, such as development of techniques for reducing the cost of modified aptamers for large-scale production, target molecule identification, biological function study and biomarker validation.

Nucleic Acids for Cancer Intracellular mRNA Study

Messenger RNA (mRNA) encodes the gene information from DNA and then decodes it into protein. The ability to detect and visualize target mRNA in living cells in real-time can offer tremendous opportunities for medical diagnostics, disease studies and drug discovery. Currently there are many traditional methods available for mRNA measurement, including reverse transcriptase polymerase chain reaction (RT-PCR) [76], gene chips [77], northern blot analysis [78] and fluorescence in situ hybridization (FISH) [79]. All of the above methods require destruction of the cells, which poses a hindrance to real-time tracking in living cells. Therefore, new analytical approaches to identify and quantify cellular mRNA in real-time are highly desired.

Molecular beacons (MBs) have offered a promising approach to intracellular biomolecular monitoring. MBs, developed in 1996 [80], are short hairpin oligonucleotide probes with one

fluorophore and one quencher flanking at each end, as shown in Figure 1-3. The loop sequence is designed for the target recognition and two stems are arranged to bring two chromophore moieties into close proximity. In the absence of target, the MB is closed, causing the quenching of fluorophore by energy transfer. Upon hybridization with its target, MB restores its fluorophore signal due to the increased space separation resulting from the spontaneous conformation change.

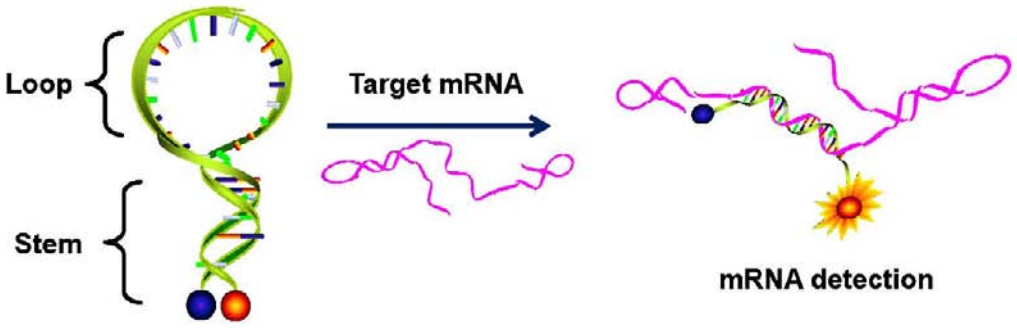

Figure 1-3. Working principle of MBs.

Basically, MBs integrate the recognition component for detection with the signal transduction component for readout. When designing MBs for intracellular mRNA monitoring, the selection of an appropriate region in mRNA as the target is the first critical step. To be accessible to the probe, the target sequence can not lie within a tight secondary structure or be bound to proteins. Additionally, the target region must have a unique sequence in order to guarantee the selectivity of the probe to this particular target mRNA. To achieve low probe background with the absence of the target, it is necessary to obtain a stable closed form. Thus, two stems, usually four to seven base pairs long and with high GC content (usually higher than 65%), are required to flank at each end of the loop portion.

The unique structural and thermodynamic properties of molecular beacons endow them with two important advantages for the intracellular monitoring. First, the light switching signal

transduction method allows MBs to detect intracellular targets without any further separation requirement, which is extremely useful for real-time detection. Second, MBs have an excellent capability to differentiate perfectly matched targets from those with single-base mismatches. These two properties make MBs promising tools for real-time intracellular mRNA monitoring.

However, the use of MBs for intracellular monitoring still has several limitations, mostly arising from the issues of signal and background, the two fundamental problems for intracellular biomolecular detection. One of the biggest challenges is biostability. Free DNA degrades after only 15-45 minutes in the cellular environment [81]. Besides that, DNA probes can be structurally disrupted by nonspecific protein binding [82]. As a consequence, MBs can yield false-positive signals. Another challenge is low sensitivity. Although it has been reported that MBs can detect as low as 10 copies of mRNA sequences [83], most biomolecular targets are mainly highly expressed biomolecules or some stimulated biomolecules resulting from several factors [84,85].

To address these problems for intracellular application, several modifications and new approaches have been developed. In terms of biostability, some nuclease-resistant building blocks were attempted in MB design, such as phosphorathioate [86,87], 2'-O-methyl RNA bases [88] and peptide nucleic acids (PNAs) [89]. However, phosphorathioate oligonucleotides have toxicity problems [90]. Also, 2'-O-methyl MBs can open up nonspecifically in cells as a result of protein binding, thus slightly reducing target specificity [91]. PNA-containing oligonucleotides tend to aggregate and fold in a way that interferes with duplex formation by their neutral charges [92]. On the other hand, locked nucleic acid (LNA) MBs demonstrate a promising candidates for intracellular detection [93]. The methylene bridge connecting the 2'-oxygen and the 4'-carbon of the ribose makes the structure of LNAs more rigid than DNA bases. This endows fully modified

LNA MBs with many advantages, including resistance to nuclease degradation, immunity to nonspecific protein binding and excellent specificity. However, fully modified LNA MBs LNAs suffer from extremely slow hybridization rates, posing an obstacle to real-time detection [93]. Therefore, the design of MBs using non-standard bases has not yielded practical molecular probes for intracellular monitoring. Chapter Three in this dissertation will describe the proposed solution later. Additionally, the use of gold nanoparticles was reported to greatly decrease the degradation of DNA MB modified on their surface [94]. However, the relevant protection mechanism was not discussed. A recent study reported that quantum dot (QD)-conjugated MBs demonstrated better resistance to nonspecific interactions with both single-stranded DNA binding (SSB) proteins and endonucleases than free MBs, while free MBs shared the same immunity to the digestion from exonucleases [95]. Thus, the authors claimed that SSB proteins and endonucleases could both be responsible for generating false-positive signals. Although SSB proteins and nucleases also present in the cytoplasm, there are fewer DNA-protein interactions in the cytoplasm than in the nucleus [87]. This report indicates that preventing nucleus accumulation by nanomaterials could be an alternative way to avoid false positive signals and improve the signal-to-background ratio, especially considering that the background yielded from the active nonspecific interactions inside the nucleus accounts for a significant portion of high background intensity.

In terms of sensitivity, dual fluorescence resonance energy transfer (FRET) molecular beacons were designed so that two beacons bind side-by-side with a donor dye and an acceptor dye in close proximity. These can substantially reduce the background signal caused by nonspecific binding and degradation [96]. Modified quenched auto-ligation probes (QUAL) using a universal linker amplified the signal and reduced the background susceptibility to

nonspecific signals. With this probe, nearly 100 signals per target were observed [97]. Superquencher MBs with multiple quenchers greatly suppressed the background as a result of the more efficient quenching [98]; however, their sensitivity inside living cells is yet to determined. QD, as a semiconductor nanoparticle which can emit very intense light, was once pursued by a group of people as a means to achieve high sensitivity of MBs. However, based on the data from currently reported QD-conjugated MBs, this goal would not be easy to realize because of incomplete quenching of the QD in the closed form of MB [95,99].

In addition to these two limitations, extremely low self-delivery efficiency into the cells is another pressing challenge for MBs. To ensure that enough probes perform their functions inside cells, an efficient delivery method is necessary. There are currently several delivery methods available for MBs, including use of microinjection, cell penetration peptide, streptolysin O, and electroporation, but they all have limitations [100]. Microinjection is the most popular method [101], but it demands high skills and is tedious, inefficient and impractical for high-throughput gene analysis. Cell penetration peptide can also deliver MBs into various types of cells efficiently [102], but its usage is limited by high cost. Streptolysin O permeabilizes cells by reversibly forming pores on the cell surface [96], but it is a toxin and would be harmful to the cells. A less popular method, eletrophoration, applies an electric field to generate transient permeabilization of the plasma membrane, but it suffers from low cell viability. Therefore, a delivery system which can realize high-throughput gene analysis, as well as provide protection to DNA-MBs during an entire delivery process, would be useful.

Other Dissertation-Related Subjects

Nucleic Acid

In order to help further understand the properties and related applications of nucleic acids, the chemical synthesis of nucleic acids and one nonstandard base, locked nucleic acid, are reviewed in the following section.

Chemical synthesis of nucleic acids

The discovery of the double helix structure of DNA by Watson and Crick [3] provided the impetus to attempt the challenging synthesis of oligonucleotides, which are nucleic acids with defined sequences. Since the first attempt in 1955 [103], the procedures for oligonucleotide synthesis have been continuously developed and optimized. Instead of a difficult and tedious task for only the most dedicated chemist, the current oligonucleotide synthesis is as easy as simply pressing a few buttons. By virtue of this automated oligonucleotide synthesis and easy modification, nucleic acid, with its inherent recognition ability, has become an ideal building block for a broad spectrum of applications.

With its high capability to synthesize long oligonucleotide strands with various modifications in high yields, the phosphoramidite method is the most commonly used synthesis method [104]. To appreciate phosphoramidite chemistry, it is necessary to understand the two key components that ensure successful synthesis: solid-phase supports and functional groups. The ideal solid-phase support used to anchor synthesized oligonucleotides 1) should have a uniform surface structure with pores large enough to contain the desired oligonucleotide, 2) should not possesss any surface functionality that may produce unwanted side products, and 3) should be available as uniform particles [105]. A solid controlled-pored glass (CPG) support is currently the most suitable and most widely used for oligonucleotide synthesis. To achieve rapid and highly efficient coupling reactions, functional groups on the phosphoramidites have been

carefully designed [106]. As illustrated in Figure 1-4, one typical phosphoramidite is composed of several different protection groups. The first and most critical functional group is a diisopropyl phosphoramidite group attached to the 3'-hydroxyl of a nucleoside, resulting in a nucleoside phosphoramidite, which ensures efficient coupling. To prevent side reactions during synthesis, primary amines of nucleotide bases are blocked by specific protection groups which are basic sensitive (as shown in Figure 1-4), so that they can be effectively removed by strong bases. On the other hand, the 5'-oxygen of the deoxyribose is capped by a dimethoxytrityl (DMT) group, which is acid labile and can selectively activate the 5'-hydroxyl under acidic conditions. Additionally, the phosphate group is protected by a base-labile 2-cyanoethyl group. Although different modifier phosphoramidites, like fluorophore and spacer, may recruit slightly different protection groups for a certain moiety, they all share similar design strategy. This strategy is also applied to the homemade phosphoramidites [107].

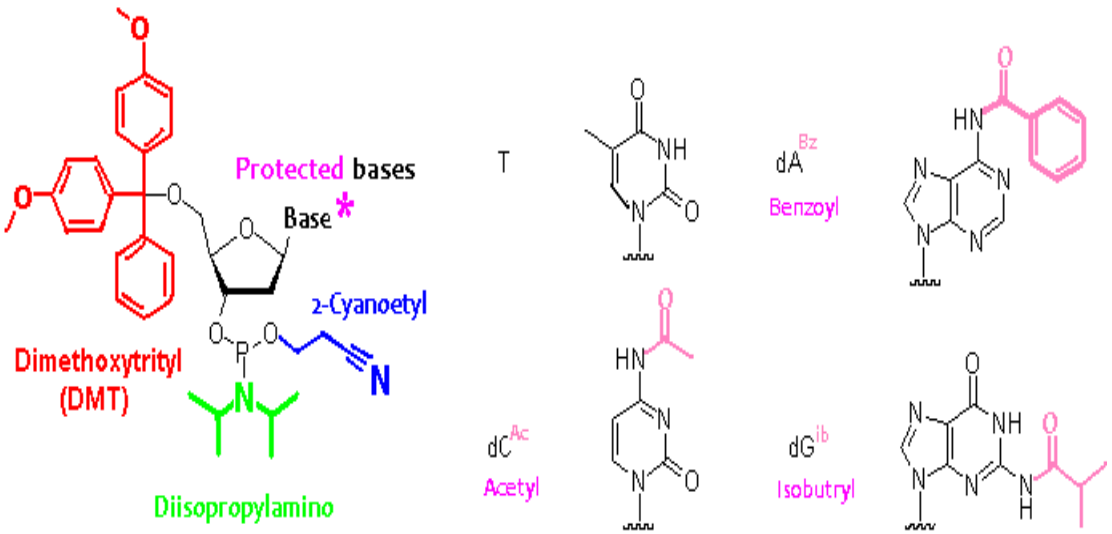

Figure 1-4. Typical structures of a protected phosphoramidite and four protected nitrogeneous bases.

Unlike enzymatically controlled synthesis, DNA chemical synthesis starts from 3' to 5'. The synthesis cycle starts with a column containing a CPG support where the 3'-hydroxyl of the

first nucleoside is attached through a long spacer arm. This support allows excess reagents to be removed by filtration and eliminates the need for purification steps during the synthesis process. The synthesis cycle involves four chemical reaction steps: detritylation, coupling, capping and oxidization (Figure 1-5). For each repetition of the phosphoramidite cycle, one new base/modifier is added to the growing sequence until the desired sequence has been completed.

Figure 1-5. Automated oligonucleotide synthesis process by phosphoramidite chemistry.

In step 1, detritylation, the DMT group is removed to activate the 5'-hydroxyl at the end of a glowing oligonucleotide chain attached to the CPG by flushing with a dilute acid solution,

either dichloroacetic acid (DCA) or trichloroacetic acid (TCA) in dichloromethane (DCM), through the reaction column. After washing away the excess acid, the 2nd step, coupling, takes place in which a phosphoramidite derivative of the next nucleotide is added to the column together with a weak acid, tetrazole. In this step, the diisopropylamine group on the 3' phosphorous in the coming nucleotide is protonated by tetrazole, resulting in a very good leaving group, which subsequently undergoes nucleophilic attack by the activated 5' hydroxyl group to form a phosphite triester linkage. Upon the completion of the coupling reaction, the column is washed to remove any unbound reagent and by-products, and then capping (step 3) is required. Since every coupling yield cannot reach 100%, there is always a small percentage of unreacted 5'-hydroxyl groups remaining on the support. This must be permanently blocked from further chain elongation to prevent formation of oligonucleotides with an internal base deletion. Capping is accomplished by acetylation of the bare 5'-hydroxyl group using a mixture of acetic anhydride and 1-methylimidazole. The capping step is followed by oxidation step (step 4) in which the newly formed phosphite triester is converted to a more stable pentavalent phosphate trimester, using iodine and water in the presence of a weak base, like pyridine. After this four-step cycle, the product is extended with a new base and is ready for a new round of conjugation.

After the synthesis is complete, the fully-protected oligonucleotide product must be cleaved from the solid support and deprotected. The deprotection method varies according to the combination of functional groups involved during the whole synthesis. Meanwhile, the deprotection method is also required to be compatible with the intended following purification techniques. For example, reverse phase HPLC is commonly used to separate the desired product. For this technique, the terminal 5'-DMT group can serve as a hydrophobic handle to facilitate the separation, so that the selected deprotection condition should be able to retain the DMT at the

end of the sequence while removing all the protection groups in the other moieties. In this case, basic conditions are usually used.

By converting into appropriate phosphoramidite derivatives, various species like fluorophores, quenchers, functional groups and linkers can be introduced into any desired position in an oligonucleotide sequence. Moreover, post-synthesis coupling can always be an alternative option for labile molecules which cannot survive the DNA synthesis process. This freedom to assemble different blocks into a nucleic acid sequence makes nucleic acid a superior building block to construct interesting tools for cancer research.

Locked nucleic acids

The three components of a nucleotide (a nucleobase, a sugar, and a phosphodiester linkage) have been prime targets for chemists to modify the natural nucleic acids [108,109]. The object is to overcome the limitations of natural nucleic acids, thereby facilitating the ease of processing oligo synthesis, enhancing affinity and selectivity, increasing nuclease resistance, improving thermodynamic properties, and furnishing the ability to cross biological membranes [110]. Locked nucleic acid (LNA) is one such product resulting from the modification of the sugar.

In 1997, an LNA, a ribonucleotide derivative with conformationally locked C3'-endo sugar conformation, was synthesized [111,112]. The first LNA monomer was based on the 2'-O-CH2-4' bicyclic structure which is now called the oxy-LNA (later termed LNA). Right after the discovery of the oxy-LNA, the bicyclic furanosidic structure was chemically modified, then the 2'-S-CH2-4' (thio-LNA) and the 2'-NH-CH2-4' (amino-LNA) bicyclic analogues[113,114], finally a series of LNA diastereoisomers [115-122] were prepared. All those LNA analogues are grouped into LNA family (Figure 1-6). While this work focuses on the structures of LNA which

have been mostly studied, several recent reviews of LNA [122-125] will provide more comprehensive coverage.

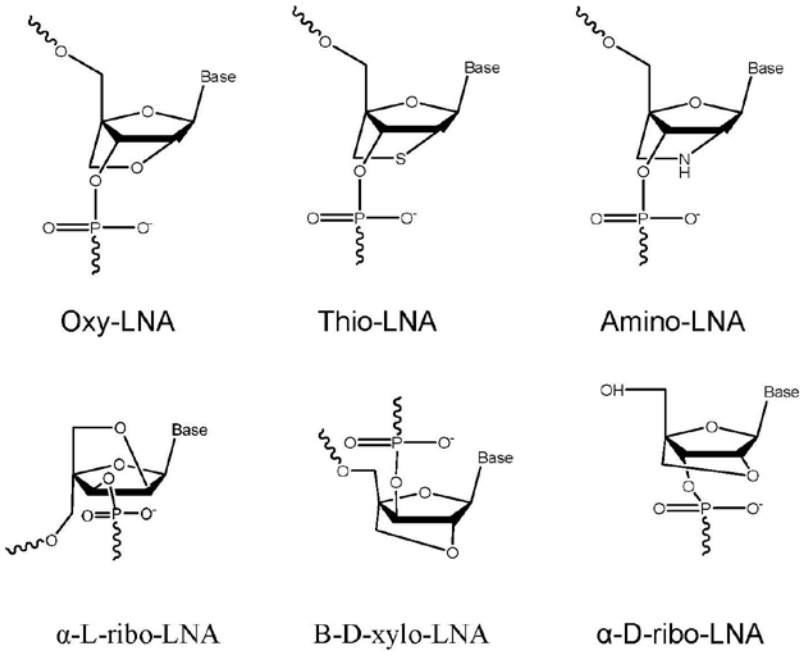

Figure 1-6.Chemical structure of LNA family[110].

According to the strict definition, an LNA is an oligonucleotide that contains one or more LNA monomer(s) [2'-O, 4'-C-methylene-ß-D-ribofuranosyl monomer (s)]. The LNA monomer is bicyclic where a ribonucleoside is linked between the 2'-oxygen and the 4'-carbon atom with a methylene unit [111,112]. Molecular modeling has predicted that bicyclic LNA nucleoside monomers should be favorably preorganized in an N-type conformation, lead to the possible formation of entropically favored with complementary DNA and RNA. X-ray crystallographic studies and NMR investigations confirmed that the LNA monomers adopt N-type sugar puckers with C3'-endo (^{3}E, P =17^0) conformation [111,112,126]. Thus, LNA is an RNA mimic, which, so far, has the highest affinity towards RNA.

Because the structures of LNAs are close to those of native nucleic acids, their characteristics are also similar. LNA duplexes display the features in common with those of their native nucleic acid anologues: Watson-Crick base pairing, nucleobases in the anti orientation, base stacking, and a right-handed helical conformation. Additionally, LNAs are soluble in water, making it possible for biological applications. Furthermore, LNA oligonucleotides can be synthesized using conventional phosphoramidite chemistry, thus allowing automated synthesis (Proligo http://www.proligo.com; Exiqon A/S http://www.exiqon.com). Moreover, LNA/DNA, LNA/RNA, LNA/phosphorothioate, LNA/2'-O-Me-RNA chimera can also be synthesized in an automated manner. Finally, because of their charged phosphate backbone, LNAs can be delivered into cells using cationic transfection vectors [127,128]. The LNAs' locked ring also overcomes some limitations of native nucleic acids. For example, LNA oligonucleotides are stable toward degradation by 3'-exonuclease [129]. Besides that, LNAs were demonstrated to have unprecedented thermal stabilities towards complementary DNA and RNA (ΔT_m/modification = +3 to +5 ^{0}C towards DNA and +4 to +8 ^{0}C towards RNA) [118,130]. Both properties indicate considerable promise in diagnostic and therapeutic applications. The exceptional stability of the LNA-modified duplexes is a function of the quenching of concerted local backbone motions (preorganization) by the LNA nucleotides in ssLNA, as a result, the entropy loss on duplex formation is reduced and the stacking of the nucleobases is more efficient [131]. Moreover, such analogues are typically more resistant to biodegradation and can therefore be used advantageously as tools in antisense or siRNA research [132]. Additionally, unlike some other sugar-modified oligonucleotide analogues, such as p-RNA or homo-DNA, LNAs can communicate with natural nucleic acids. These characteristics offer LNAs widespread applications in bioanalytical and biomedical research [123].

Nucleic Acid Aptamers

As decribed above, aptamers are single-stranded oligonucleotides that fold into unique three-dimensional structures, allowing them to bind specifically to a broad spectrum of target molecules. As mimics of antibodies, aptamers are able to recognize targets with high specificity and are able to carry therapeutic agents directly to solid tumor masses or individual cells. Since their discovery in the early 1990s [19,20], aptamers have been hailed as novel biological molecules capable of slowly replacing antibodies.

Besides recognition ability, aptamers are potentially useful as pharmaceutical agents due to their ability to modulate the activities of proteins implicated in pathological conditions. Numerous aptamers have been developed as therapeutic agents [57,133,134]. Despite being discovered less than two decades ago, an aptamer-based drug known as Macugen® or pegaptanib has already received U.S. FDA approval for the treatment of age-related macular degeneration [58,135]. Up to now, aptamers have been used for numerous applications, including sensing, separation, diagnostics, and therapeutics [22-24].

Systematic evolution of ligands by exponential enrichment (SELEX)

The method by which aptamers are selected, Systematic Evolution of Ligands by Exponential enrichment (SELEX), was independently introduced by the Gold [19] and Szostak [20] groups. In general, SELEX is a combination of *in vitro* evolution and combinatorial chemistry, involving a series of steps, including incubation, partitioning and amplification.

The process starts with the design of a large nucleic acid library pool created by solid phase technology. It is essential that this pool contain at least a few molecules having the unique conformations required to facilitate selective binding with the target. To accomplish this, the initial library sequence is randomized from 22 to 100 nucleotides in length (10^{15} different

oligonucleotide molecules for 40 random nucleotides), flanked at either side by pre-defined primer binding sites for polymerase chain reaction amplification (PCR).

In a typical round of SELEX, the first step involves incubating the library with the target under a defined buffer condition. During incubation, some sequences of the library will bind to the target molecule tightly, but other sequences will only bind weakly and a majority of the initial sequences do not bind to their target at all. A second step is therefore required to physically separate the binder: target complexes from unbound or weakly bound sequences, partitioning true binders from the others. The success of the entire process depends on this step, since separation results in the differentiation of different binders. Therefore, if the technique can eliminate most of the weak or non-binding aptamer molecules, while retaining those tightly binding to their target, then PCR will amplify mainly the tight binders. As a consequence, the enrichment process can be achieved rapidly with fewer rounds of selection. After separation, the high affinity sequences are eluted from the target molecules and then enzymatically amplified by PCR to generate a new DNA pool for the next round of SELEX. To speed up the selection process and ensure that the successful aptamer sequences are, in fact, high affinity binders, the stringency of the binding conditions (e.g. shorter incubation time, lower concentration of DNA pool) and/or elution conditions is generally increased during the later rounds. If, however, the conditions are too harsh, there is a risk of losing binders in the earlier rounds, which will result in failure of selection. Typically, it takes around 20 rounds of SELEX to obtain aptamer sequences with good affinity (for protein selection, the process would be shorter, generally around 10 rounds). After selection, the resulting oligonucleotides are subjected to DNA sequencing. The sequences corresponding to the initially variable region of the library are screened for conserved sequences and structural elements indicative of potential binding sites. Finally, the binding

potency of the aptamer candidates is verified. Despite it has been almost 20 years away from the first aptamer discovery, most aptamers are still selected by this traditional methodology. However, the involved technologies can vary from traditional capillary electrophoresis, flow cytometry to most recent microfluidic channel [136]. The overall goal for various selection approaches remain the same, that is to increase the selection efficiency with reduced time and process while fishing for ligands which bind to targets with high specificity and affinity.

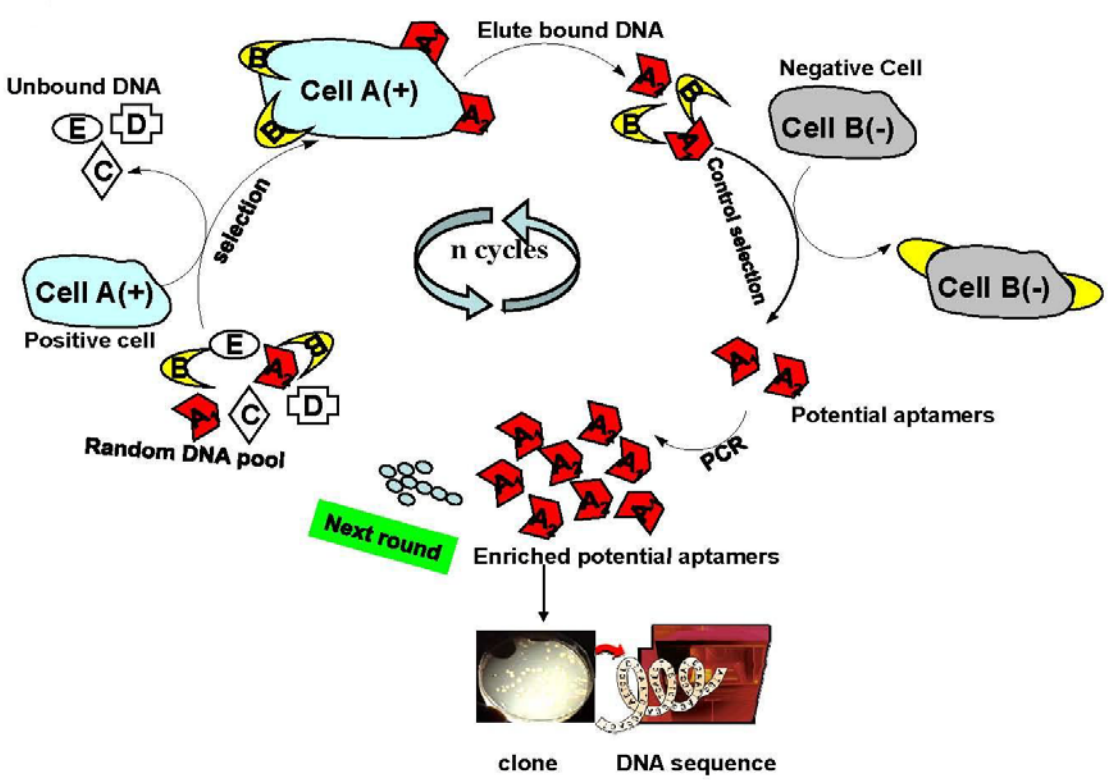

Figure 1-7. Schematic presentation of a typical whole-cell-SELEX process.

Based on this process, the Tan group recently developed a whole-cell-SELEX strategy to generate a panel of aptamers for specific diseased cells[31]. The cell-SELEX process, which is illustrated in Figure 1-7, can be performed without any prior knowledge about the target. Similar to the SELEX method, as outlined above, cell-SELEX also involves the same series of steps, including incubation, elution and amplification. However, cell-based SELEX differs in that a counter selection is introduced after a positive selection by performing similar incubation steps,

but with a negative cell line. By doing so, the common binders for regular receptors on the cell membrane are subtracted away from the resulting pools. Thus, the probability of recognizing unique molecules exclusively expressed in the target cancer cells is greatly enhanced. As discussed above, cancers originate from mutations of human genes, and these genetic alterations cause molecular changes to diseased cells, resulting in changes in cell morphology and physiology. As such, the rational selection of aptamers must take into consideration the identification of molecular differences between normal and tumor cells, and discriminate among tumor cells of different classifications, at different disease stages, or from different patients. This blind selection strategy is, moreover, an interesting method by which potential disease biomarkers can be discovered by identification of the aptamer's binding targets [137,138].

Aptamers and antibodies

As described above, nucleic acid based aptamers can perform as specific recognition molecules, just like antibodies. However, compared to antibodies, aptamers possess several inherent advantages [139-141]. As listed in Table 1-3, aptamers can be selected within two months by virtue of the automated synthesis and in vitro SELEX process, while antibody selection requires a time-consuming in vivo process involving animal models. This, in turn, requires that antibodies be generated under physiological condition, limiting their targets to extraceullar molecules which cannot be toxic to the host animal. On the contrary, versatile artificial conditions can be used in aptamer selection, and both extracellular and intracellular molecules can be its targets without any additional toxicity concerns. Although the binding specificity and affinity of aptamers are comparable to those of antibodies, aptamers have much higher inhibitory potential and much lower immunogenicity and toxicity when compared to antibodies. Unlike antibodies, aptamers are smaller in size and molecular weight, allowing higher penetration to the tissue and, as a consequence, allowing the delivery of therapeutic agents

to the tumor sites more efficiently. The aptamer's small size also allows rapid renal clearance from the system, thus reducing toxicity to healthy tissues. Automated synthesis permits aptamers to be easily reproduced with little variation, and further modification can be performed for various applications or, in the alternative, simple adjustments to the kinetic parameters can be made. Finally, aptamers are stable and chemically robust, enabling them to retain their activity, even after exposure to heat and denaturants.

Table 1-3. Comparison of aptamer and antibody's properties [139-141]

Features	Aptamer	Antibody
Production	< 8 weeks (automated, in vitro)	> 10 weeks (in vivo)
Selection conditions	Versatile	Only physiological condition
Target space	Extra- and intracellular proteins	Extracellular proteins
Selection toward toxic subjects	No	Yes
Immunogenicity and toxicity	None observed	Immune reactions observed
Molecular weight	5-25 kDa	150 kDa
Batch to bacth variation	No	Yes
Convenient chemical modification	Yes	No
Kinetic parameters (on/off rate)	Can be changed	Can not be changed
Inhibitory potential	High	Low, 1 out of 200
Shelf life	Long	Short
Physicochemical stability	Stable	Labile
Binding affinity	High	High

Given that aptamers mimic and extend many of the features of antibodies, a similar or faster development of commercial applications of aptamers in the coming few years is certain.

Micelles

Versatile nanomaterials have been successfully integrated into different aspects of cancer research, and micelle are one such interesting nanomaterial [142]. The usages of micelles in cancer research can be largely divided into two areas: separation [143] and delivery [144-146]. In this section, some basic knowledge of micelles will be presented.

Figure 1-8.Molecular structure of phosphatidyl choline.

A micelle is a dynamic species consisting of aggregated surfactant molecules in a liquid colloid. Surfactants are amphiphilic molecules which contain both hydrophilic (water-attracting) and hydrophobic (water-repelling) portions. Figure 1-7 illustrates one example of phospholipids (the most common cell membrane lipids), phosphatidyl choline. Based on the charge characteristics of their hydrophilic head groups, surfactants are generally classified into three types: cationic, anionic and zwitterionic surfactants. The hydrophobic tail portion of the surfactant can be a linear or branched hydrocarbon chain (seven to twenty-one carbons), or even an aromatic ring structure.

Amphiphilic surfactant molecules exist as discrete monomers in a very dilute solution, and they will not aggregate into micelles until the concentration reaches a breaking point called the

critical micelle concentration (CMC). It is not uncommon to obtain slightly different CMC values if different measurement methods are adopted [147]. Additionally, some factors, such as temperature and the presence of salt and organic molecules, can change the CMC value of the micelles through the interaction with water [148].

Table 1-4. The relationship between the molecular packing shape, packing parameter and lipid aggregation structures (modified from ref 149).

Critical packing shape	Packing parameter	Aggregation structure
 Cone	< ⅓	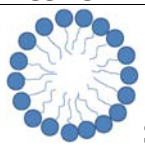 Shperical micelle
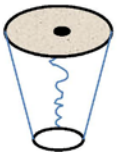 Trucated cone	⅓ - ½	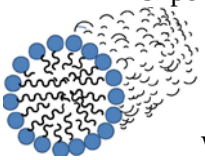 Wormlike micelle
 Cylinder	½ - 1	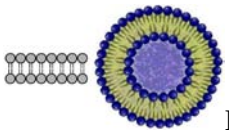 Bilayer, vesicles
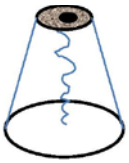 Inverted (tracated) cone	>1	 Inverted micelle

As presented in Table 1-4, the geometry of a micelle can vary from bilayer to sphere, depending mainly on the packing parameter, P, defined as follows [149]:

in which V is the volume of the hydrocarbon part of the lipid, l is the chain length of the lipid tail, and S0 is the mean cross-sectional surface area of the head group. When P is smaller than ⅓, the lipids aggregate into spherical micelles; when P is between ⅓ and ½, the aggregation will form wormlike micelles. A P value between ½ and 1 indicates the formation of a bilayer, while inverted micelles form when P is larger than 1 (see Table 1-4). However, regardless of

which structure the lipids adopt, nonpolar hydrocarbon portions of each lipid are aggregated while the polar head groups are in contact with water. The hydrophobic force is demonstrated to be the major thermodynamic driving force to stabilize the hydrated lipid aggregate [149] while the van der Waals forces between hydrocarbon chains and hydrogen bonding between the polar head groups also play a role.

Flow-Cytometric Analysis of Aptamer Binding with Cells

The abnormal growth of cancer cells may interfere with the natural expression of the cell surface markers, resulting in an over-expression or under-expression of some markers. To distinguish among diseased cells and healthy cells, flow cytometry is the popular technique to use for immunophenotyping. It is unsurprising that flow cytometry can also be applied to evaluate the binding ability of fluorophore-labeled aptamers to the cells by virtue of their antibody mimic properties. Chapter Two in this dissertation presents the utilization of flow cytometry in the aptamer-related research. To help illustrate the data, the instrumental principles of flow cytometer and related data interpretation are discussed in the following.

Basically, flow cytometers use hydrodynamic focusing principle to generate individual particles (cells in our case) to pass through the laser zone (or other light excitation source), and then measure physical and chemical properties of the individual particles simultaneously. As illustrated in Figure 1-9, the fluidics system has a central channel (through which the sample is injected) enclosed by an outer sheath that contains faster-flowing fluid. As the sheath fluid moves, the injected suspended cells are hydrodynamically focused, resulting in one cell at a time passing through the focused laser zone. As the cells intercept the light source, cells scatter light based on the sizes and shapes. A lens known as the forward scatter channel (FSC) collects the light scattered forward (typically up to 20^{o} offset from the laser beam's axis). The FSC's intensity roughly represents the particle's size; thus, it can be used to distinguish between

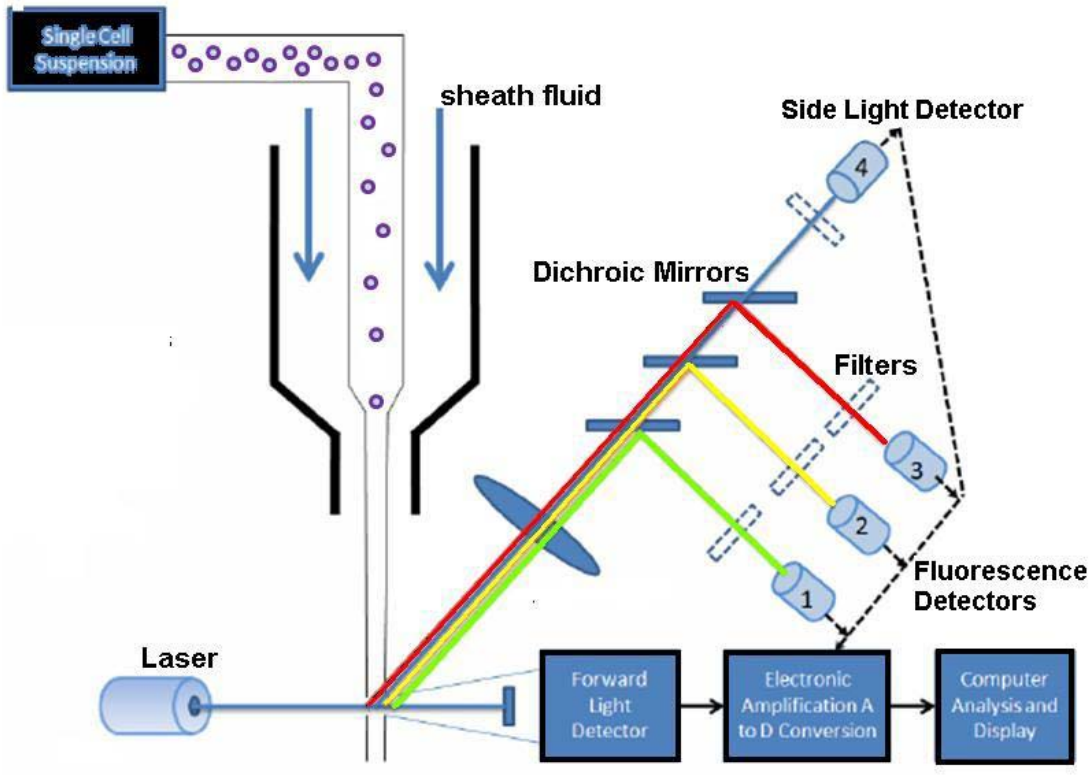

Figure 1-9. A typical flow cytometer setup. Cells are hydrodynamically injected into the fluidics system and with the aid of the sheath flow, one cell at a time passed through the optical path. As the cells intercept the laser, scattered light (forward and side) is collected. If the cells are stained with a fluorescence tags, the emitted fluorescence is collected and converted finally into a digital data set for the computer analysis and display (modified from Figure A-1 in the PhD dissertation of Prabodhika Mallikaratchy at University of Florida).

cellular debris and living cells. In contrast, another parameter, side scatter, was measured approximately at a 90^{o} to the excitation line. Unlike FSC, the side scatter channel (SSC) provides information about the granular content within a particle, such as the shape of the nucleus, the amount and type of cytoplasmic granules, or the membrane roughness. Every type of particle has its unique FSC and SSC values; therefore, a combination of these two parameters may be used to differentiate different cell types in heterogeneous samples. For instance, since dead cells have lower forward scatter and higher side scatter than living cells, we can distinguish between those two types of cells based on both FSC and SSC parameters. Additionally, if the cells are stained

with a fluorophore-labeled probe, the fluorescence signal will be collected to indicate which cells are tagged with the probe. Subsequently, both scatter and fluorescence signals from each cell are converted into analog electric signals through the photo-multiplier tube (PMT) detectors, and then further transformed into digital electric signals by analog to digital convertors (ADCs). At this point, the collected data are finally ready for the analysis by the computer.

To display and interpret data, a single-parameter histogram is commonly used. Typically, a single measurement parameter (such as forward scatter, side scatter or fluorescence) is on the x-axis while the number of events (cell counts) is on the y-axis. In this dissertation, a histogram with the events plotted as the function of fluorescence signal is used for the data analysis (Figure 2-5B for instance). After incubating target cells with aptamers and random library sequences respectively, the fluorescence intensities of cells are compared. Since the average intensity from the red curve (aptamer signal) is much higher than the one from green curve (library signal), the histograms indicate strong binding ability of aptamers.

Ideally, flow cytometry will produce a single distinct peak that can be interpreted as the positive dataset. However, in many situations, flow analysis is performed on a mixed population of cells, resulting in several peaks on the histogram. In order to identify the positive dataset, negative and/or positive control should be run on the same machine with the same conditions. For instance, to identify target cells in the human whole blood sample in Chapter Two, several control experiments are required.

Fluorescence Methods for Signal Transduction

Fluorescence measurements have been widely used for a broad spectrum of investigations in cancer research because of high sensitivity, nondestructive nature and multiplexing capabilities. Fluorescence-based nucleic acid probes may rely on the changes of emission

intensity, excitation or emission wavelength, lifetime, or fluorescence anisotropy to monitor a molecular recognition event.

Fluorescence results from a process that occurs when fluorophore molecules absorb light. When a population of these molecules absorbs the energy of the incident light, electrons of these molecules can be excited to the excited singlet states. Returning the electrons to the ground state is accompanied by an emission of photos, which results in fluorescence. This process is illustrated by the Jablonski diagram in Figure 1-10 [150,151]. In which, S0 stands for the singlet (all electrons are paired) ground state, S1 and S2 are singlet excited states, while T1 and T2 refer to the triplet (unpaired electrons) excited state. Upon light radiation, the energy of a photon is absorbed by a fluorophore and creates an excited unstable electronic singlet state (S1 or S2, the transition of the molecule from S0 state to S2 state is usually presented as a second peak at the shorter wavelength). Subsequently, the excited molecule falls to the ground vibrational level of S1 via internal conversion and/or vibrational relaxation.

When the electron returns from an excited state to the ground state S0, there is an emission of light at a characteristic wavelength (the fluorescence process). Since the lifetime of the excited state S1 (10-10-10-7 s) is longer than the vibrational relaxation time (10-12-10-10 s) as shown in Figure 1-10, vibrational relaxation usually happens before fluorescence happens, which results in a certain energy loss. Thus, the fluorescence emission spectrum is located at higher wavelengths (lower energy) than the excitation spectrum. The difference in wavelength between the maximum emission and absorption peak is known as the Stokes shift. Besides the fluorescence emission, several other pathways can also allow electrons returing from the excited singlet state to the ground state, including non-radiative decays (such as thermal relaxation) and phosphorescence (intersystem crossing to a triplet excited state).

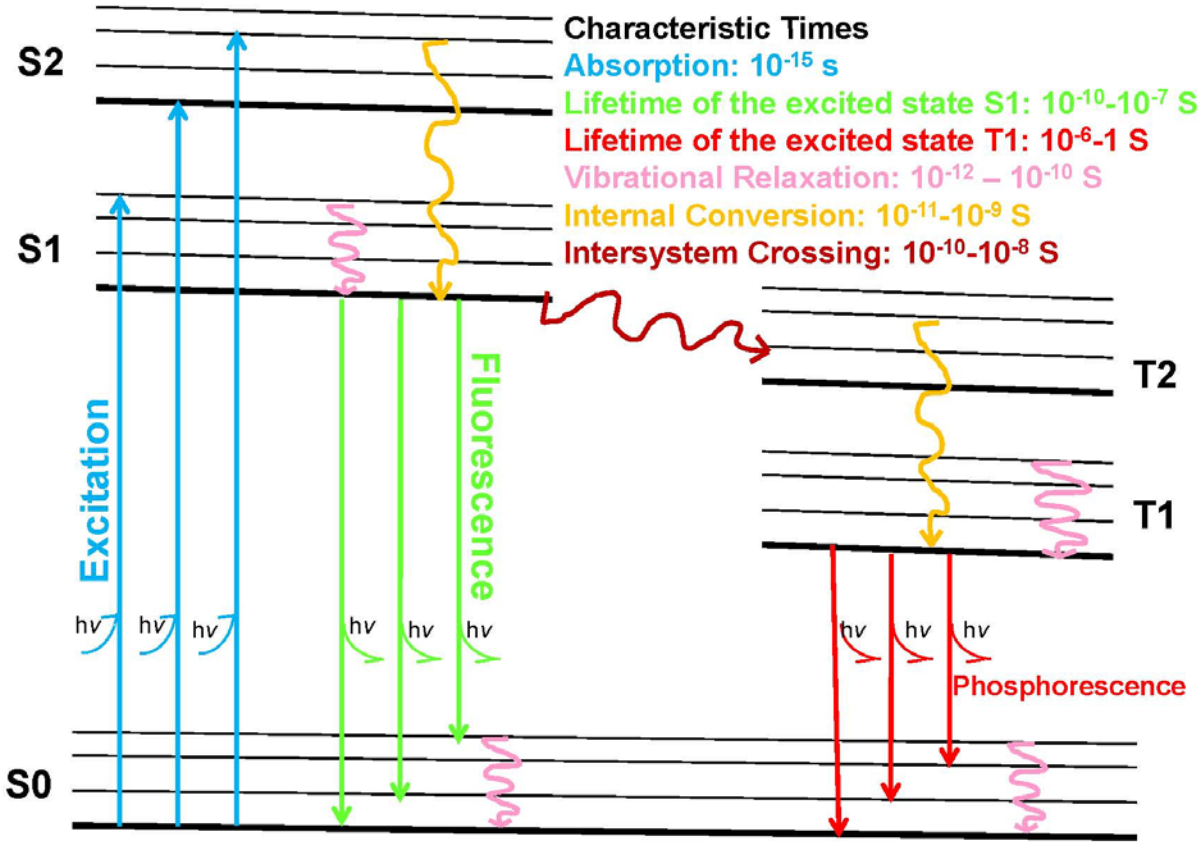

Figure 1-10.Jablonski diagram for fluorescence mechanism and characteristic times of various processes.

There are a variety of ways to quench (decrease) the fluorescence emission of a fluorophore. Two major quenching mechanisms are involved: collisional (or dynamic) quenching and static quenching. During collisional quenching, the excited molecule will experience non-radiative energy loss when colliding with other molecules (including solvent molecules) in the solution. Many molecules can be a collisional quencher, such as oxygen, halogens, amines, and acrylamide. Consequently, the excited molecule will return to the ground state without any emission of photons. The decrease in fluorescence intensity caused by collisional quenching can be described by the following Stern-Volmer equation:

$$\frac{F_0}{F} = 1 + K[Q] = 1 + k_q \tau_0 [Q]$$

F_0: Initial fluorescence intensity without quencher
F: Fluorescence intensity with quencher
K: Stern-Volmer quenching constant (M^{-1})
K_q: Bimolecular quenching rate constant ($M^{-1}S^{-1}$)
τ_0 : Fluorescence lifetime in the absence of the quencher (s)
[Q]: Concentration of quencher (M)

Based on the above equation, in aqueous solutions at room temperature with a fluorophore having 1ns fluorescence lifetime, to ensure the decreased fluorescence caused by collisional quenching is negligible, the quencher concentration should be below 1 mM. However, if two molecules are brought together by linkers, the collision rate is greatly increased and no longer controlled by diffusion rate; thus, the resulting quenching might be significant.

Unlike collisional quenching, static quenching involves the formation of a non-fluorescent complex (dark complex) between the quencher and the fluorophore in the ground state. The decrease in fluorescence intensity can be described by the following quation:

$$\frac{F_0}{F} = 1 + K_f [Q] = 1 + \frac{[FQ]}{[F]}$$

F_0: Initial fluorescence intensity without quencher
F: Fluorescence intensity with quencher
K_f: Formation constant for FQ
[FQ] : Concentration of the dark complex
[F] : Concentration of fluorophore
[Q]: Concentration of quencher

There are two simple methods available to distinguish two quenching mechanisms. The first method is to check the lifetime change. In static quenching, the lifetime does not change as the only observed fluorescence is from the uncomplexed fluorophore; therefore, the fluorophore's lifetime remains the same after quenching. In contrast, for dynamic quenching, the lifetime shows the same order of decrease as the intensity. The second method to differentiate two quenching mechanisms is to identify the effect of temperature on the quenching efficiency. In static quenching, higher temperature leads to the decreased quenching efficiency due to the

dissociation of the weakly bound complex. However, in dynamic quenching, higher temperature causes faster diffusion, thus results in more quenching.

Static quenching has been actively incorporated into the molecular probes design to study molecular recognitions. The molecular beacon, which is used in this dissertation, is one such example [152].

Scope of This Research

The scope of the research work presented here is to engineer molecular probes or nanomaterials for cancer detection, with the potential of cancer treatment and intracellular mRNA studies. First, a unique aptamer-micelle was constructed as an efficient detection/delivery vehicle toward cancer cells with enhanced selectivity. The binding ability of low affinity aptamers at physiological temperatures was greatly restored and several beneficial properties have been achieved. In a second project, a universal strategy to build practical molecular beacons for long-term real-time intracellular mRNA monitoring was proposed and completed. In this project, the designed probes demonstrated excellent biostability and good hybridization kinetics. Finally, the use of single-walled carbon nanotubes to modify nuclease-vulnerable molecular beacons was demonstrated to be an efficient way to overcome several major limitations for intracellular applications, including nonspecific interaction with nucleases and DNA binding proteins, low self-delivery efficiency and nucleus accumulation.

CHAPTER 2
DYNAMIC APTAMER-MICELLE WITH ENHANCED SELECTIVITY AS AN EFFICIENT DETECTION/DELIVERY VEHICHLE TOWARD CANCER CELLS

Introduction

This chapter discusses the construction of the aptamer-micelle based on spontaneous molecular self-assembly to perform efficient detection/delivery toward cancer cells with enhanced selectivity. Molecular self-assembly has contributed to the formation of various interesting nanomaterials, either natural or artificial, to achieve unique functions. In nature, the apoptosome [153] is one such example. Individual apaf-1 protein does not itself have a biological function; however, when forming a complex with cytochrome c, several individual proteins self-assemble into a wheel structure called an apoptosome. Once formed, the apoptosome can then recruit and activate the otherwise inactive pro-caspase-9, which can then activate other caspases and trigger a cascade of events leading to apoptosis. Learning from nature, chemists have created various artificial nanostructures. Micelles represent one such example. Polymeric micelles, functioning as drug solubilizers and carriers, have been subjected to extensive studies in the field of drug delivery [154]. More recently, a micelle constructed as a hybrid from hydrophilic oligonucleotide and hydrophobic polymer [155,156] has drawn close attention. In aqueous solutions, this type of amphiphilic block copolymer can self-assemble into a three-dimensional spherical micelle structure or a nanorod-like micelle structure [157]. This type of micelle has been shown to efficiently carry a variety of cargos to cells, including antisense oligonucleotides [158] and drug molecules [159]. To perform efficient targeted delivery, folic acid, a type of cancer cell recognition molecule modified on a piece of short complementary DNA, was clicked onto micelles based on Watson-Crick base pairing [159].

Aside from Watson-Crick base pairing, single-stranded oligonucleotides can recognize other target molecules based on noncovalent interactions, such as hydrophobic interaction and

hydrogen bonding. This type of oligonucleotide ligand is known as an aptamer, which can tightly bind to specific target molecules, such as small molecules, proteins, and even cancer cells [19,20,31]. Compared to antibodies, aptamers possess a few critical advantages, such as small size, lack of immunogenicity, and ease of synthesis and modification [160,161]. We believe that attaching a hydrophobic tail to the end of an aptamer should result in a highly ordered micelle-like structure. In this type of aptamer assembly, the aptamer strand would not only act as the building block for the nanostructure, but also perform a recognition function to its specific target. Furthermore, densely packing aptamers on such an assembly could create a multivalent effect, leading to greatly improved binding affinity of the aptamers. Engineering this type of aptamer-micelle can be simple and could result in enhanced binding capability to its specific targets. Micelles are also considered to be dynamic and soft materials. Since the cell membrane is basically a dynamic lipid bilayer, a "soft" nanomaterial might produce some interesting interactions with it, particularly where such interactions involve cell permeability and drug delivery. In fact, we have generated a pool of aptamers specifically targeting various cancer cells [31-33], thus paving the way for the construction of aptamer-micelles with applications in diagnosis and targeted therapy.

Experimental Section

Materials

Unless specified, chemicals were purchased from Sigma-Aldrich (St. Louis, MO) and used without further purification. DNA synthesis reagents were purchased from Glen Research (Sterling, VA). The single-walled carbon nanotubes (SWNTs) were purchased from Unidym, Inc. with <5wt% ash content (CAS number: 7782-42-5). CellTracker^{TM} Green BODIPY (C2102) and Qdot 705 streptavidin conjugate (Q10161MP) were purchased from Invitrogen. All flow cytometry data were acquired with a FACScan cytometer (Becton Dickinson Immunocytometry

Systems, San Jose, CA). Ramos (CRL-1596, B-cell line, human Burkitt`s Lymphoma), CCRF-CEM (CCL-119, T-cell line, human Acute Lymphoblastic Leukemia), K562 (CCL-243, chronic myelogenous leukemia (CML), and HL60 (CCL-240, acute promyelocytic leukemia) were obtained from ATCC. The NB4 cell line was kindly provided by Shands Hospital. All cell lines were cultured in RPMI 1640 medium (ATCC) supplemented with 10% fetal bovine serum (FBS) (heat inactivated, GIBCO) and 100 IU/mL penicillin-streptomycin (Cellgro). The wash buffer contained 4.5 g/L glucose and 5 mM $MgCl_2$ in Dulbecco's PBS (Sigma). Binding buffer used for the aptamer binding assays was prepared by adding yeast tRNA (0.1 mg/mL) (Sigma) and BSA (1 mg/mL) (Fisher) into the wash buffer to reduce background binding.

Synthesis of Lipid Tail Phosphoramidite.

Synthesis of compound 1: A solution of stearoyl chloride (6.789 g) in $ClCH_2CH_2Cl$ (50 ml) was slowly added to a solution of 1,3-diamino-2-dydroxypropane (1.0 g) in $ClCH_2CH_2Cl$ (100 ml) and TEA (2.896 g). The reaction mixture was stirred for 2 hours at room temperature and then heated up to 70 °C overnight. The solution was then cooled down to room temperature, filtered, and the solid was washed with CH_2Cl_2, CH_3OH, 5% $NaHCO_3$ and ethyl ether. After drying under vacuum, the solid turned to white (compound 1, yield: 90%).

Synthesis of compound 2: Compound 1 (5.8 g) was dissolved in anhydrous CH_2Cl_2 (100 ml), and DIEA (8.6 ml) was injected into it. The solution was cooled on an ice bath, and 2-Cyanoethyl N,N-diisopropylchlorophosphoramidite (4.2 mL, 16.72 mmol) was added under dry nitrogen. After stirring at room temperature for 1 hour, the solution was heated to 60 °C for 90 minutes. After cooling to room temperature, the solution was washed with 5% $NaHCO_3$ and brine, dried over Na_2SO_4 and concentrated by vacuum. The product was purified by precipitation

from concentrated CH_2Cl_2 into CH_3CN to afford compound 2 (4g, 55% yield) as white solids. ^{31}P NMR ($CDCl_3$) 154 ppm.

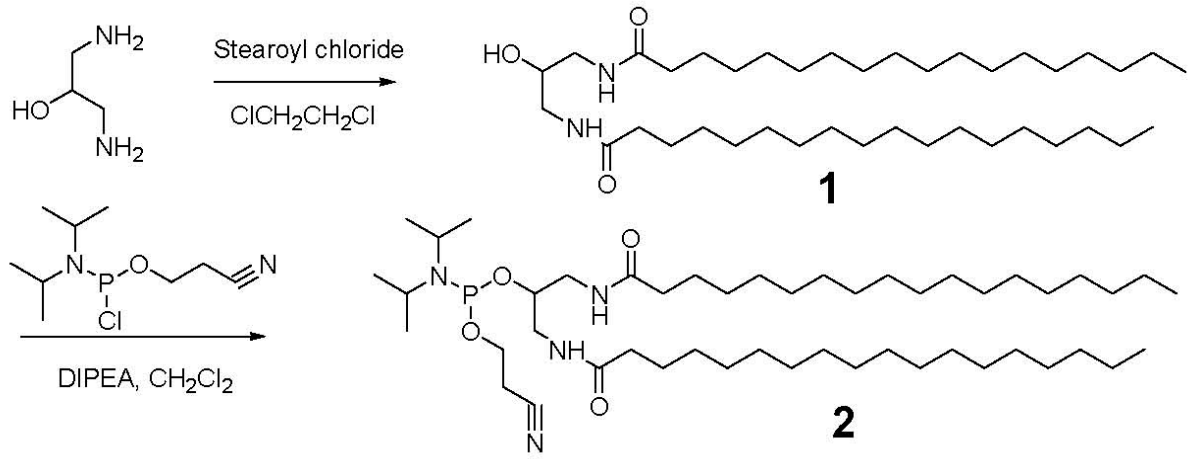

Synthesis of Aptamer-Lipid Sequence

An ABI3400 DNA/RNA synthesizer (Applied Biosystems, Foster City, CA) was used for the preparation of all DNA sequences. All oligonucleotides were synthesized based on solid-state phosphoramidite chemistry at a 1 µmol scale. The aptamer-lipid sequences listed in Table 2-1 were synthesized in controlled-pore glass columns with a 3'-(6-FAM), TAMR or biotin TEG covalently linked to the CPG substrate. The complete aptamer-lipid sequences were then deprotected in AMA solution (concentrated ammonia hydroxide:methylamine = 1:1) at 65 ^{0}C for 15 minutes for FAM/biotin labeling or a solution of methnol: tert-butylamine: water (1:1:2) at 65 ^{0}C for 3 hours for TMR labeling. A ProStar HPLC (Varian, Walnut Creek, CA) with a C8 column (from Alltech, Deerfield, IL) was used for probe purification. Deprotected sequences were purified with a linear elution gradient with TEAA (triethylammonium acetate) in acetonitrile changing from 20% to 70% over a 30 min period. The collection from the first HPLC separation was then vacuum dried. Spacer phosporamidite 18 was used as the linker between DNA and lipid tail. Lipid tail phosphoramidite dissolved in methylene chloride was directly coupled onto the sequence by the synthesizer. The synthesis of lipid tail phosphoramidite is

described in the above section. A Cary Bio-300 UV spectrometer (Varian, Walnut Creek, CA) was used to measure absorbance for probe quantification.

Preparation of TDO5-Micelles with Different Aptamer Densities

Aqueous TDO5-lipid/library-lipid solution and aqueous PEG-lipid solution were diluted in different centrifuge tubes by addition of at least 5-fold volume of acetone. Subsequently, the two solutions were mixed well together and put in a vacuum drier to evaporate away the acetone leaving only an aqueous solution. By adjusting different molar ratios of TDO5-lipid/library-lipid and PEG-lipid solutions at this first step, TDO5-micelles/library-micelles with different aptamer/library densities could be achieved.

Micelle Characterization

TEM images were obtained after negative staining with 1% aqueous Uranyl Acetate using a transmission microscope (Hitachi H-7000). The TEM samples were dropped onto standard holey carbon-coated copper grids. Dynamic Light Scattering measurements were carried out at room temperature using a Brookhaven ZetaPALS analyzer. Aptamer-lipids were dissolved in PBS buffer. using a transmission microscope (Hitachi H-700).

Flow Cytometric Analysis

To demonstrate the cell-specific targeting capabilities of aptamer-lipids, fluorescence measurements were made using a FACScan cytometer (Becton Dickinson Immunocytometry Systems, San Jose, CA). The binding was performed by the following procedure. 250 nM aptamer-lipid/library-lipid in binding buffer was added to about 1 million cells in the individual flow tubes. The prewarmed mixture was incubated at 37 ^{0}C in a cell incubator for various time periods. After incubation, the cells were immediately washed twice with cold washing buffer. The fluorescence was determined by counting 15,000 events.

Competition assays to measure the off rate of the aptamer-cell interacton (K_{off}) were performed as follows. An aptamer concentration of 250nM was incubated with cells for 20 minutes at 4 ^{o}C for 20 minutes to allow the aptamer to bind to the target in the cell membrane. After the incubation, the cells were washed to remove unbound aptamer. Finally, the labeled cells were incubated with 2.5 uM unlabeled aptamer at 4 ^{o}C for various incubation times. The mean fluorescence intensity was measured at different incubation times after a brief vortexing of the cell mixture. K_{off} was obtained by fitting the dependence of the binding percentage over time to the equation $Y = Y0 + A_{exp} (K_{off}X)$ where Y is binding percentage and X is time. The fluorescence intensity before the displacement was normalized to 100% binding. Additionally, the equilibrium dissociation constants (K_d) of the aptamer-cell interactions were obtained by fitting the dependence of fluorescence intensity of specific binding on the concentration of the aptamers to the equation $Y= B_{max}X/(K_d + X)$ by SigmaPlot (Jandel, San Rafael, CA).

Preparation of Au NP-TDO5/library Conjugates

Gold nanoparticles (Au NP, 13 nm) were prepared [162] and modified with Neutravidin by the reported method. Then either an excess of biotin and Cy5 co-labeled TDO5 aptamer or library was mixed with the Neutravidin-modified Au NP, and the complexes were rocked at room temperature for at least half an hour. After removal of unbound DNA by centrifugation, the conjugates were directly used in cell binding studies.

Preparation of SWNT/TDO5-Lipid or SWNT/Library-Lipid Complexes

SWNTs were ultrasonicated (Fisher Scientific, Model 100) for 1 hour. Then about 60 mg/L SWNT was mixed with 5 μM TDO5-lipid or library-lipid aqueous solution. The mixture was ultrasonicated for another 30 minutes. Then the probe/nanotube solution was centrifuged at 20,000*g* for 15 minutes. The pellet, comprising impurities and large aggregates of nanotubes at the bottom of the centrifuge tube, was discarded and the supernatant was dialyzed against 1.5L

water (Spectra/MWCO1MDa) for 3 days. The water was changed 6 times during the dialysis period. The resulting solution was stored at 4 ^{o}C.

Preparation of Biotin-TDO5-Micelles Doped with Dyes

Dye-doped aptamer-micelles were prepared by the precipitation and membrane dialysis method. 15 pmol of dry biotin-TDO5-lipid was dissolved in 20 μL ethanol, and then mixed well with 6.74 nmol CellTracker^{TM} Green BODIPY. The solution was then added dropwise into 100 μL deionized water while stirring. After stirring for about 3 hours to evaporate the ethanol, the aqueous solution was dialyzed against 1.5 L water (Spectra/MWCO3500) for 2 days. The water was changed 5 times during the dialysis period. Finally, the solution was filtered through a 0.22 um filter to remove any undesirable aggregates and stored at 4 ^{o}C.

Preparation of NBD-Labeled Liposome

27.4 μM POPC (Avanti) and 1.3426 mM NBD-PC (Avanti) (2% NBD-PC in the lipid mixture) were mixed in a chloroform solution, the solvent was evaporated by a stream of nitrogen and vacuum, and the lipids were allowed to hydrate in PBS buffer. The resulting multilammellar vesicles were put through five freeze-thaw cycles and then extruded through a polycarbonate filter with pore diameter of 100 nm (Whatman).

Determination of CMC of Aptamer-Micelle

10 μM of pinacyanol chloride solution in distilled water was mixed with TDO5-micelles with various concentrations from 0.2 nM to 150 nM. The solutions were left to sit for hours before taking the pictures.

Cytotoxicity Assays

Cellular toxicity of DNA-lipid was assessed using the CellTiter 96 Cell Proliferation Assay (Promega, Madison WI), according to the manufacturer's instructions. Cells were cultured in 96-well microtiter plates in complete growth medium with various library-lipid or library

concentrations for 2 days, with 500,000 cells/mL as the starting cell density. As a positive control, 10% DMSO was incubated under the same conditions.

Confocal Imaging

Cell images were made with a confocal microscope setup consisting of a Leica TCS SP5 Laser Scanning Confocal Microscope. For real-time monitoring, the fluorescent images were taken every minute at a fixed depth. 2 uM cell tracker dye and/or about 4.5 uM aptamer-lipid were/was incubated with the cells in complete cell medium at 37 oC. For the co-localization experiment, cells were incubated with TMR-TDO5-lipid (250nM) in RPMI-1640 complete medium at 37 oC for 3 hours, and then AF633-transferrin (60nM) was added 30 minutes before the termination of incubation. Incubation was stopped by placing the cell on ice immediately after washing with cold washing buffer.

Flow Channel Device Preparation and Incubation under Continuous Flow

For micelle-buffer incubation, a PDMS flow channel was used. PDMS devices were fabricated using a process similar to what is described in the literature [39,163]. The layout of the device was designed in AutoCAD and printed on a transparency using a high-resolution printer. The pattern on the transparency was transferred to a silicon wafer via photolithography. The silicon wafer was etched to a depth of 25 μm in a deep reactive ion etching machine. The resulting silicon wafer with the desired pattern served as a mold to fabricate a number of PDMS devices. Sylgard 184 (Corning) reagents were prepared and thoroughly mixed by following the manufacturer's instructions. After being degassed to remove bubbles, the mixture was cast on top of the silicon mold. After being cured at room temperature, the PDMS layer was peeled off the silicon mold. Two wells at both ends of the channel and one well in the middle of the channel were created by punching holes in the PDMS. The PDMS slice was reversibly attached to a clean 50× 45 mm cover glass (Fisher) to form a device. Avidin- and

biotin-aptamer solutions were added to the wells at both ends of the channel (sgc8 aptamer for CCRF-CEM on the left side; TDO5 aptamer for TDO5 on the right side) and were sucked through channels by applying a vacuum to the middle well of the channel. Then the corresponding cell solutions were put to the corresponding end-wells, sucked slowly through the entire channel by applying a vacuum to one of end-wells, and incubated at 37 ^{o}C for 5 minutes. After washing, the DNA-micelles diluted in binding buffer were continuously flushed through the channel at 300 nL/s for 5 minutes by connecting a microsyringe pump (World Precision Instruments, Inc.) to the end-well of the channel (dynamic incubation). The channel was ready for confocal imaging after three washing steps. In between experiments, the PDMS devices were cleaned by sequential sonication in 20% bleach with 0.1 M NaCl and then 50:1 water:versaclean (Fisher) at 40 ^{o}C, followed by rinsing in deionized H_2O and drying under N_2.

For micelle-blood incubation, a simplified flow channel made from double glass slides glued together by a double sided tape. Instead of a microsyringe pump, a piece of filter paper was used to suck the solutions through the channel with average flow rate of about 300 nL/s.

Results and Discussion

Aptamer-Micelle Construction

As indicated in the scheme (Figure 2-1A), we have attached a simple lipid tail phosphomidite with diacyl chains onto the end of an aptamer inserted with a PEG linker. This amphiphilic unit self-assembled into a spherical micelle structure, as demonstrated in the TEM image (Figure 2-2A). The aptamer used in this case is called TDO5. As shown in Figure 2-2A, the TDO5-micelle has an average diameter of 68±13nm, which is consistent with the hydrodynamic diameter measured by Dynamic Light Scattering of 67.22nm (Figure 2-2B).

When optimizing our selective aptamer-micelles, we found that the hybrid from lipid tails plus a short length of DNA (short DNA-lipid) can result in nonspecific binding with cells within

a short time period. As shown in Figure 2-3, only after 30 minutes, strong fluorescence signals were observed. However, this nonspecific interaction problem can be greatly reduced by simply elongating the DNA by inserting more random DNA bases. The hybrid from the lipid and a total 89mer DNA length demonstrated the least nonspecific binding within 2 hours of incubation with cells. To facilitate DNA synthesis pursuant to the construction of aptamer-micelles for further studies, we replaced the random DNA bases by a PEG linker of similar length, using a spacer phosphoramidite 18. In this case, 24 units of PEG were inserted between a TDO5 aptamer sequence and lipid tail (Figure 2-1A).

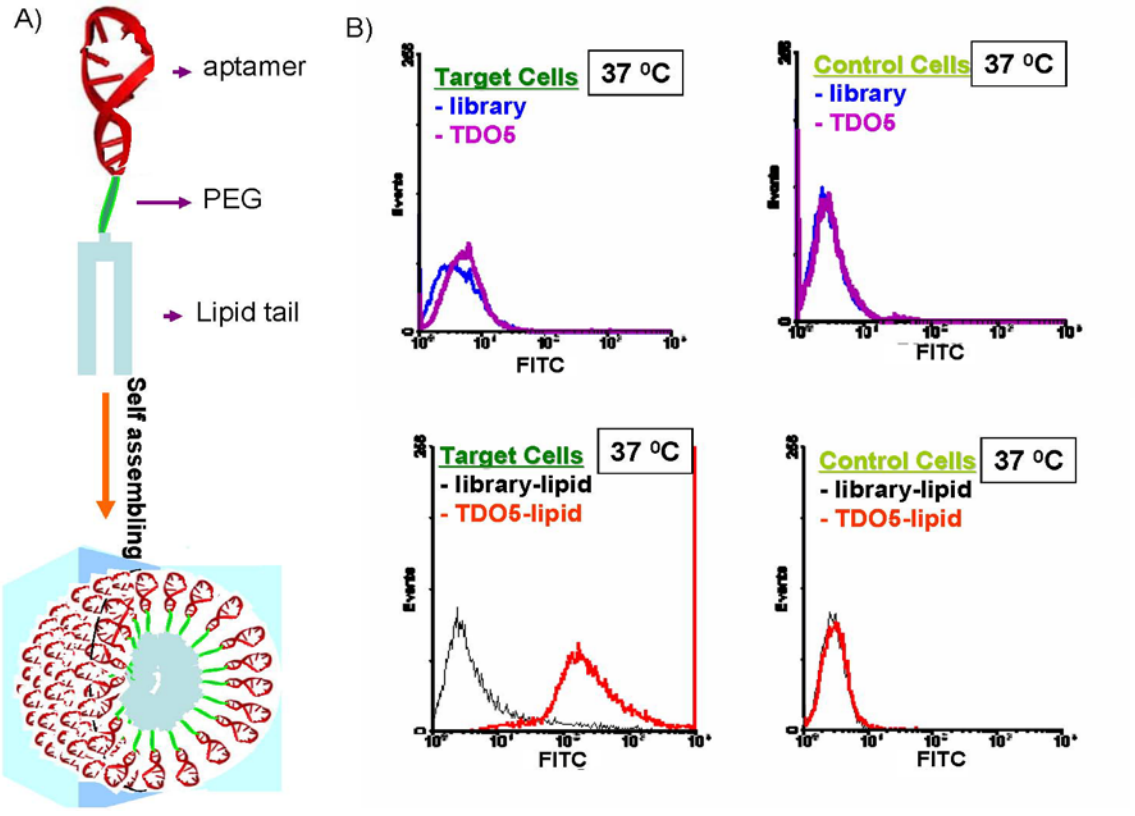

Figure 2-1.A) Schematic illustration of aptamer-lipid formation. All the related sequences are listed in Table 2-1. B). Flow cytometric assay to monitor the binding of free TDO5 (250nM) and TDO5-lipid (250nM) with Ramos cells (target cells) and HL60 (control cells) at 37 ^{0}C for 5 minutes. The blue and black curves represent the background binding of unselected DNA library and TDO5-lipid respectively. The purple and red curves represent the binding of TDO5 and TDO5-lipid, respectively.

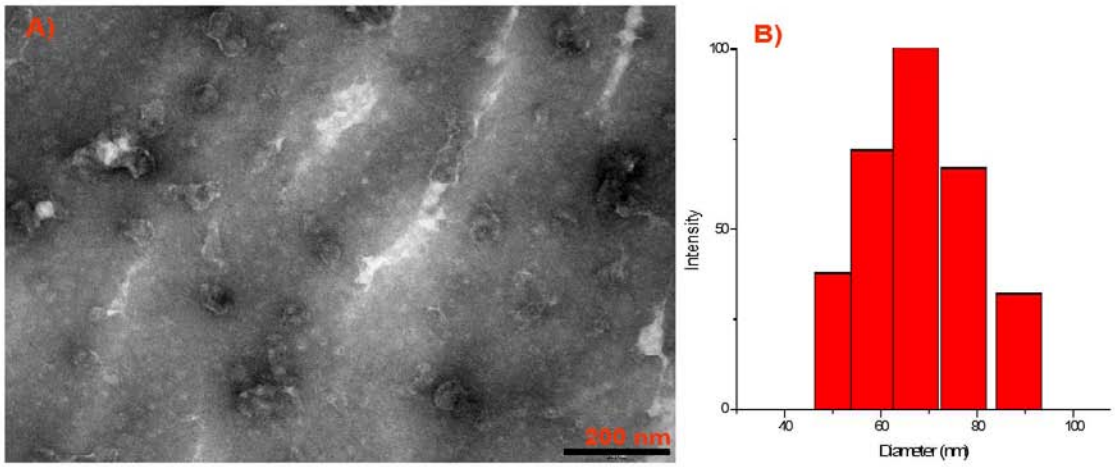

Figure 2-2.TEM image after negative staining by 1% aqueous Uranyl Acetate (A) and Dynamic light scattering histogram (B) of TDO5-micelles.

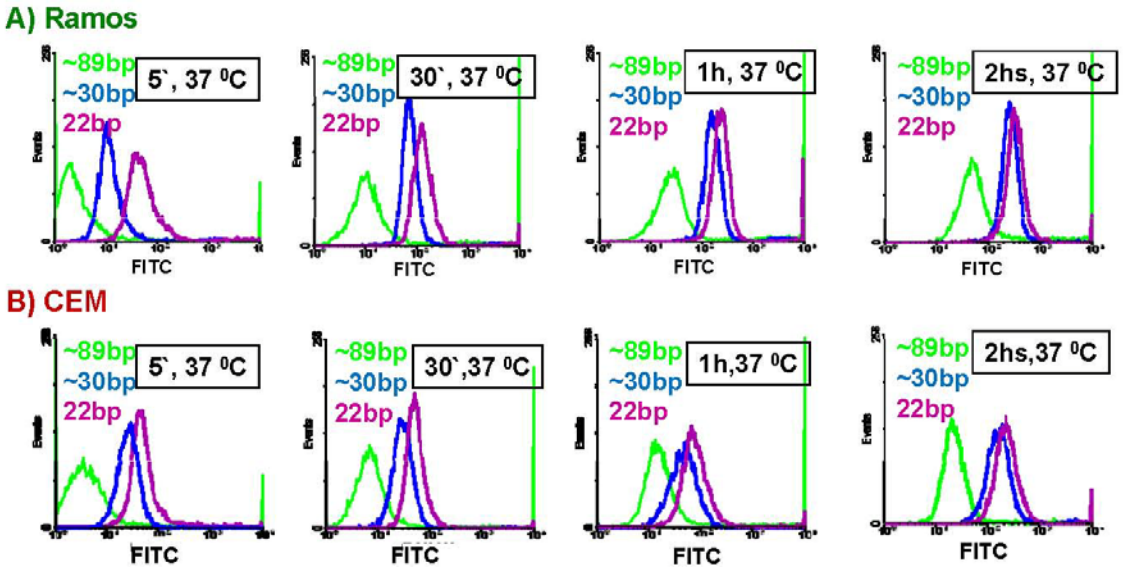

Figure 2-3.Effect of the length of oligonucleotide on the nonspecific interactions between DNA-lipids and different cell lines, including Ramos (A) and CCRF-CEM (B). The green, blue and purple curves represent the hybrids from lipid tails with oligonucleotides of about 89, 30, and 22 base pairs, respectively.

Enhanced Binding at Physiological Temperature

Interestingly and surprisingly, the formation of an aptamer-micelle was found to enhance the binding capability of otherwise low-affinity aptamers at physiological temperature. TDO5 is such an aptamer and was selected specific to Ramos cells (a B-cell lymphoma cell line) [32]. At

4 ºC, TDO5 showed high affinity and selectivity for its target protein, immunoglobulin heavy mu chain (IGHM) receptor on the cell surface [138], which indicates that this surface cell membrane protein has an upregulated expression in Ramos cells. On the other hand, TDO5 did not bind with Ramos cells at 37 ºC (Figure 2-1B), a condition which could seriously hinder its potential *in vivo* applications. However, when TD05 is used for micelle formation, the TDO5-micelle was also found to have excellent binding selectivity at 37 ^{0}C. As shown in Figure 2-1B, when binding with target cells, about 80-fold enhancement in fluorescence intensity was observed for TDO5-lipid, while no binding shift was found with control cells.

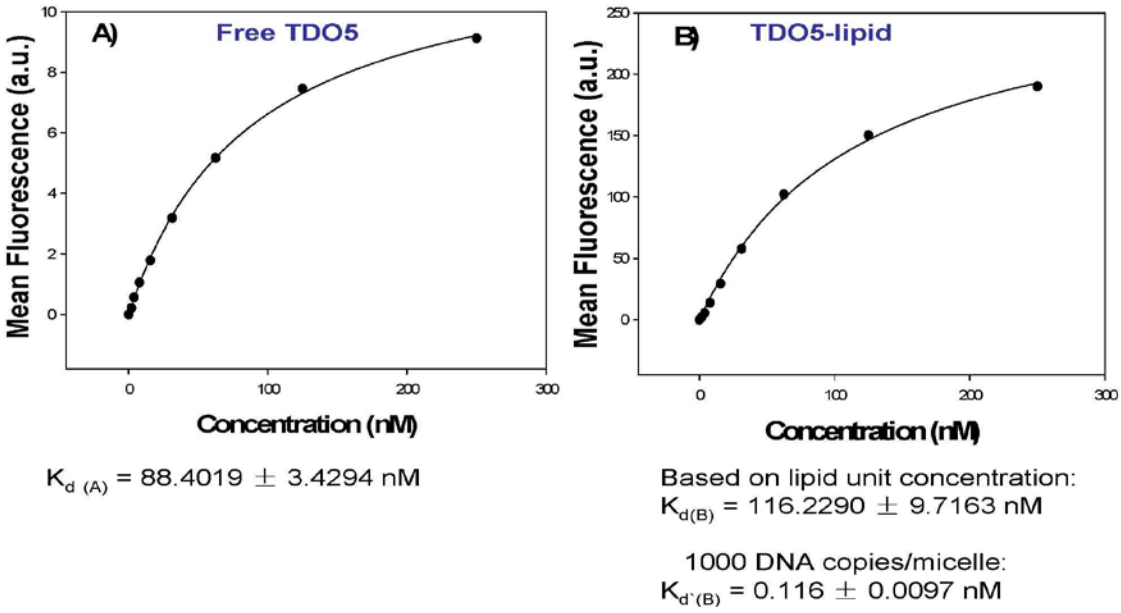

Figure 2-4. Flow cytometry to determine the binding affinity of free FITC-TDO5 aptamer (A) and FITC-TDO5-lipid (B) to target cells (Ramos cells). The nonspecific binding was measured by using fluorescein (FITC)-labeled unselected library DNA or library DNA-lipid. The mean fluorescence intensity of target cells was obtained by subtracting the mean fluorescence intensity of nonspecific binding. Although the dissociation rate of aptamer-lipid is similar to that of free aptamer, if based on aptamer-lipid unit concentration, the dissociation rate of aptamer-micelles is much smaller if assuming 1000 DNA-lipid units per micelle particle.

The dissociation constants of the aptamer-micelles were also investigated. Since a similar size of polymer micelle (60nm) was estimated to have 1000 copies of units [164], one TDO5-

micelle (68nm) is assumed to have the same estimated unit numbers. As shown in Figure 2-4, the TD05 micelle has a Kd of 116 nM. If one TDO5-micelle has 1000 copies of DNA-lipid units, the dissociation constant after constructing the micelle structure would be greatly decreased from 88 nM (for free TDO5) to 0.116 nM (for TDO5-micelle). This approximate 750-fold increase in binding affinity might be ascribed to the multivalent effect from multiple aptamer binding.

Based on these findings, the lipid tail plus linker modification can be a universal strategy to promote the binding abilities of low-affinity aptamers, as demonstrated by the improved binding behaviors observed after attaching lipid tails onto the end of two other low-affinity aptamers, KK and KB (Figure 2-5).

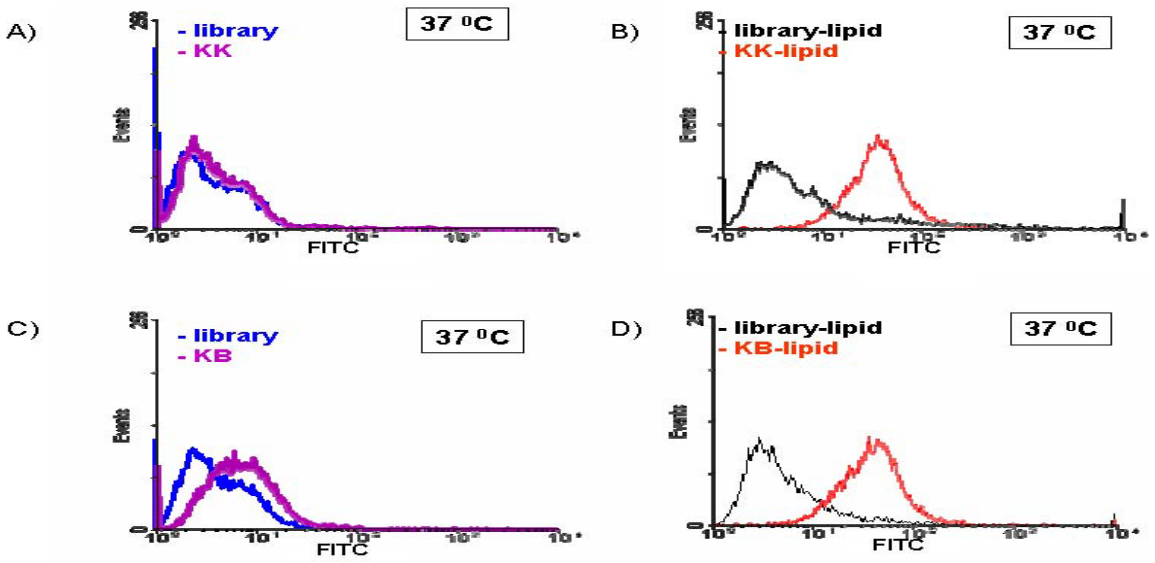

Figure 2-5. Flow cytometric assay to monitor the binding of free aptamer (250 nM) and aptamer-lipid (250nM) with target cells (K562) at 37 ^{0}C for 5 minutes. FITC-KK (A) and FITC-KB (C) aptamers either bind weakly or do not bind at all to the target cells. However, FITC-KK-lipid (B) and FITC-KB-lipid (D) show increased binding to the target cells.

Extremely Low k_{off}

Generally, a low off rate tends to indicate that the binding is strong and difficult to be replaced. Therefore, the k_{off} rate of our aptamer-lipid was examined by a competition experiment,

which was designed to test the micelle's binding strength in comparison to single aptamers. As shown in Figure 2-6, after one day of competition with unlabeled TDO5 aptamer, almost all the bound labeled TDO5 was replaced. Plotting the competition data of free TDO5 showed an exponential decay with a k_{off} of -4.4×10^{-5} S^{-1} (R^2 = 0.93844). In contrast, after the same competition time, a very low percentage of bound TDO5-micelles was replaced by free TDO5 with a k_{off} of -1.5×10^{-6} S^{-1} (R^2 = 0.23481). We noticed that the coefficient for the data fitting in the TDO5-micelle case is quite low, which indicates that the off rate pattern of TDO5-micelle might not be the same as the exponential pattern. Similar low off rates and low R^2 were observed for the other two aptamer-micelles based on KK and KB aptamers (Figure 2-7A).

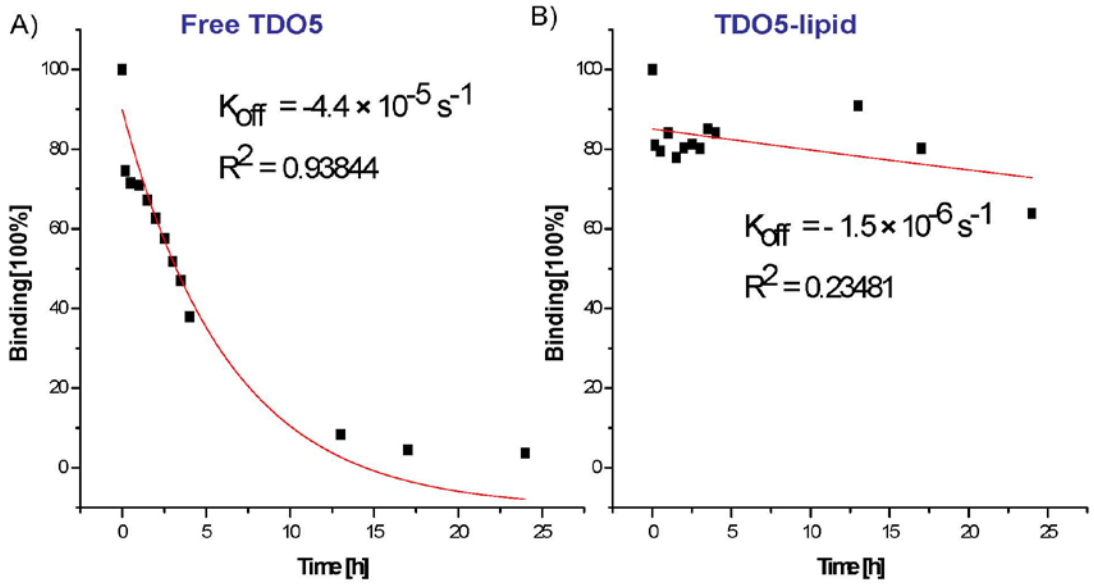

Figure 2-6.Time course of displacement of FITC-TDO5 (A) or FITC-TDO5-lipid (B) bound onto the target cells by competition with an excess of non-labeled TDO5. Cells were incubated with binding buffer containing 250 nM FITC-labeled probes for 20 minutes at 4 ^{o}C. Then 2.5 μM non-labeled TDO5 was added to the cells, and flow cytometric measurements were carried out at times as shown in the x-axis. The fluorescence intensity before the displacement was normalized to 100% binding. The fluorescence intensity of each data point was normalized to the binding percentage

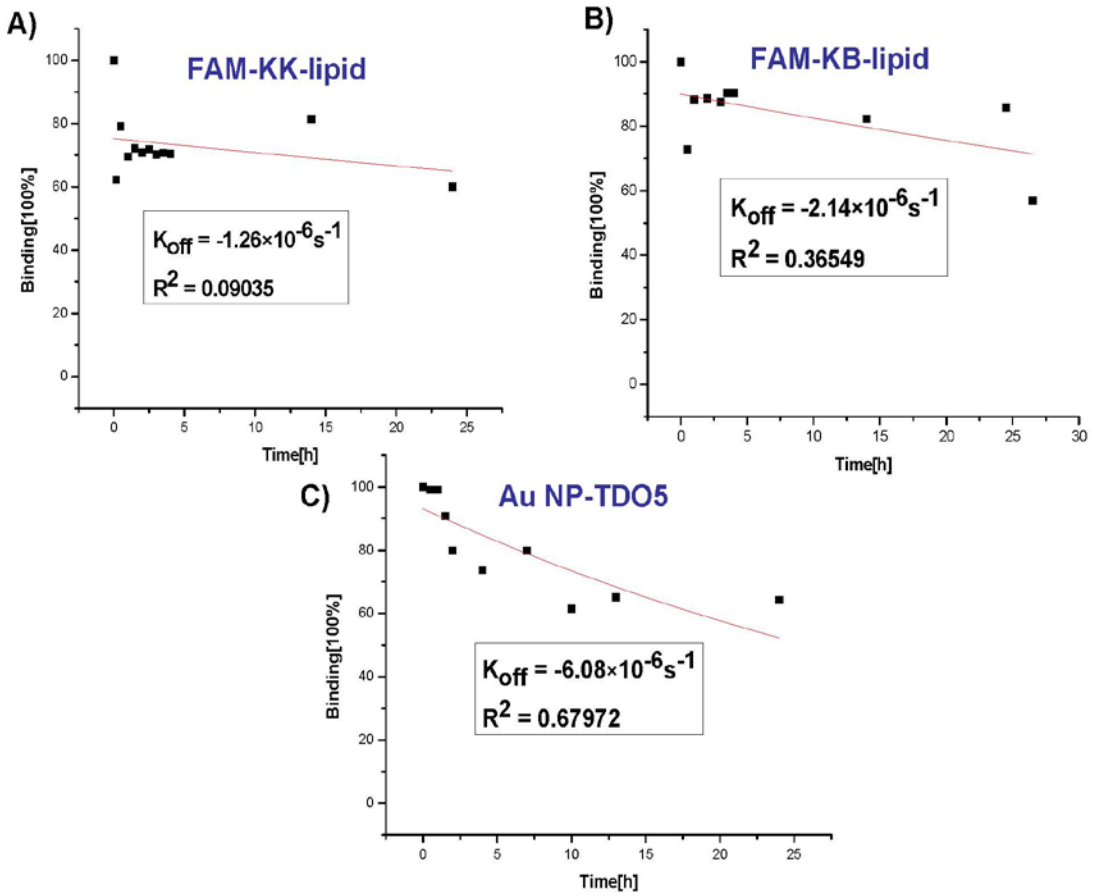

Figure 2-7.Time course of displacement of FAM-KK-lipid (A), FAM-KB-lipid (B) and Cy5-TDO5-Au NP conjugate (C) bound onto the target cells (K562 for A and B; Ramos for C) by largely excess of non-labeled corresponding aptamers (KK for A, KB for B, TDO5 for C). Cells were incubated with binding buffer containing 250 nM FAM-labeled probes for 20 minutes at 4^{o}C. Then, 2.5 μM non-labeled TDO5 was added to the cells, and flow cytometric measurements were carried out at times as shown in the x-axis. The fluorescence intensity before the displacement was normalized to 100% binding. The fluorescence intensity of each data point was normalized to the binding percentage, as well. The graphs show that the dissociation rates of the aptamer-nanomaterial complexes are all much slower than those of corresponding aptamers.

Based on these extremely low off rates, and considering the fact that both aptamer-lipid and cell membrane have hydrophobic and hydrophilic portions, we hypothesize that the integration of aptamer-lipid into the cell membrane can be facilitated by the lipid tail and that the preferred thermal stability does not allow such aptamer-lipid to easily diffuse out. In order to determine whether our aptamer-micelles could fuse with cell membrane, we doped TDO5-micelles with a special dye that only fluoresces inside cells (CellTracker™) (see scheme in

Figure 2-8A). As shown in Figure 2-8B and 2-8C, after incubating the cells with free cell tracker for 12 hours, a strong fluorescence signal was observed inside the cells, while a very weak fluorescence signal was present after 2 hours of incubation. In contrast, it was only after an incubation lasting more than 2 hours with dye-doped TDO5-micelles that most of the cells produced a strong fluorescence signal (Figure 2-8D). To determine whether some or all the aptamer-micelles remained on the cell surface, we post-incubated streptavidin-quantum dots 705 (QD705) with the cells after binding biotin-labeled TDO5-lipid to the cells. Figure 2-8E shows a strong red fluorescence signal around the cell membrane, which indicates that at least some of the aptamer-lipid remained bound to the cell membrane after the dye was released. Exposing the cells to strong UV illumination for a long time leads to cell apoptosis and the leakage of activated fluorescent cell tracker dyes into the incubation buffer. As shown in Figure 2-8E, a strong green fluorescent signal was observed outside the apoptotic cells, while a clear QD705 halo remained where the cell membrane would have been, indicating the integration of the aptamer-lipid into the membrane (Figure 2-8E inset). Based on our real-time monitoring of the fluorescence from the cell tracker at room temperature (Figure 2-8F), fusion of the micelles with the cell membranes occurs within minutes.

The above experiments reveal the potential fusion between aptamer-micelles and the cell membrane. Thus, the interaction process between aptamer-micelles and cells is proposed to be fluidic in nature, involving specific interaction induced nonspecific insertion (see the related information for detailed hypothesized mechanism and related experiments at the end of this section).

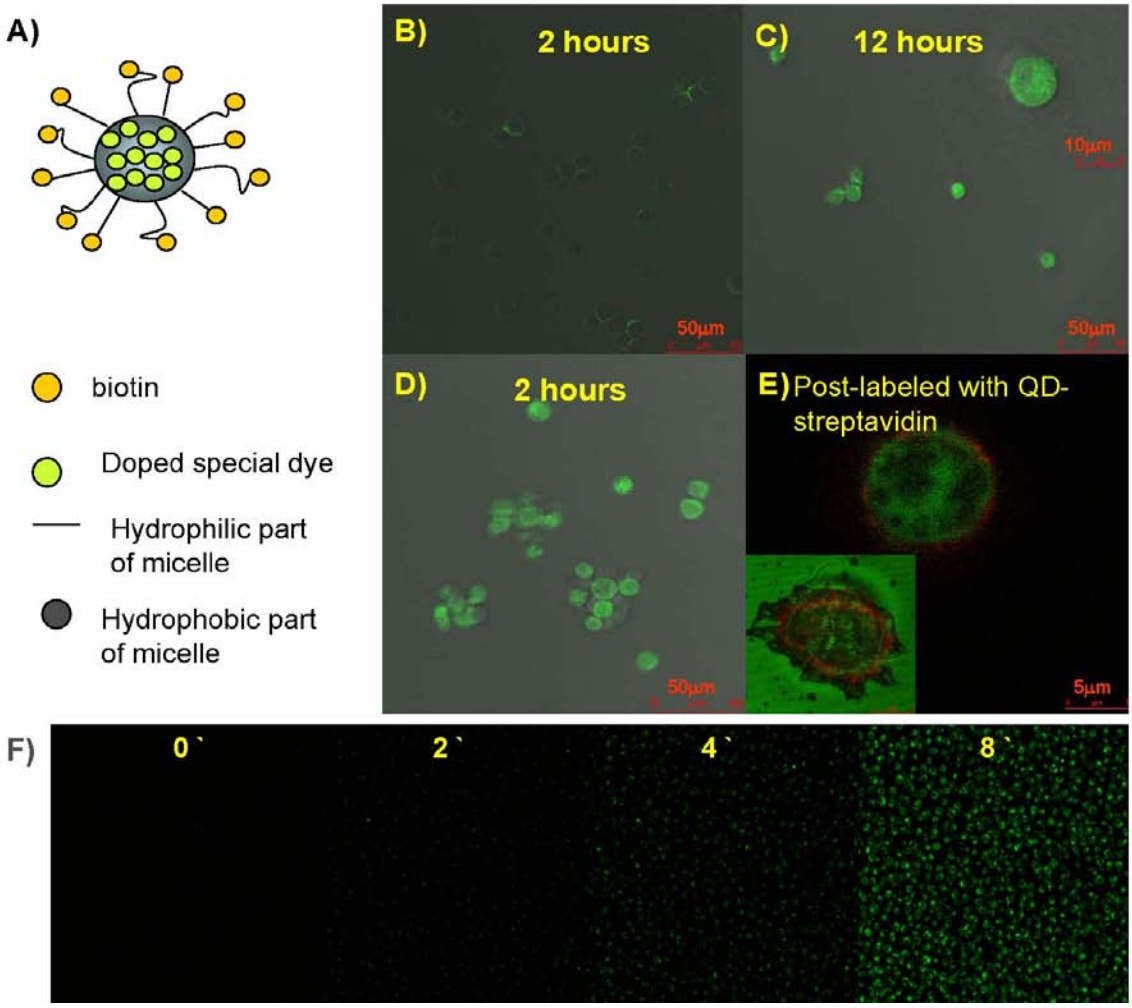

Figure 2-8. Flow cytometric assay to monitor the binding of FITC-TDO5-lipid or FITC-library-lipid with human whole blood sample (male, single donor human whole blood in Na Heparin, Innovative Research) at 37 ^{0}C for various time periods. The black, green and red curves represent the fluorescence intensities from blood cells only, unselected DNA library-lipid and TDO5-lipid, respectively.

TDO5-Micelle Helps Cell Internalization

Although some of the aptamers by themselves lack an internalization pathway, the introduction of this novel nanostructure formation allows the aptamer-lipids to ultimately penetrate the cells they target. As shown in Figure 2-9, while most of the micelles remained on the cell surface after long incubation, a clear fluorescence signal inside the cells, which was confirmed by optical imaging with confocal Z-axis depth scanning, was observed. Since TDO5

alone does not internalize, we reasoned that another mechanism, possibly related to membrane recycling, and might be contributing to this phenomenon. To investigate the intracellular distribution of TDO5-lipid, we co-stained the cells with Alexa633-labeled transferrin, which is commonly used to identify the location of endosomes [165]. The co-localization of the aptamer-lipid with transferrin indicated that the internalized aptamer-lipids were inside endosomes (Figure 2-9). This interesting internalization pathway created by the attachment of the lipid tail, as detailed above, can widen aptamer applications in therapy requiring drug delivery inside the cells. The signal from outer cell membrane should be from the ones which have bound onto the cell membrane but not entered cell yet or have been recycled out to the cell membrane after going inside.

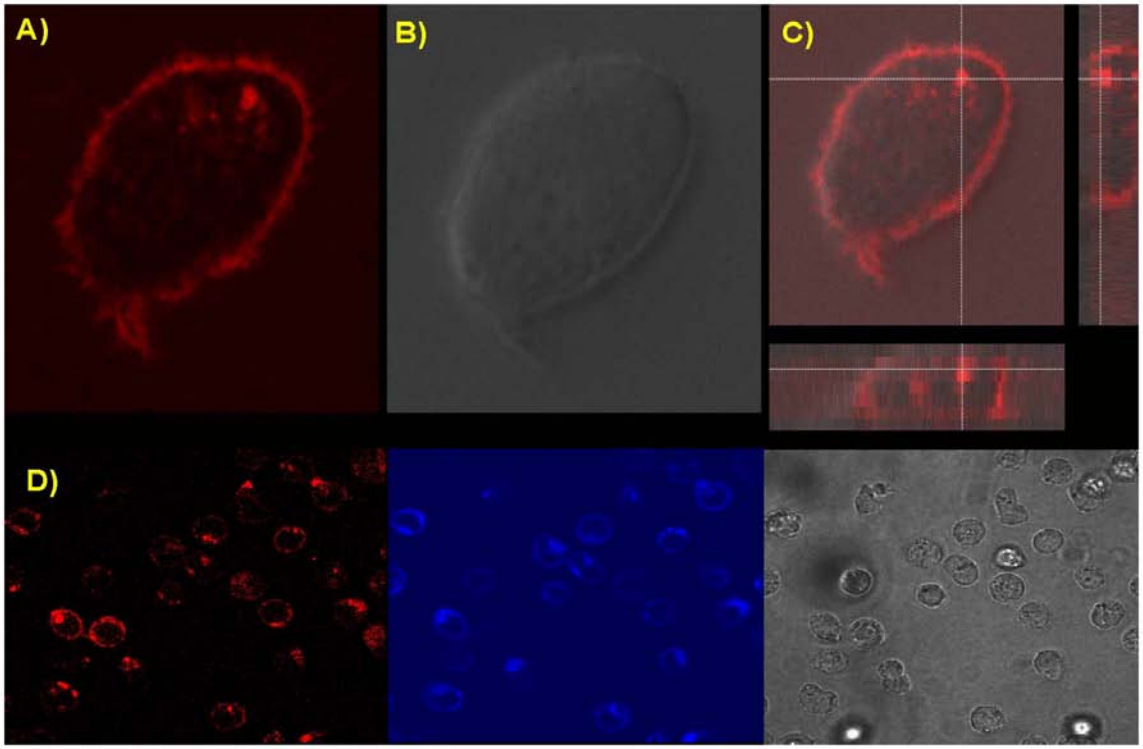

Figure 2-9.The enlarged fluorescence image (A), bright field image (B), and stack image after Z-depth scanning (C) of Ramos cells after incubation with TMR-TDO5-lipid in complete cell medium at 37 ^{0}C for 2 hours. The cross marked in image C indicates that the brightest fluorescence signal comes from inside the cell. (D) Co-localization of TMR-TDO5-lipid (red) and AF633-transferrin (blue) in endosomes.

Rapid Identification with High Sensitivity

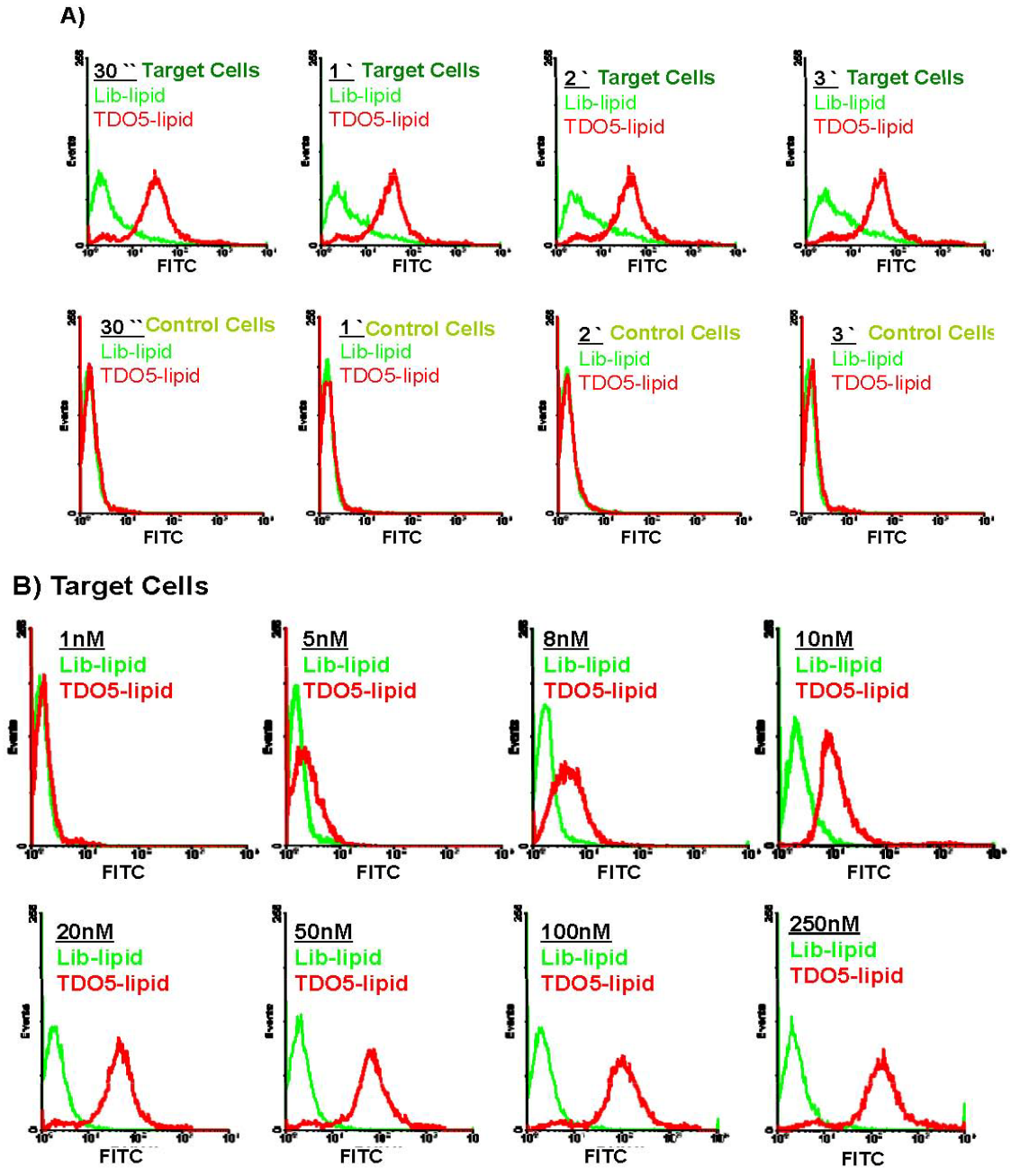

Figure 2-10. Flow cytometric assay to monitor the binding of 250nM TDO5-lipid or library-lipid with Ramos cells (target cells) and HL60 (control cells) at 37 ^{0}C for various incubation times (A), or various concentrations of TDO5-lipid/ library-lipid with target cells at 37 ^{0}C for 5 minutes (B). The green and red curves represent the background binding of unselected DNA library-lipid and TDO5-lipid, respectively.

This TDO5-micelle demonstrated extremely rapid recognition of the target cells. As shown in Figure 2-10A, after an incubation of only 30 sec at 37 ^{0}C, a 45-fold enhancement in fluorescence intensity was observed for TDO5-lipid upon binding with target cells. Again, no significant binding was observed for the control cells. Although a targeting time shorter than 30 seconds might be possible, we did not attempt it because of experimental difficulties. Since every piece of DNA-lipid is labeled with one single FITC dye at the 3' end, one recognition event from one aptamer-lipid can induce multiple-dye staining to target cells. Therefore, this aptamer-micelle structure is suggested to provide an additional signal enhancement. We varied TDO5-lipid/library-lipid concentrations from 250 nM to 1 nM and incubated them with one million cells, respectively. As shown in Figure 2-10B, even at about 0.005 nM (or 5 nM, based on DNA-lipid concentration), noticeable fluorescence shift was still observed upon binding with target cells.

Trace Cell Detection in Whole Blood Sample

To evaluate the detection ability of TDO5-micelle in a complex environment, we spiked one million target cells/control cells directly in 50 uL human whole blood sample (about 310 million cells) and then incubated the DNA-micelles with the cell mixture at 37 ^{0}C for 5 minutes. Based on the flow data shown in Figure 2-11, obvious binding shift was observed when binding to the target cells, but no significant binding shift happened in the control cell mixture. Similar to control, no binding shifts happened in the absence of spiked target cells in whole blood sample (see Figure 2-12). These flow data prove that the aptamer-micelle can detect trace target cells selectively, even in a complex environment.

Meanwhile, when we lengthened the incubation time from 5 minutes to 2 hours, smaller binding shifts were observed (Figure 2-12). It is suggested that the instability of nucleic acid in

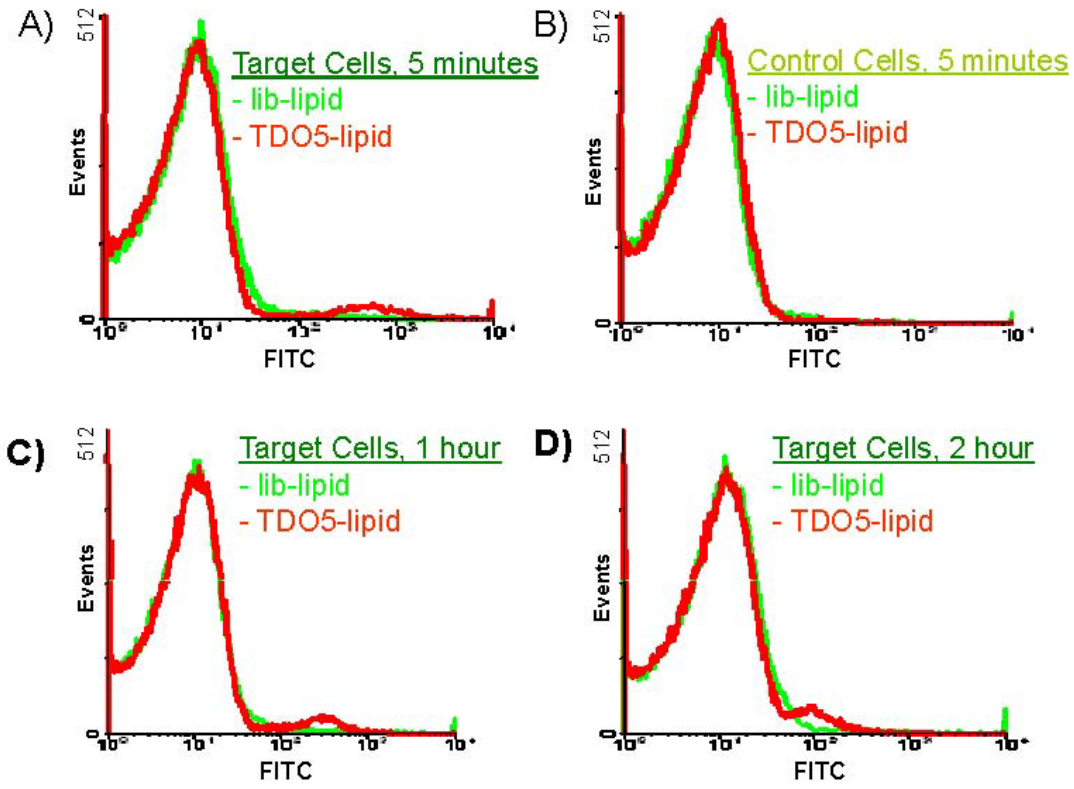

Figure 2-11. Flow cytometric assay to monitor the binding of 250nM TDO5-lipid or library-lipid with trace Ramos (target cells, A) and CCRF-CEM (control cells, B) in human whole blood sample at 37 ^{0}C for 5 minutes. By mixing 1 million cells with 25 uL male whole blood (about 155 million blood cells), 1 million cells with 50 uL male whole blood (about 310 million blood cells), 1 million cells with 100 uL male whole blood (about 620 million blood cells), and 0.5 million cells with 100 uL male whole blood (about 620 million blood cells), the cell percentages were adjusted to 0.64%, 0.32%, 0.16% and 0.08%, respectively. The green and red curves represent the binding of unselected DNA library-lipid and TDO5-lipid, respectively.

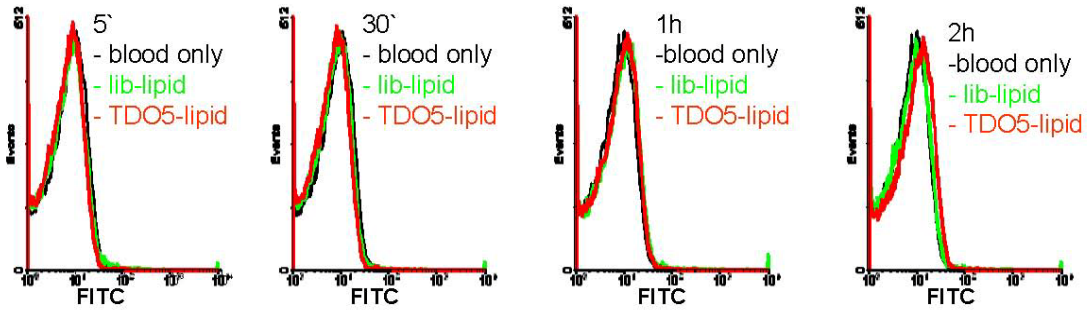

Figure 2-12. Flow cytometric assay to monitor the binding of FITC-TDO5-lipid or FITC-library-lipid with human whole blood sample (male, single donor human whole blood in Na Heparin, Innovative Research) at 37 ^{0}C for various time periods. The black, green and red curves represent the fluorescence intensities from blood cells only, unselected DNA library-lipid and TDO5-lipid, respectively.

plasma at 37 ^{0}C after long incubation is the main reason for the reduced binding shifts [166]. It can therefore be concluded that the presence of fewer intact aptamer-lipids leads to lower binding signals.

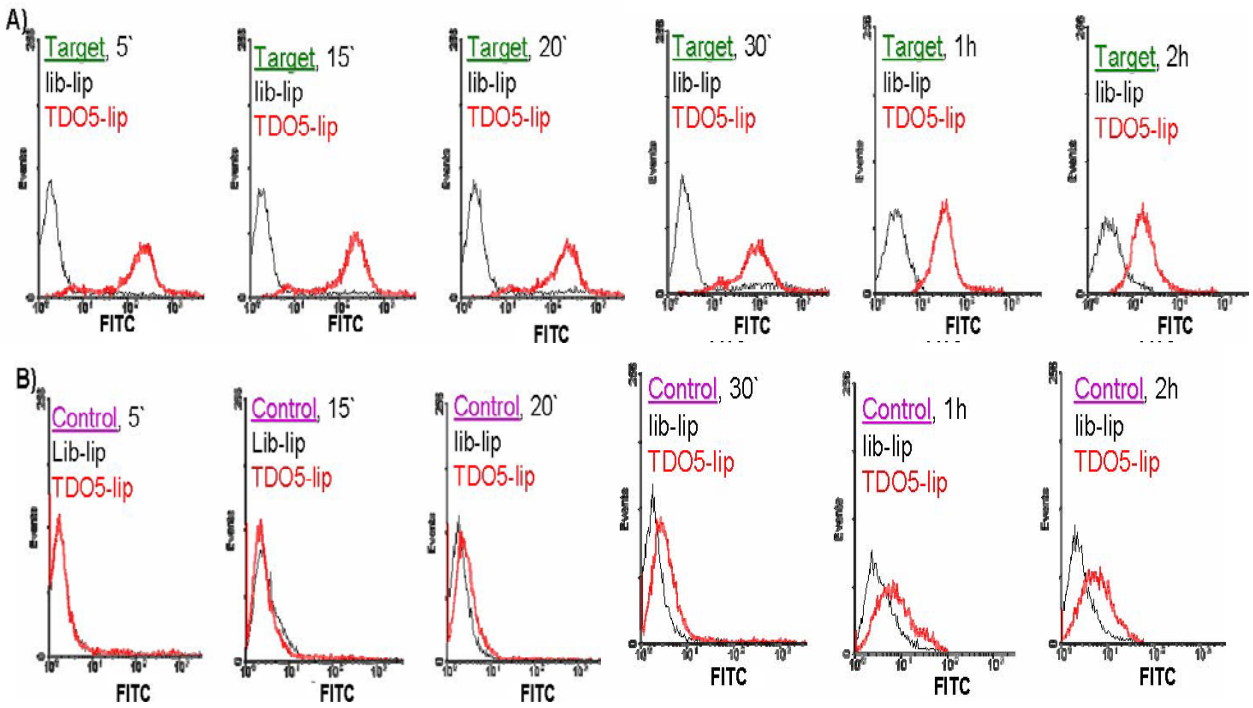

Figure 2-13.Flow cytometric assay to monitor the binding of FITC-TDO5-lipid (250nM) with target cells (Ramos) (A) or control cells (HL60) (B) at 37 ^{0}C for different time periods.

We do not believe that the higher nonspecific binding of DNA-micelles after long incubation in this complex environment causes the smaller binding shifts. As shown in Figure 2-12, the nearly identical fluorescence intensities of library-lipid were observed irrespective of the incubation time with whole blood cell mixture. Comparing the increased nonspecific bindings with increased incubation time in pure buffer sample, as shown in Figure 2-13, we think that the difference in total cell numbers in these two different cases may well lead to different nonspecific interaction patterns. Since the total cell number is extremely high per whole blood cell mixture sample (about 311 million cells), but much lower for the pure buffer incubation

(only 1 million cells), the micelle concentration per cell should be extremely low. This leads to the absence of significant nonspecific binding, even after 2 hours of incubation for whole blood cell mixture.

Aptamer-Micelle Targeting in a Flow Channel under a Continuous Flow

To investigate whether aptamer-micelles can be used for selective targeting under the dynamic fluid conditions of blood circulation, a simplified flow channel was used to mimic the circulatory environment. While we understand there is a significant difference between the fluidic channel and the blood vessel, we believe that this flow dynamic study will give us hint about future possibilities in using this micelle system as a detection/delivery system with dynamic specificity. As shown in the scheme in Figure 2-14A, two biotin-labeled aptamers (biotin-sgc8 and biotin-TDO5) were individually immobilized onto either side of a glass channel using avidin-biotin interactions. Following this step, their corresponding target cells (CCRF-CEM for sgc8 and Ramos for TDO5) were flowed through and captured by the immobilized aptamers. In this way, two different cell zones were established in the flow channel: CCRF-CEM in the control cell zone and Ramos in the target cell zone for TDO5 aptamer.

As the first step, the targeting ability of aptamer-micelle spiked in a simple pure binding buffer system at 37 ^{0}C inside the flow channel under continuous flushing was evaluated. For micelle-buffer incubation, either FITC-TDO5-micelle or FITC-library-micelle diluted in binding buffer was continuously flushed through the two cell zones sequentially at 37 ^{0}C for 5 minutes at 300 nL/s. The same results were observed irrespective of which direction the DNA-micelle was sucked through the two types of cell zones. A representative result after micelle-buffer incubation with FITC-TDO5-lipid is presented in Figure 2-15A. In this case, strong fluorescence signal was seen from the target cell zone, but no noticeable fluorescence signal from the control cell zone. In contrast, no fluorescence signal was observed in either cell zone after incubating

with a control FITC-library-micelle or free FITC-TDO5 aptamer at 37 ^{0}C (Figure 2-15BC), which indicates that TDO5-micelle enhances TDO5 aptamer's binding ability at 37 ^{0}C.

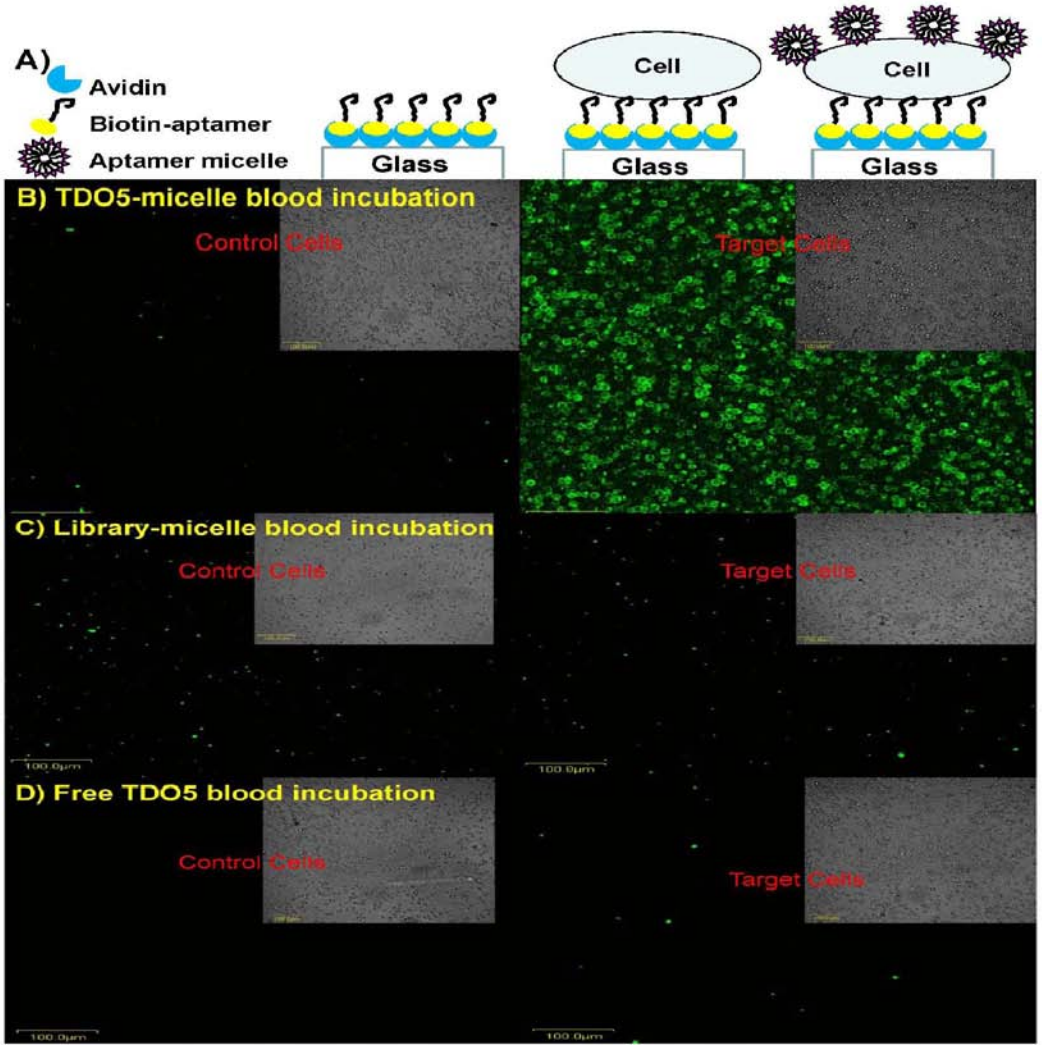

Figure 2-14. Simplified flow channel response to cell staining assay. (A). Stepwise immobilization scheme of the flow channel. Representative images of the bright field and fluorescent images of control cells (CCRF-CEM) and target cells (Ramos) captured on the flow channel surface incubated with FITC-TDO5-micelle (B), or FITC-library-micelle (C) or free FITC-TDO5 (D) spiked in human whole blood sample under continuous flow at 300nL/s at 37 ^{o}C for 5 minutes. All the scale bars are 100 μm.

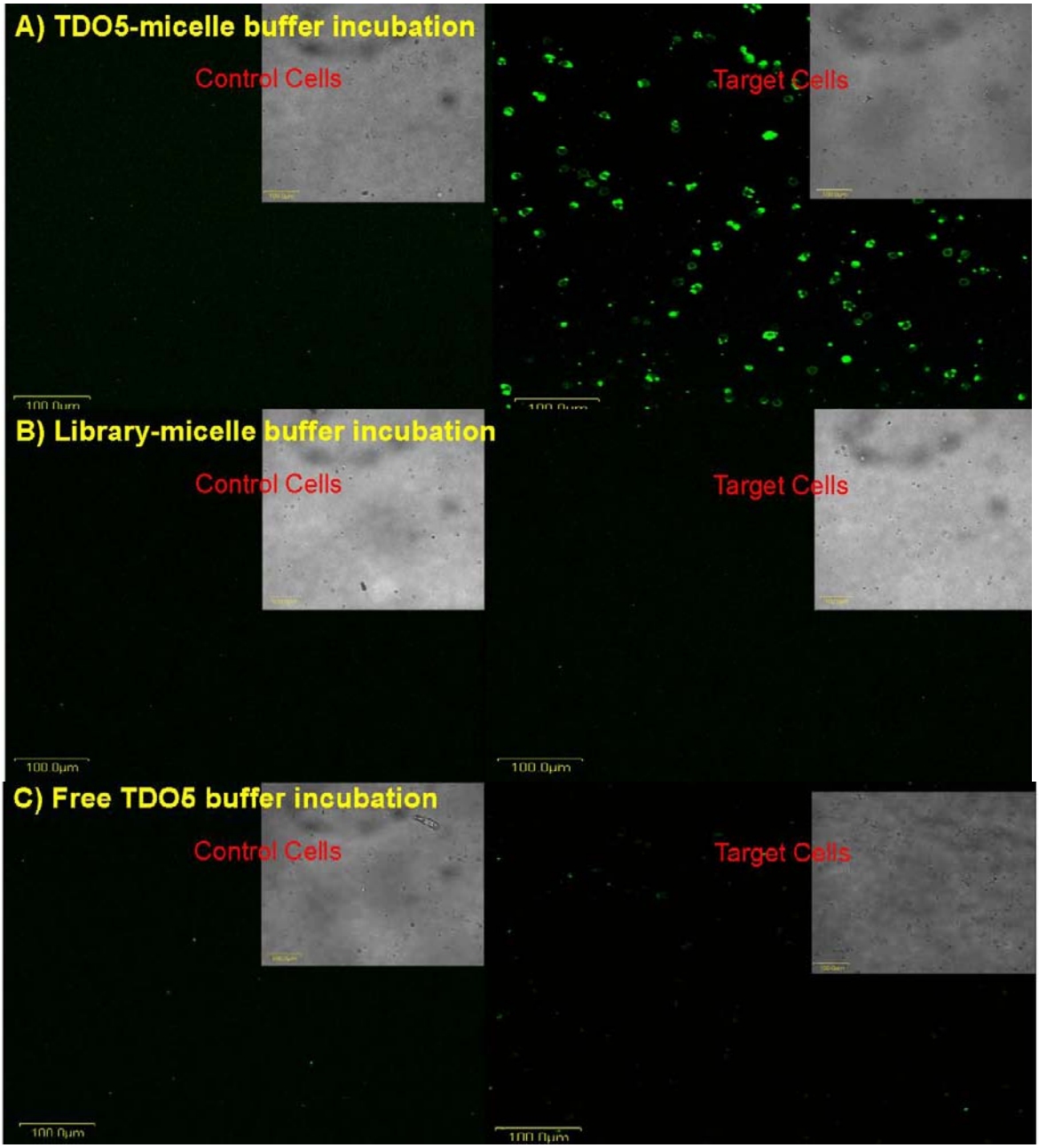

Figure 2-15.Representative images of the bright field and fluorescent images of control cells (CCRF-CEM) and target cells (Ramos) captured on the flow channel surface incubated with FITC-TDO5-micelle (A), or FITC-library-micelle (B) or free FITC-TDO5 (C) spiked in pure buffer solution under continuous flow at 300 nL/s at 37 ^{o}C for 5 minutes. All the scale bars are 100 μm.

As the second step, blood circulation in living systems was mimicked to further test the targetting ability of aptamer-micelle in complex human whole blood sample. This was accomplished inside the flow channel under continuous flushing at 37 ^{0}C. To avoid cleaning difficulties, a simplified flow channel made of double glass slides was preferred over a PDMS flow channel for micelle-blood incubation. Representative results after micelle-blood incubation are presented in Figure 2-14B. As in the micelle-buffer incubation system, strong fluorescence signal was seen from the target cell zone after incubation with TDO5-micelle spiked in whole blood sample, but no noticeable fluorescence signal from control cell zone was seen. In contrast, no fluorescence signal was observed in either cell zone after incubating with a control FITC-library-micelle spiked in whole blood sample.

Circulation velocity in living systems might be much faster than 300 nl/s in most locations [167]. Nonetheless, we still expect that aptamer-micelles would be capable of recognizing target cells to a degree at least equal to, if not better than, that which is shown in this dynamic incubation channel with a faster circulation rate. Based on our *in vitro* study of the effect of the incubation time on cell recognition ability using fixed cell numbers (Figure 2-13), increasing incubation time resulted in a decrease of selectivity; thus, a shorter incubation time might either have no effect at all, or might even lead to better binding selectivity, especially considering the rapid identification ability of aptamer-micelles. These results indicate that the aptamer-micelle can perform selective recognition in a complex environment that mimics [167] blood circulation.

Moreover, this aptamer-micelle was found to have low CMC and low cytotoxicity to the cells (Figure 2-16, Figure 2-17). As such, this type of aptamer-micelle is proposed to be an efficient drug delivery vehicle for target cells without the need for internalization of the aptamer's target molecule. Instead, aptamer-lipids can simply interact with the cell membrane

and quickly release the doped hydrophobic molecules into the cells. Meanwhile, however, through membrane replacement, aptamer-lipids can permeate cells by a process of endocytosis. Thus, this type of aptamer-micelle offers two kinds of drug delivery pathways: direct releasing of doped drug and internalization by direct drug-aptamer-lipid conjugation. Finally, by replacing PEG-lipid with therapeutic aptamer drug-lipid, the heterogeneous aptamer-micelle can specifically deliver aptamer drugs around the target cell surface. For instance, by lipid tail plus linker modification, we can construct a lipid molecule from Macugen, an FDA-approved aptamer selected against vascular endothelial growth factor (VEGF). By replacing PEG-lipid in Figure 2-18 with Macugen-lipid, we expect that this aptamer-micelle will be able to draw all the Macugen-lipids to a specific tumor cell surface, which would greatly increase the localized drug concentration to enhance inhibition potency.

CMC Determination of TDO5-Micelle by Pinacyanol Chloride

In the present study, pinacyanol chloride, a well-known useful dye for determining the critical micelle concentration of anionic surfactants, was used. As in previous reports [168-170], the color change of pinacyanol chloride from red to blue occurs in a concentration range not very far from the CMC of the anionic surfactant. The blue color above the CMC is characterized by two absorption bands, α- and β-bands at 607 and 562 nm, and the red color below the CMC, by the γ-band around 480 nm. The γ -band results from the aggregate formed by the dye, while the α- and β-bands are attributable to the solubilization of the dye into the micelle. Therefore, the estimated CMC of TDO5-micelle can be assigned to the concentration range where the blue color begins to fade into red. As shown in Figure 2-16, the estimated CMC of TDO5-micelle could be around 20 nM (based on TDO5-lipid unit concentration).

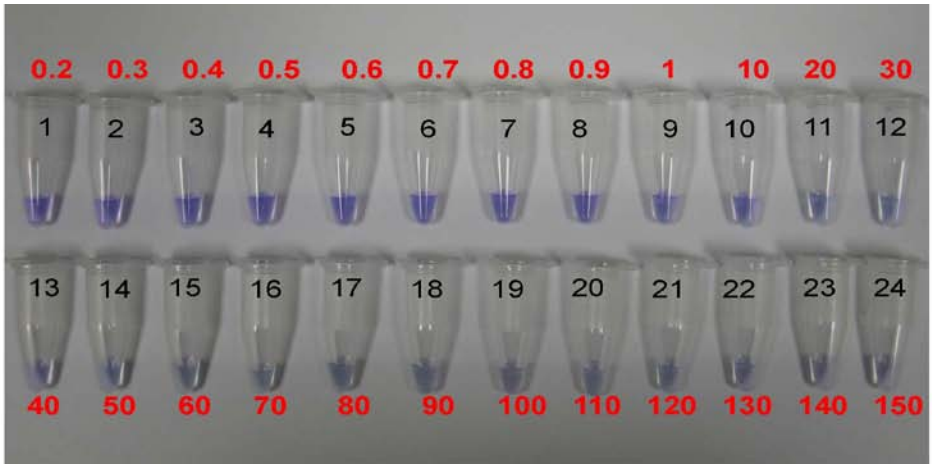

Figure 2-16.The determination of estimated CMC of TDO5-micelle by the color change of pinacyanol chloride. The red numbers on the top or the bottom of the centrifuge tubes are the concentration of TDO5-lipid mixed with 1×10^{-5} M pinacyanol chloride (based on TDO5-lipid unit concentration; concentration unit is nM). From left to right, top to bottom, from tube 1 to tube 24, the TDO5-lipid concentrations are 0.2, 0.3, 0.4, 0.5, 0.6, 0.7, 0.8, 0.9, 1, 10, 20, 30, 40, 50, 60, 70, 80, 90, 100, 110, 120, 130, 140, 150 nM, respectively.

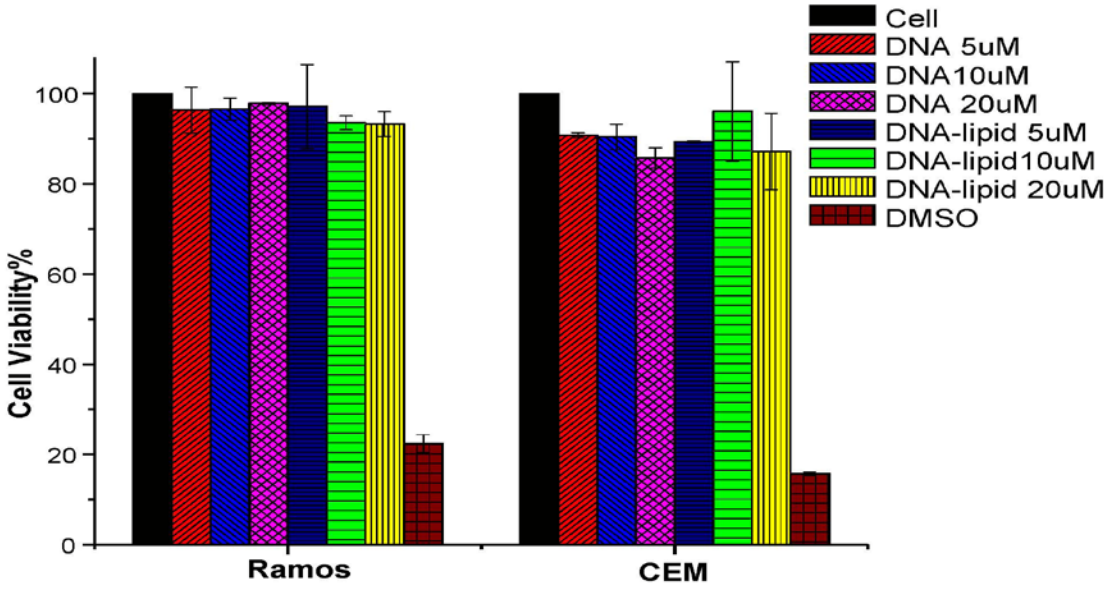

Figure 2-17.The cell viability affected by library-lipid with various concentrations, which was determined by CellTiter 96® AQueous One Solution Reagent on a plate reader. As one type of positive control for MTT assay, 10% DMSO was added to cells. The total incubation time is 2 days.

Effect of Aptamer Density on the Selective Binding of Aptamer-Micelles

The effect of aptamer density on selective binding was investigated by mixing FITC-TDO5-lipid with FITC-PEG-lipid in different molar ratios: 0:1, 1:1 and 10:1 (PEG-lipid versus TDO5-lipid). As shown in Figure 2-18, even at an aptamer density of 9% (10:1 molar ratio of PEG-lipid/TDO5-lipid), the aptamer-micelles still demonstrate selective binding ability at 37 0C after incubation with cells for 5 minutes. As aptamer density decreases, the binding shift is observed to become smaller. First, this indicates that a certain aptamer density is required to preserve target cell recognition at physiological temperatures for this type of aptamer-micelle. Second, a certain amount of multivalent binding might also be important.

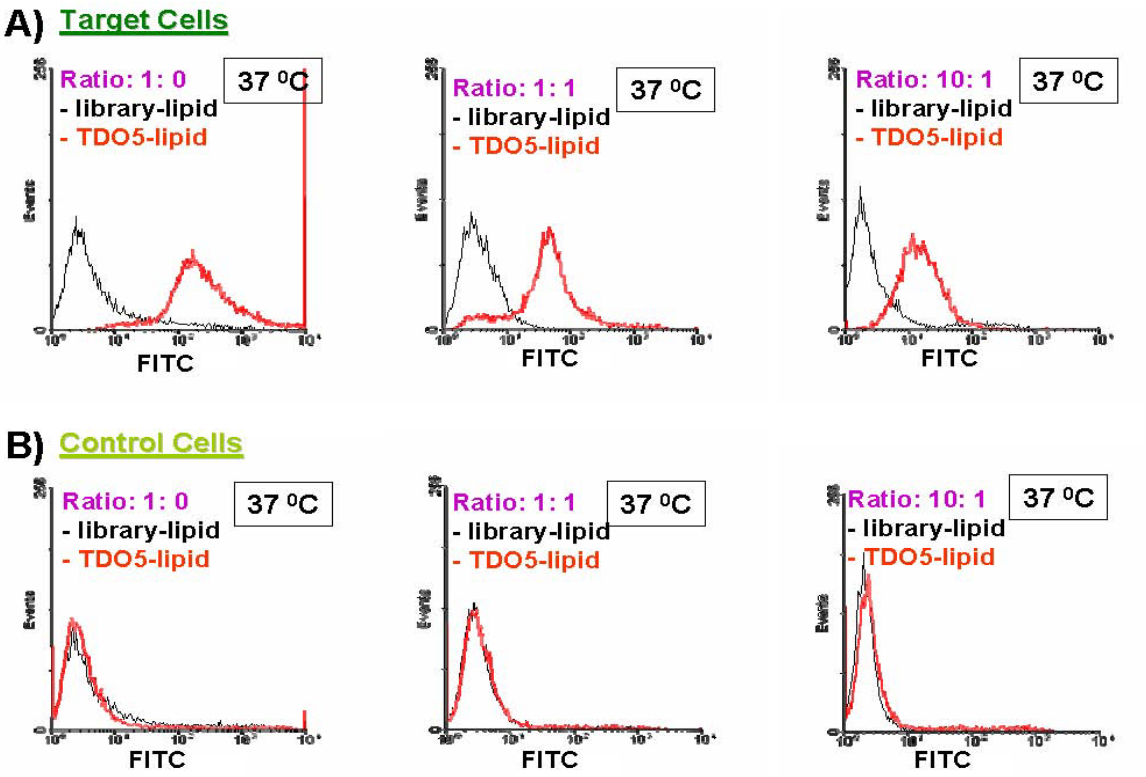

Figure 2-18.Flow cytometric assay to monitor the binding of TDO5-lipid or library-lipid with Ramos cells (target cells, A) and HL60 (control cells, B) at 37 ^{0}C for 5 minutes after mixing with different ratios of PEG-lipid. The molar ratios between FAM-DNA-lipids and FAM-PEG-lipid are 1:0, 1:1, and 10:1. The black and red curves represent the background binding of unselected DNA library-lipid and TDO5-lipid, respectively.

Hypothesized Mechanism about the Interaction Between Aptamer-Micelle and Cells

All aptamer-micelles (TDO5-micelle, KK-micelle, KB-micelle) show improved binding abilities. Similar improvement in binding ability should be expected by conjugation of single aptamer to other types of "solid" nanomaterials. However, when TDO5 was conjugated or complexed with 13nm Au NPs and SWNTs (single-walled carbon nanotubes), the complex did not show restored binding when temperature was raised to 37 ^{0}C (Figure 2-19).

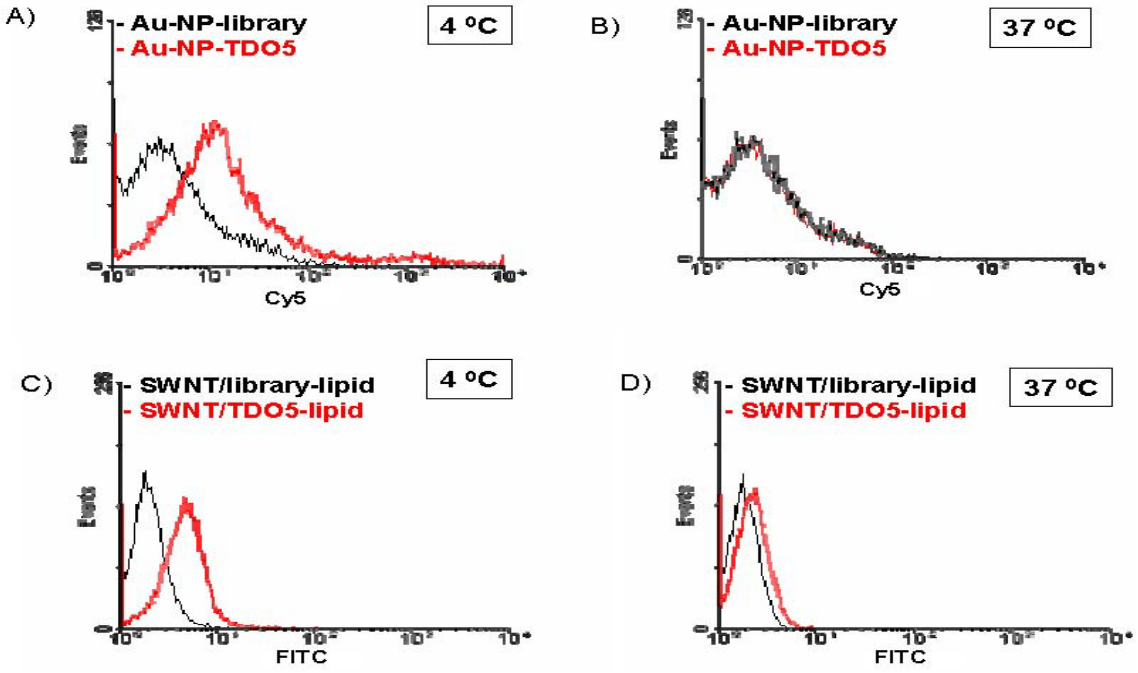

Figure 2-19.Flow cytometric assay to monitor the binding of two other types of nanomaterial-aptamer conjugates/complexes, including gold nanoparticles-TDO5 (A, B) and single-walled carbon nanotubes (SWNTs) complexed with FITC-TDO5-lipid (C, D), with target cells at 4 ^{0}C for 20 minutes and 37 ^{0}C for 10 minutes.

In fact, both kinds of nanomaterials ("soft" nanoparticles (micelle) and "solid" nanomaterials (Au NPs and SWNTs)) showed completely opposite binding behaviors to the target cells at 37 ^{0}C, although they presented similar binding abilities at 4 ^{0}C. These differences might be ascribed to two possible mechanisms, including the multivalent effect by the presence

of multiple aptamers on the nanomaterial surface, or the fluidic nature of the aptamer-micelles. To explain these interesting observations, the two mechanisms are under investigation.

Since both types of nanomaterials have greatly improved dissociation constants at 4^0C, multivalent effect should exist for both of them. This would not, however, explain why the two types of nanomaterials would have different binding patterns at physiological temperature. Thus, we believe that multivalent effect would not be the main reason for these interesting observations.

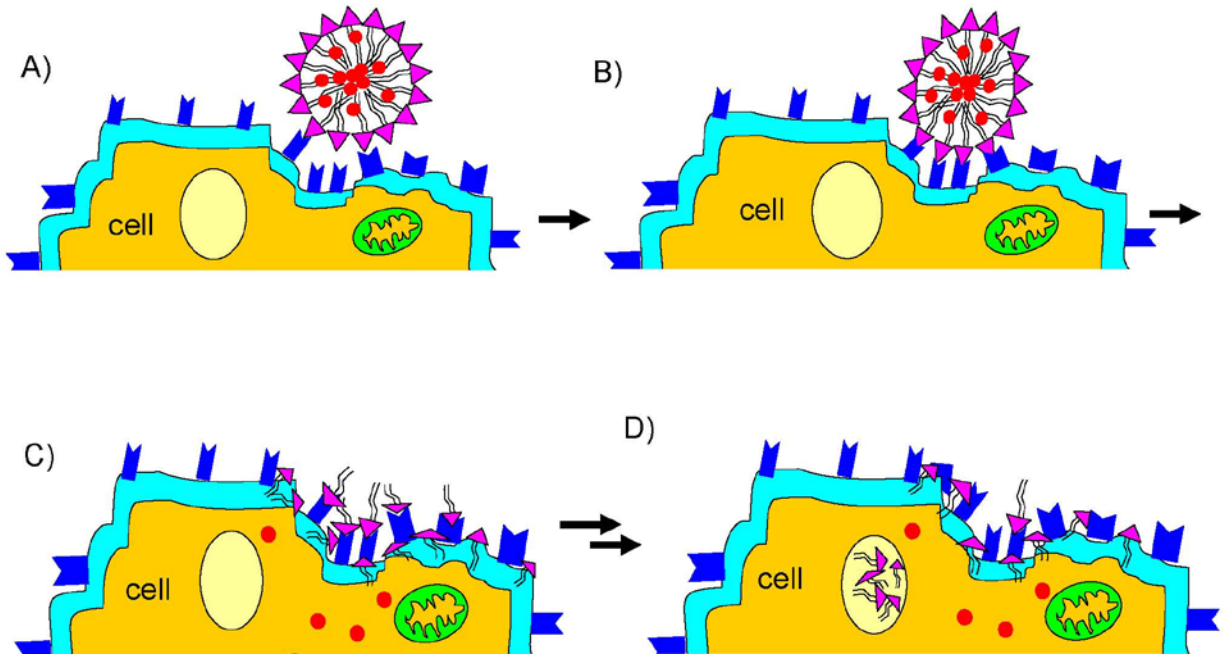

Figure 2-20.Scheme depicting the hypothesized interaction between dye-doped aptamer-micelle and cells. (A) At the first step, one or two aptamers on the aptamer-micelle surface have weak interactions with target proteins on the cell membrane. (B) At the second step, the fluidic nature of the aptamer-micelle leads to the rearrangement of aptamer-lipid units to make more and stronger interactions with multiple target proteins on the cell membrane; meanwhile, the aptamer-micelle is drawn closer to the cell membrane. (C) At the third step, the aptamer-micelle fuses with cell membrane and releases the doped dye. (D) After multiple processes, some of the aptamer-lipids localize in the endosome inside the cells, while the others remain on the cell membrane. However, since the structure of hydrophobic lipid tails pointing toward aqueous solution is not favored, most of the bound aptamer-lipids flip and insert into the cell membrane with or without weak interaction between aptamer heads and target proteins.

Instead, we believe that the fluidic nature of aptamer-micelles plays an important role in preserving the binding ability of the otherwise low-affinity aptamers. Similar to the lipid bilayers in the cell membrane [171], aptamer-lipids are in constant motion in the aptamer-micelle, although the micelle itself is relatively stable. We therefore hypothesize that a four-stage process occurs when aptamer-micelles are incubated with cells (see scheme in Figure 2-20). We assign these stages to each of four steps: A through D. In step A, when the temperature is raised to 37 ^{0}C, TDO5 undergoes a conformational change, which leads to the weak binding with target protein, wherein the K_{on} rate is slow, while the K_{off} rate is fast, resulting in an insignificant apparent binding shift of free TDO5. This occurs during step A, when only a couple of individual aptamer-lipids have weak interactions with a couple of receptor proteins. At step B, however, the lipid units rearrange their relative position to some extent, leading to more individual aptamer-lipids having a better fit into the binding pockets of more target proteins. Because the aptamer-micelle has localized multiple aptamers, the binding interactions between the TDO5 ligands and the target proteins have an additive effect, increasing the binding ability of the aptamer-micelle. This step is critical, and it is speculated to be the main reason for a difference in binding ability. TDO5/SWNTs are unable to retain their binding affinity at 37 ^{0}C, presumably because the aptamer moieties are fixed onto the surface of the SWNT. Therefore, although it might also have localized multiple weak interactions by the presence of the multiple aptamers, its binding status could not be favored under the dynamic binding equilibrium. By contrast, in step B, the whole micelle is drawn much closer to the cell membrane as a result of the weak, but additive, interactions. Additionally, for the same reason, the local concentration of aptamer-micelle is greatly increased, which further increases the possibility of interaction between micelle and cells. In step C, because the micelle is in close proximity to the cell membrane, it disintegrates and

fuses with the cell membrane. After multiple cellular processes, some aptamer-lipids that have fused with the cell membrane will further permeate the cell during a process of membrane recycling, while others remain on the cell membrane. This is step D. Some aptamer-lipids, which originally bind to the target proteins, might flip and insert into the cell membrane with or without any interaction with proteins since the structure with hydrophobic tail pointing into aqueous solution would not be thermodynamically favored. In this proposed mechanism, the kinetic trap which favors a long live of whole micelle structure near the cells to ensure aptamers function as a specific recognition ligand is critical and previous step for nonspecific disintegration of micelle into the cell membrane.

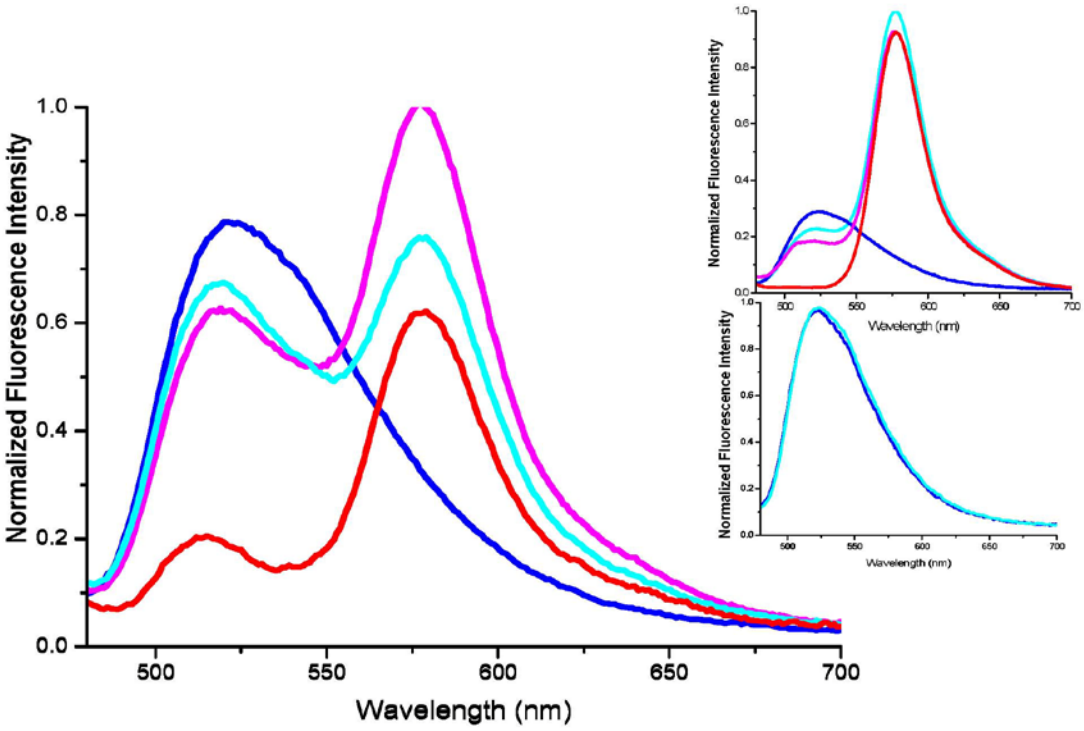

Figure 2-21.Fluorescence emission spectra of NBD-PC: POPC, TMR-DNA-lipid and mixture (NBD-PC: POPC in the presence of TMR-TDO5-lipid) in PBS buffer (pH7.4): NBD-PC: POPC (blue curve), TMR-TDO5-lipid (red curve), mixture (light green curve), mixture after adding Triton (purple curve). Instead of TMR-TDO5-lipid, TMR-DNA (inserted upper graph) and no dye labeled TDO5-lipid (inserted bottom graph) were mixed with NBD-PC: POPC with or without the presence of Triton, respectively.

To investigate the possibility of fusion in step C, we first utilized liposomes to mimic the cell membrane lipid bilayer. By mixing NBD-labeled liposomes (NBD-PC: POPC) and TMR-labeled DNA-lipid, we monitored lipid bilayer-DNA lipid interactions by Fluorescence Resonance Energy Transfer (FRET). As shown in Figure 2-21, the blue curve represents the NBD emission spectrum from NBD-liposome only, and the red curve represents the TMR emission spectrum from TMR-micelle only. After the two materials were gently mixed, an increase in TMR emission and a decrease in NBD emission were observed by exciting NBD-labeled liposome, indicating that FRET had occurred between the two probes. By further adding Triton X-100, which was reported to induce complete loss of FRET (100% membrane fusion) [172], further increase in TMR emission was observed, indicating that FRET was indeed caused by the fusion of DNA-micelle with liposome lipid bilayer. Control experiment by mixing NBD-liposome with TMR-DNA shows no occurrence of FRET, nor did FRET occur in the absence of mixing dye-labeled liposome with DNA-lipid. These findings indicate that TMR-micelle can fuse with cell membrane mimic liposome. These buffer experiments, combined with the observations mentioned in the main text (extremely low off rate and fast release of doped dye into the cells), indicate that the micelle can disintegrate and fuse with the cell membrane (described in step C). This process is a specific binding from multiple aptamers inducing nonspecific insertion.

As mentioned in the main text, the results shown in Figure 2-9 demonstrate the possibility of internalization in step D.

Conclusions

In summary, we have developed an aptamer-micelle assembly for efficient detection/delivery targeting specific cancer cells. This aptamer-micelle enhances the binding ability of the aptamer moiety at physiological temperature, even though the corresponding free

aptamer loses its binding ability under the same condition. The merits of aptamer-micelles include greatly improved binding affinity, low K_{off} once on the cell membrane, rapid targeting ability, high sensitivity, low CMC values, and the creation of a dual drug delivery pathway. Most importantly, the aptamer-micelles show great dynamic specificity in flow channel systems that mimic drug delivery in the blood system. All of these advantages endow this unique assembly with the capacity to function as an efficient detection/delivery vehicle in the biological living system.

Table 2-1. List of all oligonucleotides used in this work

Name		Sequence
aptamer-lipids and library-lipid	FAM-TDO5-lipid	5`-lipid tail-$(CH_2CH_2O)_{24}$-AAC ACC GGG AGG ATA GTT CGG TGG CTG TTC AGG GTC TCC TCC CGG TGA-FAM-3`
	Biotin-TDO5-lipid	5`-lipid tail-$(CH_2CH_2O)_{24}$-AAC ACC GGG AGG ATA GTT CGG TGG CTG TTC AGG GTC TCC TCC CGG TGA-biotin-3`
	TMR-TDO5-lipid	5`-lipid tail-$(CH_2CH_2O)_{24}$-AAC ACC GGG AGG ATA GTT CGG TGG CTG TTC AGG GTC TCC TCC CGG TGA-TMR-3`
	KK-lipid	5`-lipid tail-$(CH_2CH_2O)_{24}$-ATC CAG AGT GAC GCA GCA GAT CAG TCT ATC TTC TCC TGA TGG GTT CCT AGT TAT AGG TGA AGC TGG ACA CGG TGG CTT AGT-FAM-3`
	KB-lipid	5'- lipid tail-$(CH_2CH_2O)_{24}$-ACA GCA GAT CAG TCT ATC TTC TCC TGA TGG GTT CCT ATT TAT AGG TGA AGC TGT-FAM-3'
	Library-lipid	5'- lipid tail-$(CH_2CH_2O)_{24}$-(N)n *-FAM -3'
Aptamers and library	FAM-TDO5	5`-AAC ACC GGG AGG ATA GTT CGG TGG CTG TTC AGG GTC TCC TCC CGG TGA-FAM-3`
	FAM-KK	5`-ATC CAG AGT GAC GCA GCA GAT CAG TCT ATC TTC TCC TGA TGG GTT CCT AGT TAT AGG TGA AGC TGG ACA CGG TGG CTT AGT-FAM-3`
	FAM-KB	5`-ACA GCA GAT CAG TCT ATC TTC TCC TGA TGG GTT CCT ATT TAT AGG TGA AGC TGT-FAM-3'
	FAM-library	5`- NNN NNN NNN NNN NNN NNN NNN NNN NNN NNN NNN NNN NNN NNN NNN NNN-FAM -3'
	TDO5 for Au NP	5`-Cy5-AAC ACC GGG AGG ATA GTT CGG TGG CTG TTC AGG GTC TCC TCC CGG TGA TTT TTT TTT TTT TTT-biotin -3`
	Library for Au NP	5`-Cy5-NNN NNN NNN NNN NNN NNN NNN NNN NNN NNN NNN NNN NNN NNN NNN TTT TTT TTT TTT TTT-biotin -3`
	Biotin-TDO5 for flow channel	5`-AAC ACC GGG AGG ATA GTT CGG TGG CTG TTC AGG GTC TCC TCC CGG TGA TTT TTT TTT T-biotin-3`
	Biotin-sgc8 for flow channel	5`-ATC TAA CTG CTG CGC CGC CGG GAA AAT ACT GTA CGG TTA GAT TTT TTT TTT-biotin-3`

*N is random base, and n is equal to the base number of corresponding aptamers.

CHAPTER 3
NUCLEIC ACID BEACONS FOR LONG-TERM REAL-TIME INTRACELLULAR MONITORING

Introduction

Advanced cancer research, especially disease process study, as well as drug discovery protocols, presuppose the need for superstable molecular probes for use in long-term real-time gene monitoring inside living cells, as well as in vivo monitoring inside animals. Such probes should be able to resist nuclease digestion and avoid cellular protein binding. One probe, the molecular beacon (MB) [96,173-177], promises to meet these requirements. The MB is a short hairpin oligonucleotide probe which produces a fluorescence signal upon hybridizing to specific nucleic acids. Although MBs have been used for real-time intracellular detection, DNA-MBs are known to yield false positive signals. This results from multiple intracellular interactions that degrade DNA-MBs, or change their conformation, through processes such as endogenous nuclease degradation and/or stem-loop structure disruption by nucleic acid binding proteins [85]. Consequently, a biostability problem arises which has been addressed by incorporating nuclease-resistant building blocks, such as phosphorothioate [86], 2‘-O-methyl RNA bases [88], peptide nucleic acids [89], and locked nucleic acids (LNA) [93], into MB designs. Among these candidates, MBs with LNA bases have demonstrated adequate biostability in vitro [93,178]. Nevertheless, the overall effectiveness of fully modified LNA MB is compromised by extremely slow hybridization rates. A practical LNA based MB for long-term real-time mRNA monitoring inside the living cells is yet to realize. In this chaper, we report the design of effective MBs and evaluate their pratical applications inside the living cells.

Experimental Section

Chemicals and Reagents

The MBs prepared are listed in Table 3-1. DNA and LNA synthesis reagents were purchased from Glen Research (Sterling, VA). Deoxynuclease I, ribonuclease H, and single-stranded binding protein were purchased from Fisher.

Table 3-1. Optimized LNA-MBs for Intracellular Experiments

optimized LNA-MBs	Sequence
β-actin MB	5'-Cy3-C*AG*T*CG*A*GGAAGGAAGGCTGGAAGAG*C*G*A*C*T*G*-BHQ2-3'
MnSOD MB	5'-Cy3-C*CTAGC*C*AGTTACATTCTCCCAGTTGATT*G*C*T*A*GG*-BHQ2-3'
control MB	5'-AF488-*CTAGC*T*C*T*AAA*T*CAC*T*AT*GG*T*CGC*G*C*T*AG*-BHQ1-3'

Note: Italic letters represent LNA bases, and underlined letters are bases for the MB stem.

Equipments

An ABI3400 DNA/RNA synthesizer (Applied Biosystems, Foster City, CA) was used for all MB probes and DNA target preparation. A ProStar HPLC (Varian, Walnut Creek, CA) with a C18 column (Econosil, 5μ, 250 mm× 4.6 mm) from Alltech (Deerfield, IL) was used for probe purification. A Cary Bio-300 UV spectrometer (Varian, Walnut Creek, CA) was used to measure absorbance for probe quantitation. Fluorescence measurements were performed on a Fluorolog-Tau-3 spectrofluorometer (Jobin Yvon, Inc., Edison, NJ). The protein concentrations in the cell lysate were determined with Bio-Rad protein assay dye reagent concentrate (Bio-Rad Laboratories Inc.) by comparing with a bovine serum albumin (BSA) calibration curve. Cell images were taken with a confocal microscope setup consisting of an Olympus IX-81 inverted microscope with an Olympus FluoView 500 confocal scanning system and tunable argon ion laser (458 nm, 488 nm, 514 nm) and a green HeNe laser (543 nm) with two separate photomultiplier tubes (PMT) for detection. A 40× 0.6 NA air objective was used. A Leiden microincubator with a TC-202A temperature controller (Harvard Apparatus, Holliston, MA) was used to keep the cells at 37 ℃ during injection and monitoring. An EXFO Burleigh PCS-6000-

150 micromanipulator was used for positioning the injector tip. An Eppendorf Femtojet microinjector with 0.5 μm Femtotips was used to inject the MBs into the cells. Image acquisition and analysis were conducted with the FluoView software.

Molecular Beacon Synthesis

All oligonucleotides were synthesized based on solid-state phosphoramidite chemistry at a 1 μmol scale. All LNA MBs labeled by FAM were synthesized with controlled-pore glass columns with a 3'-Dabcyl molecule covalently linked to the CPG substrate. FAM phosphoramidite was used to couple to the 5' end of the sequence. The complete MB sequences were then deprotected in concentrated ammonia hydroxide at 65oC overnight and further purified with reverse phase high-pressure liquid chromatography (HPLC) on a C-18 column and ion-exchange HPLC (Dionex DNAPacTM PA-100 column (40 × 250 mm, or semipreparative), 30%-70%, 45 min gradient 1 M NaCl/20 mM NaOH, pH 12). For the MBs labeled with Cyanine 3(Cy3), FAM phosphoramidite was replaced by Cy3 phosphoramidite, and 3'-Dabcyl CPG was replaced by 3'- Blackhole Quencher 2 (BHQ2) CPG. For the MBs labeled with AF488, off-column synthesis was required. The synthesis began with 3'-Blackhole Quencher 1 (BHQ1) CPG and ended with 5'-amino-modifier C6 phosphoramidite. After that, the sequence was purified and deprotected by 2% acetic acid to activate the amino group. Then, off-column synthesis was conducted in sodium carbonate buffer (pH=9) with Alexa Fluor 488 carboxylic acid succinimidyl ester (Invitrogen) with 10-fold higher concentrations.

Hybridization Kinetics Study

Hybridization experiments were obtained using 100 nM of MBs and 500 nM targets in a total volume of 150 μL. The buffer used was 20 mM Tris-HCl (pH 7.5) containing 5 mM MgCl2 and 50 mM NaCl. The fluorescence intensities were measured as a function of time.

DNase I Sensitivity

To test the nuclease sensitivity of MBs, the fluorescence of a 150 ul solution containing 20 mM Tris-HCl (pH 7.5), 5 mM MgCl2, 50 mM NaCl and 100 nM MBs was monitored as a function of time at room temperature. Two units of ribonuclease-free DNase I were added and any subsequent fluorescence change was recorded.

RNase H Sensitivity

To test the susceptibility of molecular beacon-target mRNA hybrids to the digestion of ribonuclease H, 100 nM of MBs were incubated with the same concentration of RNA target as indicated in the above buffer. After the hybridization reached equilibrium, 12 units of ribonuclease H were added, and the subsequent change in fluorescence was monitored as a function of time.

Protein Binding Study

Gel electrophoresis was performed to study the interactions between Single-Stranded DNA Binding Protein (SSB) and MBs. In the buffer containing 20 mM Tris-HCl (pH 7.5), 5 mM MgCl2 and 50 mM NaCl, 5 μM MB was first incubated with the same concentration of SSB. After one hour, the solution was analyzed in a 3% agarose gel at 100V in TBE buffer for 50 minutes. The gel was then stained by Coomassie blue G 250 stain solution (Bio-Rad) for one hour and washed with de-ionized water for 30 minutes. The image of the resulting gel was achieved by scanning on a regular scanner.

Cell Lysate Preparation

A 75 cm^2 flask of ~95% confluent MDA-MB-231 was washed with serum-free medium (Leibovitz's L-15 medium with l-glutamine, ATCC) for 1 h in the incubator. After removal of the serum-free medium (SFM), the cell cultures were suspended in 3 mL of ice-cold detergent-free buffer (50 mM Tris-HCl, pH 7.4, 1 mM EDTA, 2 mM EGTA, 0.33 M sucrose, 1 mM

dithiothreitol) containing a broad-range protease inhibitor cocktail (Roche Molecular Biochemicals, Indianapolis, IN). The cells were then scraped off the flask using a plastic cell scraper and passed five times through a 27 $^1/_2$ gauge needle. The samples were fractionated by centrifuge at 1000*g* for 10 min at 4 ℃ to isolate the nuclei, and the supernatant was the cytosolic fraction. After one more washing with the detergent-free buffer, the nuclei pellet was resuspended in a lysis buffer (20 mM HEPES, 1 mM EDTA, 2 mM EGTA, 150 mM NaCl, 0.1% sodium dodecyl sulfate (SDS), 1% Igepal, and 0.5% deoxycholic acid, pH 7.5) containing a broad-range protease inhibitor cocktail (Roche Molecular Biochemicals) and mixed for 90 min at 4 °C to ensure full membrane lysis. After centrifugation at 1000*g*, the supernatant was the nuclear fraction. Each fraction's protein concentration was determined, using the Bradford protein assay, and was stored at −80 ℃ until use.

Biostability Study with Cell Lysate

With the fluorometer, the fluorescence intensity change of MBs was monitored upon the addition of 2 μL of 4 μg/mL cell lysate fractions (nuclear or cytosolic fraction) into the 100 nM MB solutions. The buffer used was 20 mM Tris-HCl (pH 7.5) containing 5 mM $MgCl_2$ and 50 mM NaCl.

Imaging and Data Collection

All the cellular fluorescent images were collected by the confocal microscope using laser excitation. The control MB with AF488 was excited at 488 nm and collected at 520 nm. The MnSOD MB and β-actin MB with Cy3 was excited at 543 nm and collected at 570 nm. The probe solution used in the experiments contains a 4 μM concentration of each MB in 20 mM Tris, 50 mM NaCl, and 5 mM $MgCl_2$ buffer. Images were taken every minute or every other minute. The microscope shutter was opened only long enough to allow the laser to illuminate the injected cells while a fluorescence image was collected at each of the required time points to

avoid unnecessary dye photobleaching and any damage to the cells. A region surrounding each of the injected cells was used to determine the average fluorescence intensity for each channel at each time point. These average intensities for each cell at each time point were recorded and plotted against the time frame. For long-time imaging, some cells might change their shapes or move slightly. The signal region for analysis was accordingly adjusted to achieve more accurate data. The data collection was stopped when the injected cell changed its shape, a circumstance which raised some concerns about cell viability. The relative fluorescence intensities were calculated by directly comparing the current intensity with its intensity at the beginning state for each case. For data given in Figure 2c, the relative fluorescence intensity ratios were calculated by the average ratios from the final five points divided by the monitoring starting point (for the cases without LPS treatment) or by the data points right before LPS treatment (for the cases with LPS treatment). The error bars represent the standard deviation from the calculated five data points for each case.

Results and Discussion

MB Design and *in vitro* Characterization

We demonstrated that MBs made entirely of LNA improves biostability and sequence selectivity greatly *in vitro* [93]. However, we discovered that the overall effectiveness of fully modified LNA-MBs can be compromised by extremely slow hybridization rates. To overcome the limitations of MBs in intracellular measurements, we made design modifications by mixing LNA and DNA bases in both the stem and loop of a MB, resulting in MBs that can effectively measure intracellular events with extremely high biostability (Table 3-1). As shown in *in vitro* testing (Figure 3-1), these MBs combine long-term stability with excellent sensitivity, selectivity, and fast hybridization kinetics.

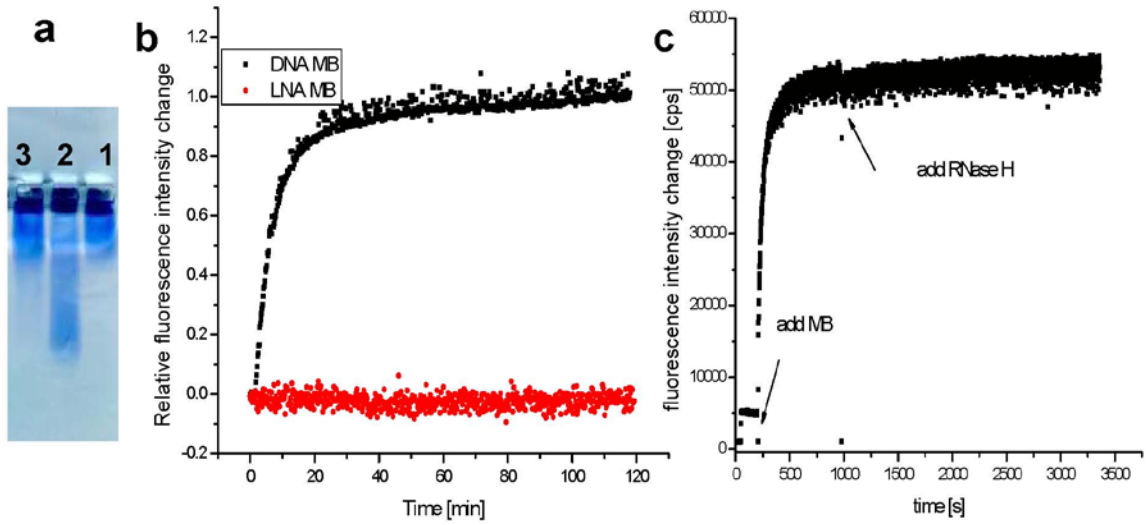

Figure 3-1. Representative *in vitro* biostability experiments of the optimized LNA-MBs. (a) Gel electrophoresis of SSB solutions containing no MBs (lane 1); the optimized LNA-MBs (lane 2). Under the experimental conditions, SSB migrates significantly slower than the negatively charged MB and will only migrate when it is in complex with the MB. Thus, the representative gel electrophoresis result for an optimized LNA-MB showed little SSB binding. (b) Fluorescence signal change of LNA and DNA-MB upon the addition of ribonuclease-free DNase I. In the DNase I assay, the fluorescence intensity increases as the DNA-MB is digested by DNase I, which nonspecifically cleaves phosphodiester bonds. On the other hand, LNA-MBs had no response to the addition of excess DNase I. (c) Fluorescence signal change of LNA-MB upon the addition of RNase H. The RNase H assay mimics false negative results that can occur when target mRNA is degraded once it is hybridized with the DNA-MB. RNase H specifically cleaves RNA strands that are hybridized with DNA, thereby decreasing the target concentration and allowing the MB to reform the hairpin structure. No noticeable signal decrease was observed when RNase H was added to the duplex of RNA: LNA-MB.

Our design strategy consisted of two steps. First, in order to maintain the fast hybridization rate, the MB stem was consistently composed of 50% LNA in an alternating fashion. Such optimized LNA-MBs would then have a fast response to excess complementary target DNA (Figure 3-2). When compared to DNA-MBs, it is precisely this hybridization behavior which makes it possible to use these LNA-MBs to track gene expression levels in real time. Second, we gradually increased the LNA percentage in the loop starting from 50% until the LNA-MB satisfied the biostability screening criteria (Figure 3-1).

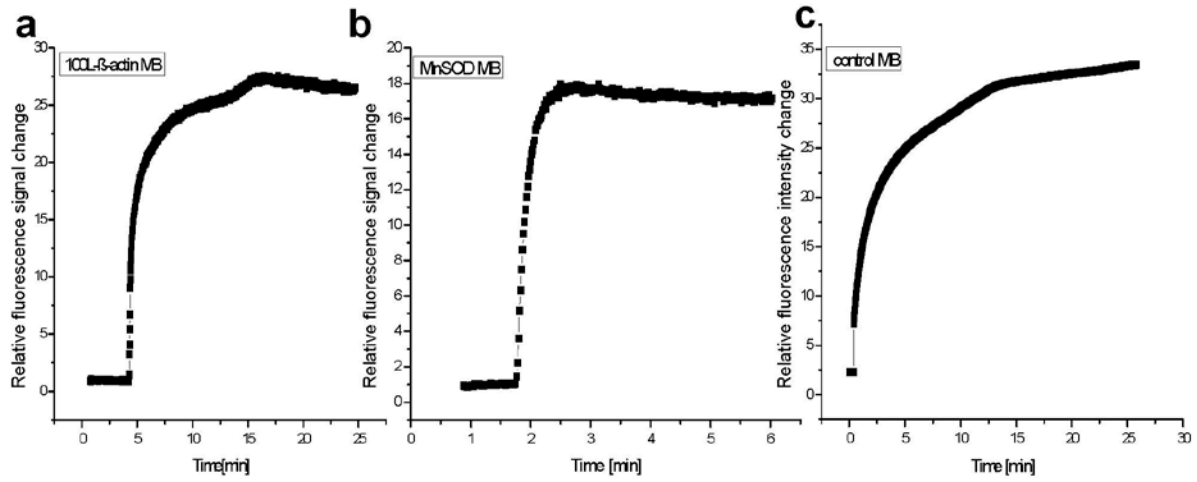

Figure 3-2. *In vitro* hybridization kinetics of the optimized LNA-MBs. Ten-fold excess cDNAs (CTCTTCCAGCCTTCCTTCCT; AATCAACTGGGAGAATGT AACTG; GCGACCATAGTGATTTAGA) were added to all three optimized LNA-MBs. The hybridization experiments were performed at room temperature in 20 mM Tris-HCl (pH 7.5) buffer containing 5 mM $MgCl_2$ and 50 mM NaCl.

The biostability screening criteria are to test LNA-MBs with various amounts of LNA by three types of experiments: single-stranded DNA binding protein (SSB) interaction, DNase I, and ribonuclease H (RNase H) digestion. The *in vitro* biostable LNA-MBs which passed all three *in vitro* biostability tests were termed optimized LNA-MBs, as listed in Table 3-1, and they were then used for further study inside living cells.

MB *in vitro* Testing with Cellular Samples

Before we attempted to use the LNA-MBs for intracellular measurements, we tested them with cytosolic and nuclear fractions of MDA-MB-231 cells. DNA-MB was used for a comparison, and the results are shown in Figure 4-3. When the cell lysate was added to the DNA-MB solution, we saw a significant fluorescence increase over time. In contrast, there was no such fluorescence increase for any of the optimized LNA-MBs, clearly demonstrating that the LNA-MB can sustain biostability for a long period of time, even with cell lysate samples. This finding enabled us to test the feasibility of the LNA-MB as a long-term molecular probe for

mRNA monitoring inside living cells. To accomplish this, the LNA-MB was microinjected into living cells, and their hybridization with nucleic acid targets was monitored through fluorescence by confocal microscopy. The LNA sequences showed little nucleus accumulation problem inside MDA-MB-231 cancer cells; therefore, the average fluorescence intensities around the injected cells were determined for data analysis.

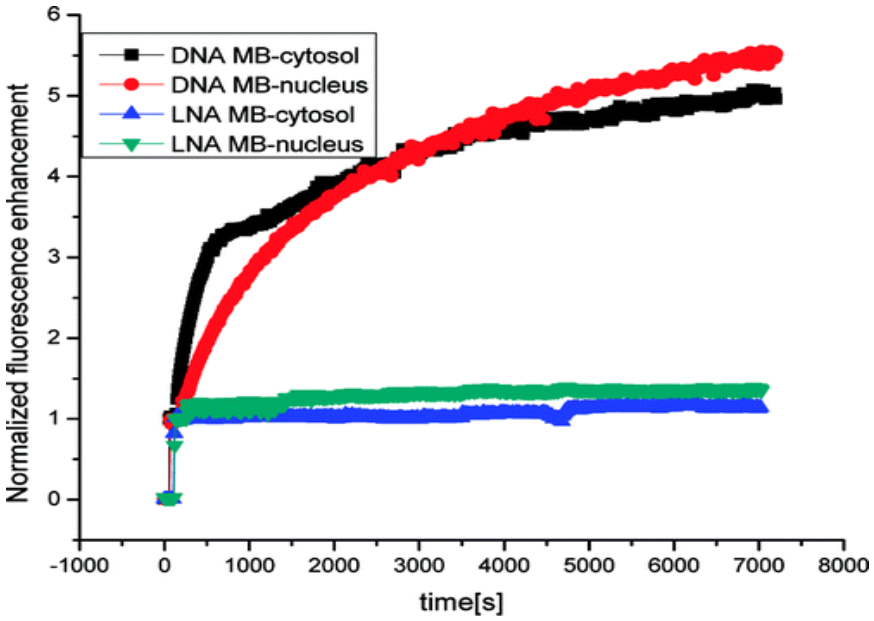

Figure 3-3. Normalized representative fluorescence intensity changes of DNA-MB and LNA-MB with cytosolic and nuclear fractions from MDA-MB-231 cell lysate. The DNA-MBs had a significant fluorescence increase over time, while the LNA-MBs had no significant fluorescence changes.

Long-Term Monitoring Inside Living Cells

The LNA-MB was observed to monitor mRNA expression inside a living cell for more than 5 h. To further evaluate the biostability and mRNA detection ability of LNA-MBs in living cells, we used LNA bases to synthesize both control MB and MnSOD MB, which were co-injected into MDA-MB-231 cancer cells. The control LNA-MB and MnSOD LNA-MB were made with donor fluorophores (Alexa Fluor (AF488) and Cyanine (Cy3), respectively). Because their excitation and emission wavelengths do not overlap, both beacons could be imaged simultaneously in our confocal system [179]. In this experiment, lipopolysaccharide (LPS) was

used to stimulate MnSOD mRNA expression inside living cells [180]. The control LNA- MB had no complement inside the cells. Therefore, we determined that the signal from the control LNA-MB would be stable, as long as the MB was not degraded by nucleases or nonspecifically opened by protein binding. As shown in Figure 3-4a,b, the fluorescence signal of the control MB did not change noticeably, even after 5.5 h (1.5 h before LPS treatment plus another 4 h after treatment). At the same time, the MnSOD LNA-MB was effective in monitoring MnSOD mRNA expression over a 5.5 h period. Also, as shown in Figure 3-4a, there is a slow fluorescence increase in the MnSOD LNA-MB before LPS induction, whereas the fluorescence stays flat for the control MB. As the basal level of MnSOD is very low inside the cell, the number of newly formed hybrids caused by hybridization is slowly increased over time. We tested multiple cells, which showed the same trend as that discussed above, and the relative fluorescence signal changes from the injected cells are plotted in Figure 3-4c. Overall, these results showed that the basal MnSOD expression level in MDA-MB-231 cells was low, but that MnSOD mRNA could be highly expressed with LPS treatment. In addition, the hybridization kinetics of LNA-MBs inside the cells (with either synthetic complement DNA or native mRNA, Figure 3-2, 3-5) was within minutes. The prolonged signal increase, as seen in Figure 3-4a, suggests a continuously induced mRNA expression. Because the signal for the control MB inside the living cells during the same time period was not changed, the long-term stability of the LNA-MBs was further confirmed. The small fluctuation of signal enhancement ratios among these cells only reflects a cell-to-cell gene expression variation. These cell-to-cell differences might have been a consequence of some membrane ruffling and cell morphology changes during the monitoring period, as indicated in the time-lapse images shown in Figure 3-4b.

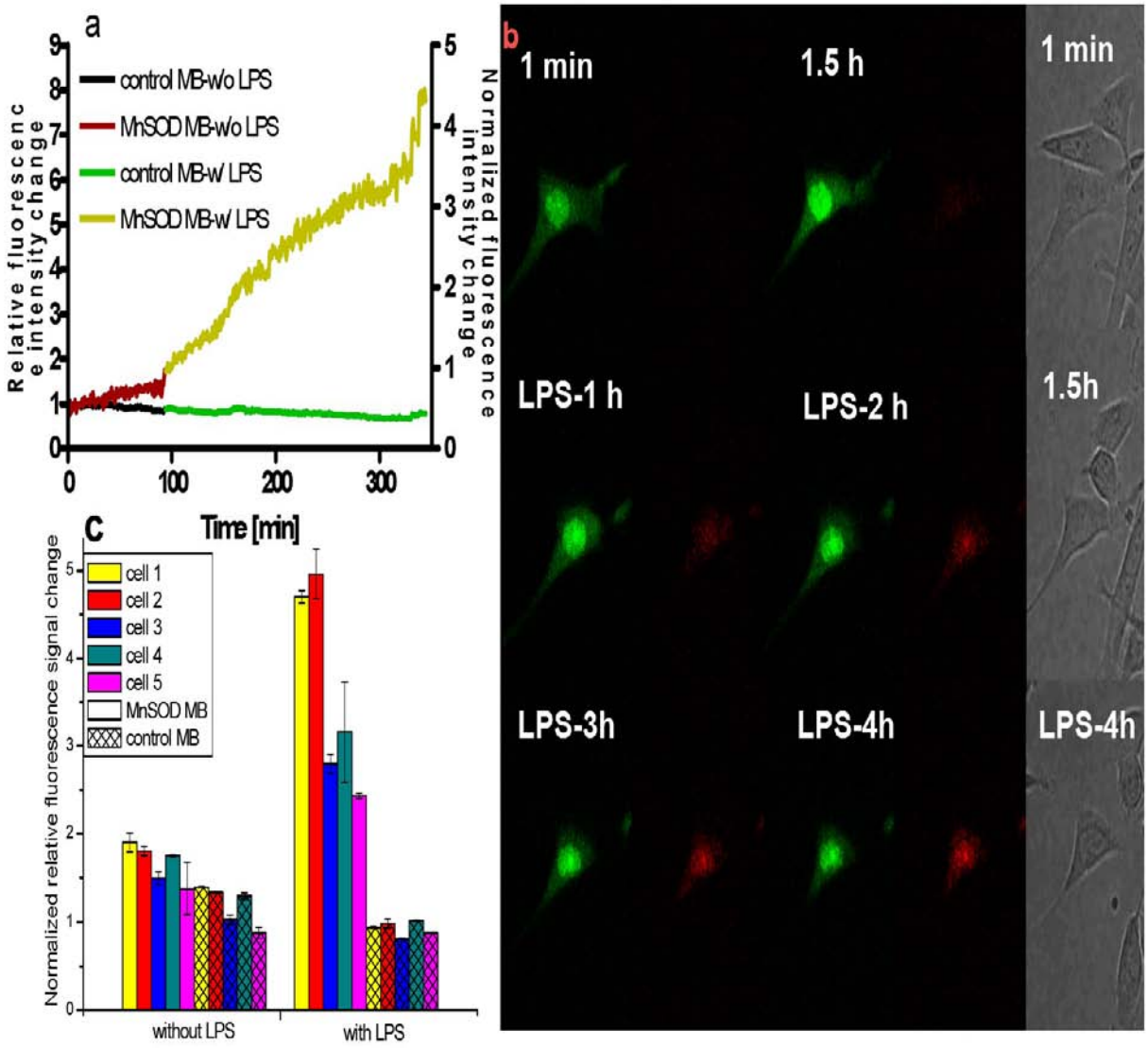

Figure 3-4. Representative microinjection experiments. (a) Relative fluorescence signal changes of control MB and MnSOD MB during 1.5 h without LPS treatment and during 4 h with LPS treatment. The *y*-axis represents the signal changes relative to the initial fluorescence signal directly after microinjection (Supporting Information). **(**b**)** Time-lapse of control MB (green) and MnSOD MB (red) inside a MDA-MB-231 cell. The control MB fluorescence did not change over time, but that for MnSOD changed significantly as the gene expression was stimulated by LPS. **(**c**)** Histograms of relative fluorescence signal change of MnSOD MBs (no pattern) and control MB (cross-hatched pattern) without LPS and with LPS treatments within different cells.

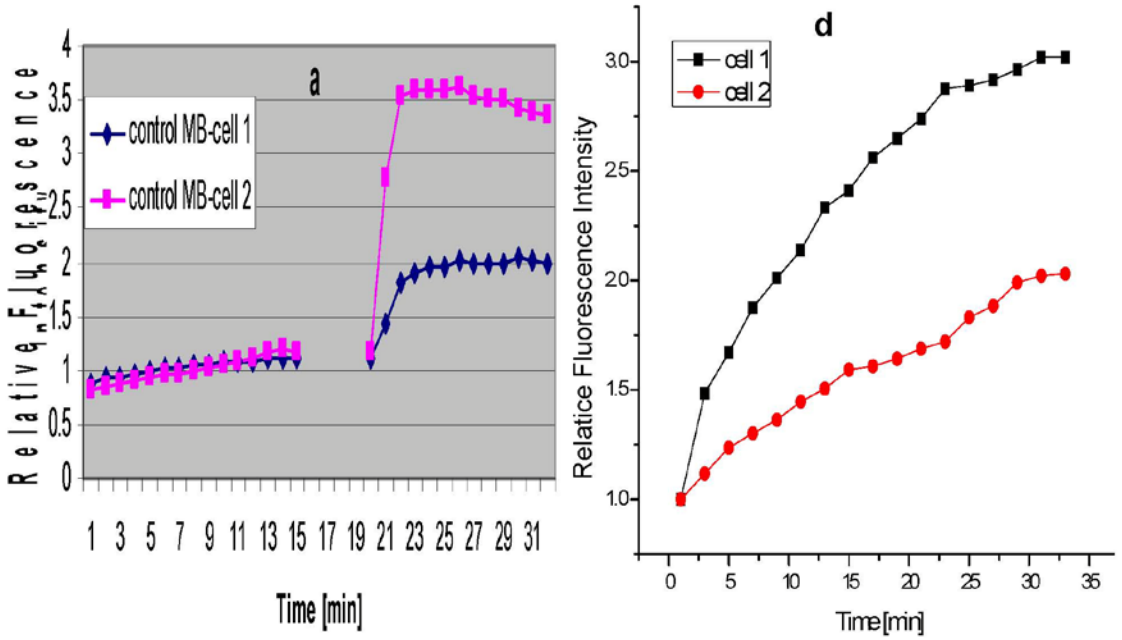

Figure 3-5. *In vivo* hybridization kinetics of the optimized control LNA-MB and ß-actin MB. (a) The first segment represents two typical time course measurements of the fluorescence intensity of two cells after optimized LNA control MB is injected into the cells. The second segment illustrates the hybridization kinetics of control MB with excess cDNA (GCGACCATAGTGATTTAGA) introduced into the same cells. (b) Time course fluorescence intensity measurements of the optimized LNA ß-actin MB with native mRNA in two living cells.

Long-Term Stability of MBs

The LNA-MBs are also shown to be effective for nucleic acid monitoring, even after 24 h inside living cells. To demonstrate this, the control LNA-MB was injected into a cell and incubated for 24 h before the cell was used for nucleic acid hybridization studies. A target complementary DNA solution was injected into the cell 24 h after the original control LNA-MB injection. Time-lapse fluorescence images (Figure 3-6) show that the control LNA-MB remains functional, even after incubating inside the cells for 1 full day. We also tested the enhancement of the LNA-MB by adding cDNA for the LNA-MB, both immediately after MB injection and 24 h later. The signal enhancements in both cases are about the same, 2.26 for immediate second-injection (standard deviation is 32.9%) and 2.02 for delayed second-injection (standard deviation

is 4.24%). The fact that the LNA-MB showed the same response to complementary DNA after 24 h of incubation inside a living cell proves that the LNA-MBs can be used for long-term monitoring of gene expression inside living systems.

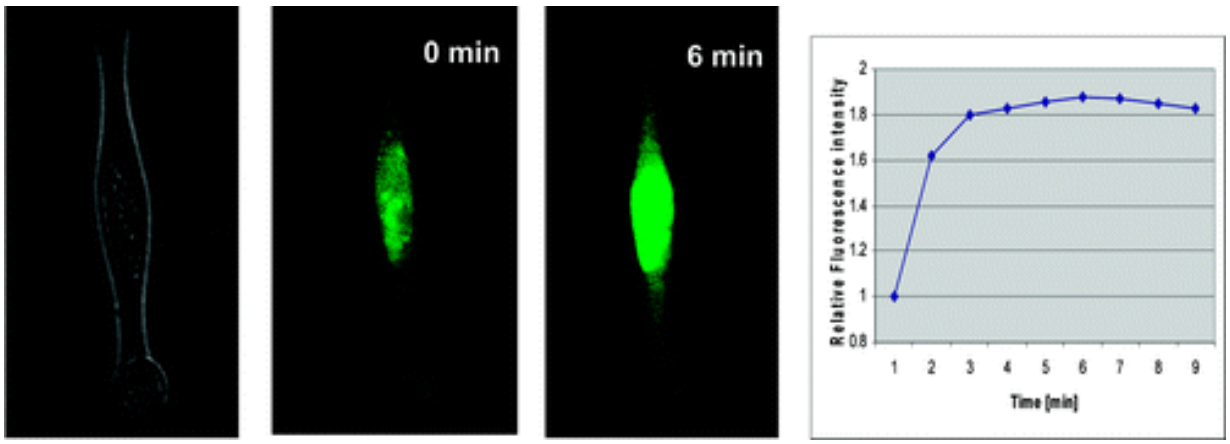

Figure 3-6. Time-lapse fluorescence images after microinjection of excess cDNA into the same cell which has been injected by the optimized control MB after 24 h.

Conclusions

We have created LNA-MBs that have superior resistance to enzymatic cleavage and protein binding and that retain their functions inside cells, even after 24 h of incubation. To put this into perspective, DNA-MBs degrade after about 15-45 minutes in the cellular environment [81]. In contrast, the newly designed LNA-MBs provide outstanding biostability which extends their application to long-term real-time intracellular gene monitoring and possible *in vivo* monitoring inside living animals. In particular, we will be able to study gene expression levels within a single cell, making it possible to carry out experiments in which specific cells within a tissue or tumor can be monitored over long time periods. Examples include (1) following gene expression in a single cell as it differentiates, (2) observing specific cells during development, (3) measuring cellular responses to drugs, and (4) studying specific cellular reorganization processes in cancer, i.e., tumor cell migration and angiogenesis. The superstability of the newly designed

LNA-MBs makes them an effective tool for many *in vivo* studies and monitoring where stability of the molecular probe is needed for a protracted period of time.

CHAPTER 4
CARBON NANOTUBES PROTECT DNA STRANDS DURING CELLULAR DELIVERY

Introduction

As noted in Chapter One, for efficient intracellular mRNA monitoring, an ideal molecular probe should not only have an adequate biostability, but also should overcome two other major problems: extremely low self-delivery efficiency of nucleic acids into the cell and serious nucleus accumulation. Insterestingly, by the DNA probe/SWNT (single-walled carbon nanotube) complexes, all three problems have been simultaneously addressed. Although SWNTs have been intensively studied for 18 years, this is the first report about SWNTs' protection ability for their DNA cargos from nonspecific intracellular interactions. Thus, this chapter focuses on the protection ability SWNTs have endowed to their DNA cargos, while introducing other benefits SWNTs bring to DNA probes for their applications in intracellular mRNA monitoring.

Bioanalytical and biomedical applications to cancer cells, particularly those which involve probe delivery for intracellular gene monitoring and targeted drug delivery, depend upon uninhibited transport of DNA, RNA, or drug molecules into living cells. However, some cargos, such as DNA, are easily degraded by cellular enzymes or digested by cellular nucleases. This problem is compounded by the fact that most delivery systems take several hours to transport cargos into cells; therefore, a delivery system which can provide protection for DNA cargos during prolonged transport would be useful. To this end, inorganic nanomaterials, including nanoparticles, nanotubes, and nanowires, have exhibited promising physical properties which make them useful as molecular transporters [142,181-189]. To date, however, only a few nanomaterials, such as silica nanoparticles [181], silica nanotubes [187], and gold nanoparticles [94], offer viable protection properties. Aside from these, the most promising of all may be single-walled carbon nanotubes (SWNTs) which have been shown to shuttle various types of

cargos into a wide range of cell types. These include the biologically and medically more relevant T cells and primary cells, which are difficult to transfect by traditional delivery methods [190,191]. Therefore, this research investigates whether SWNTs can, additionally, provide protective properties similar to silica or gold nanoparticles, thus ultimately shielding bound DNA sequences from cleavage during in vivo cellular delivery. By evaluating biostabilities using DNA molecular beacon as the model system, other benefits which this SWNT modification method endows to DNA probe are investigated as well.

Experimental Section

Materials and Instruments

The sequences of DNA and RNA oligonucleotides prepared are listed in Table 4-1. DNA synthesis reagents were purchased from Glen Research (Sterling, VA). The SWNTs were purchased from Unidym, Inc. with <5 wt % ash content (CAS number: 7782-42-5). An ABI3400 DNA/RNA synthesizer (Applied Biosystmes, Foster City, CA) was used for all MB probes and DNA target preparation. A ProStar HPLC (Varian, Walnut Creek, CA) with a C18 column (Econosil, 5 μm, 250× 4.6 mm) from Alltech (Deerfield, IL) was used for probe purification. A Cary Bio-300 UV spectrometer (Varian, Walnut Creek, CA) was used to measure absorbance for probe quantitation. Fluorescence measurements were performed on a Fluorolog-Tau-3 spectrofluorometer (Jobin Yvon, Inc., Edison, NJ). Cell images were conducted with a confocal microscope setup consisting of an Olympus IX-81 inverted microscope with an Olympus FluoView 500 confocal scanning system. A 40 × 0.6 NA air objective was used.

Synthesis of Molecular Probes

All oligonucleotides were synthesized based on solid-state phosphoramidite chemistry at a 1 μmol scale. Both molecular probes listed in Table 4-1 were synthesized with controlled-pore glass columns with a 3′-Black Hole Quencher 2 molecule (BHQ2) covalently linked to the CPG

substrate. The complete MB sequences were then deprotected in concentrated ammonia hydroxide at room temperature overnight and further purified with reverse phase high-pressure liquid chromatography (HPLC) on a C18 column with a linear elution gradient with TEAA (triethylammonium acetate) in acetonitrile changing from 20 to 70% over a 30 min period. The collection from the first HPLC separation was then vaccuum-dried, incubated in 200 μL 80% acetic acid for 15 min, incubated with 200 μL of ethanol, and vaccuum-dried before the second round of HPLC. The HPLC was performed on a ProStar HPLC Station (Varian, CA) equipped with a fluorescent and a photodiode array detector.

Table 4-1. Probes and Oligonucleotides Used in This Work

name	Sequence
MnSOD probe	5′-TTTTTTTTTTTTTTTTTTTT(CH2CH2O)$_{36}$Cy3-CGAGCCAGTTACATTCTCCCAGTTGATTGCTCGG−BHQ2−3′
Random DNA probe	5′-Cy3-CCTAGCTCTAAATCACTATGGTCGCGCTAGG-BHQ2−3′
MnSOD cDNA	5′-AATCAACTGGGAGAATGTAACTG-3′
GT	5′-GTGTGTGTGTGTGTGTGTGTGTGTGTGT-3′

Synthesis of GT/SWNT

Because of radioactive safety concerns and laboratory facility limitations, the SWNTs were cut before complexing with radioisotope-labeled GT sequence. The SWNTs were treated with a strong acid mixture (nitric acid/sulfic acid = 3:1) and sonicated for 24 h. After washing with water, 1 mg/L treated SWNT was mixed with 0.1 μM GT sequence labeled with ^{32}P at room temperature and rocked for 24 h. The resulting complex was directly used for the digestion test.

Synthesis of MnSOD Probe/SWNTs

Since neutral SWNTs are the popular form for cellular application, we wanted to investigate its protection ability during cellular delivery. The SWNTs were ultrasonicated by sonic dismembrator (Fisher Scientific, Model 100) for 1 h. Then about 200 mg/L SWNT was mixed with 20 μM MnSOD probe aqueous solution. The mixture was sonicated for another 45 min to 1 hour. Afterwards, the probe/nanotube solution was centrifuged at 22 000*g* for 6 h. The

pellet comprising impurities and aggregates of nanotubes at the bottom of the centrifuge tube was discarded, and the supernatant was collected and ultracentrifuged for another 6 h at 22 000*g*. The supernatant is the MnSOD probe/SWNTs, which turned out to be soluble. After dialysis, the complex was stored at 4 °C. The solubilized SWNTs are not well-dispersed individual nanotubes, but a mixture of nanotube bundles and individual nanotubes.

Cellular Experimental Procedures

MDA-MB-231 cells (ATCC, HTB-26) were cultured in Leibovitz's L-15 medium with 2 mM l-glutamine supplemented with 10% fetal bovine serum (all reagents from Invitrogen). Cells were plated into chambered coverslides 1 day before the experiments so that cells would be about 90% confluence during the experiments. The concentrated MnSOD probe/SWNTs were added to each well at a final concentration of about 25 mg/L. The incubations were carried out at 37 °C air atmosphere for 12 h. After incubation, the cell medium was decanted from the well, and the cells were washed thoroughly. To stimulate MnSOD mRNA expression, cells were incubated in 1 μg/mL LPS from *E. coli* serotype 055:B5 (Sigma) for 4 h prior to cellular imaging. The control experiments were conducted under the same conditions, but without LPS stimulation.

Results and Discussion

Protection in GT/SWNT

To investigate the protective properties of SWNTs, a 30-base-paired single-stranded DNA (ssDNA) oligonucleotide with repeating GT sequence (GT) was used as the model sequence. This sequence has been demonstrated to wrap onto the SWNT surface [192,193]. Radioisotopic labeling and denaturing PAGE gel were then used to monitor the digestion of DNA by DNase I, which can nonspecifically cleave ssDNA and dsDNA. The efficacy of the method was first tested to determine whether SWNTs could affect the mobility of bound DNA. To accomplish

this, both GT/SWNT complex and free DNA were treated with DNase I, and aliquots were collected at 5, 15, and 60 min time points. Aliquots were heated at 95 ℃ for 5 min before running the denaturing PAGE gel. As shown in Figure 4-1, the mobility of both GT and GT/SWNT sequences remains the same (lanes 1 and 2), which demonstrates that SWNTs do not inherently affect the mobility of their bound DNA. Having determined the viability of the method for monitoring digestion in the GT/SWNT complex cases, the same model and protocol were used to determine the effect of cleavage. Accordingly, the results of the cleavage assay show increased digestion of GT as a function of time, but no digestion for GT/SWNT, even after 60 min of digestion (Figure 4-1, lanes 3−5 and lanes 6−8, respectively). These experiments demonstrate that GT DNA is protected from DNase I cleavage when it is in complex with the SWNTs. Although protection from enzymatic cleavage is a useful property for DNA delivery into cells, it is also important that DNA probes be functional when in complex with SWNTs.

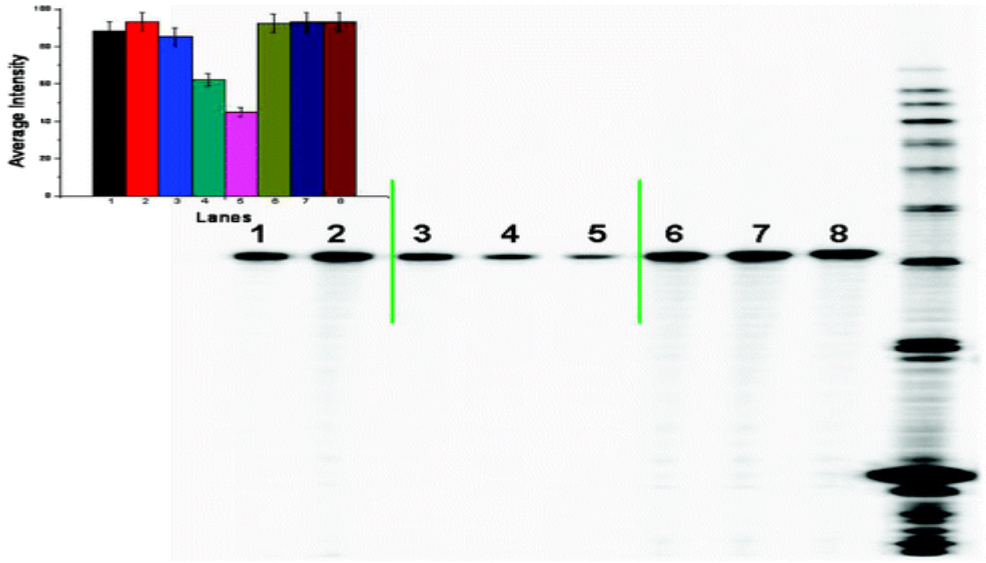

Figure 4-1. Polyacrylamide gel electrophoresis (PAGE) of free GT sequence and GT/SWNT complexes by 15% gel. Lanes 1 and 2 are the intact GT sequence and GT/SWNT complexes; lanes 3−5 are the GT sequence after DNase I digestion for 5 min, 15 min, and 1 h; lanes 6−8 are the GT/SWNT complexes after DNase I digestion for 5 min, 15 min, and 1 h; lane 9 is the 10 base pair DNA marker. The gel band intensity for each lane is plotted in the upper left corner graph.

Design and Characterization of MnSOD/SWNTs

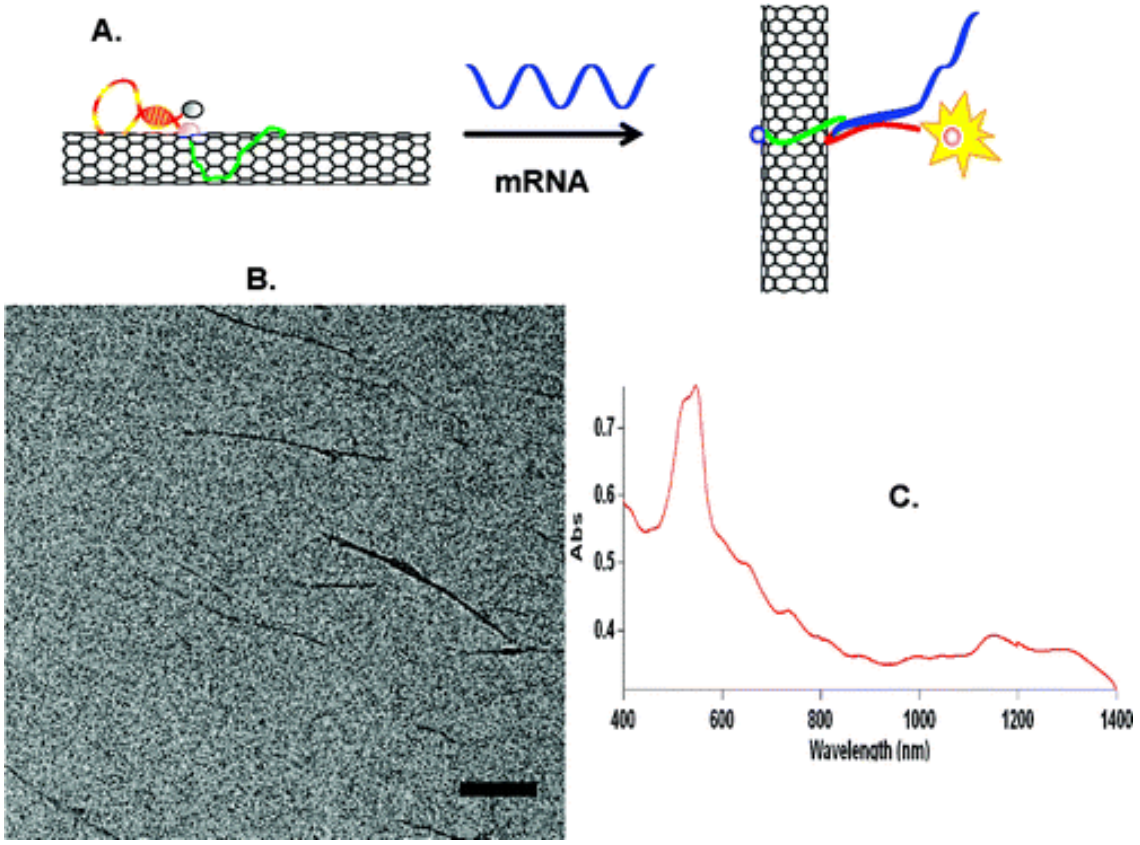

Figure 4-2. (A) Possible interaction between MnSOD probes, the SWNTs, and target mRNA; (B) TEM image of MnSOD probe/SWNTs (the scale bar represents 100 nm); (C) absorption spectrum of the probe in H_2O.

In order to demonstrate that SWNTs can protect functional DNA probes from enzymatic cleavage, a specific DNA probe was first modified and complexed with the SWNTs (possible interaction is shown in Figure 4-2 A). This DNA probe, which showed increased fluorescence upon binding manganese superoxide dismutase (MnSOD) mRNA [179], was further modified with polyT [193] to increase binding to the SWNT. In the absence of target cDNA (cDNA), our previous study [194] demonstrated that the designed probe forms a hairpin structure and adsorbs onto the SWNTs at room temperature, resulting in low signal intensity from the MnSOD probe/SWNTs. This low signal intensity was mainly a consequence of quenching from the Black Hole Quencher 2 (BHQ2), but it could have also been the result of quenching from the SWNTs

[195]. On the other hand, in the presence of target cDNA, the hybridization event separated the fluorophore from the quencher, or SWNTs, thus causing the signal enhancement shown in Figure 4-3. This demonstrates that the MnSOD probe/SWNTs could still respond to the target cDNA and that, consequently, the bound DNA was still functional.

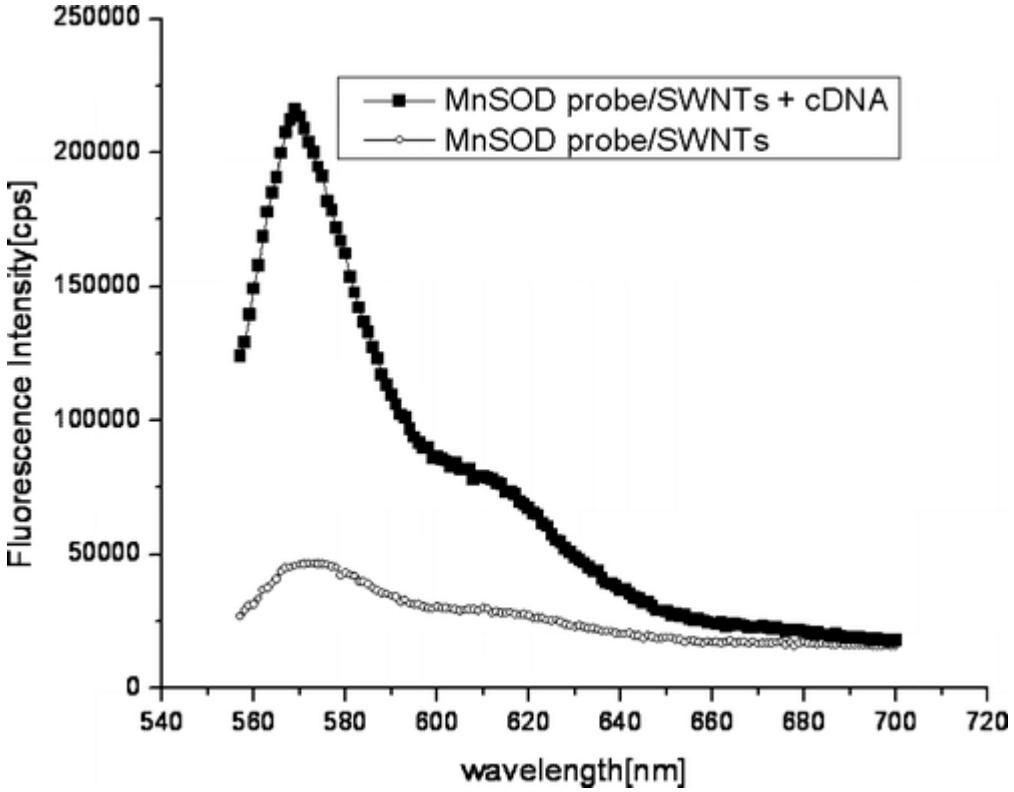

Figure 4-3. Emission fluorescence spectrum of MnSOD probe/SWNTs in the presence and absence of 10-fold excess target cDNA.

Protection Test in Buffer

Since the functional sensitivity of the MnSOD probe/SWNTs could be retained, we next tested its ability to resist nuclease cleavage in pure buffer. First, a fluorescence-based assay was performed as follows. One unit of DNase I endonuclease was added to separate solutions of 50 nM free MnSOD probes and probe/SWNTs. In this assay, if the probe is digested by DNase I, the fluorescence intensity will increase because the donor dye molecule will separate from the quenchers. Experiments for both free MnSOD probes and MnSOD probe/SWNTs were

performed under identical conditions. As shown in Figure 4-4 left, probe/SWNTs showed little degradation and, correspondingly, little fluorescence, while the free MnSOD probes showed a significant fluorescence increase, indicating increased degradation. These preliminary results therefore demonstrate that MnSOD probe/SWNTs could be immune to cleavage by DNase I. Next, the interactions of free MnSOD probes and probe/SWNTs with single-stranded DNA binding protein (SSB) were investigated. This was necessary because, intracellularly, DNA probes are subject to nonspecific binding by proteins, which can produce false positive signals. One such protein is the ubiquitous single-stranded DNA binding protein [82]. As shown in Figure 3-4 right, free probes had a 6-fold increase of fluorescent signal compared to MnSOD probe/SWNTs when incubated with SSB. Since the probe/SWNT complex showed little response to excess SSB, these results demonstrate that it may well be protected from this form of interference during intracellular experiments.

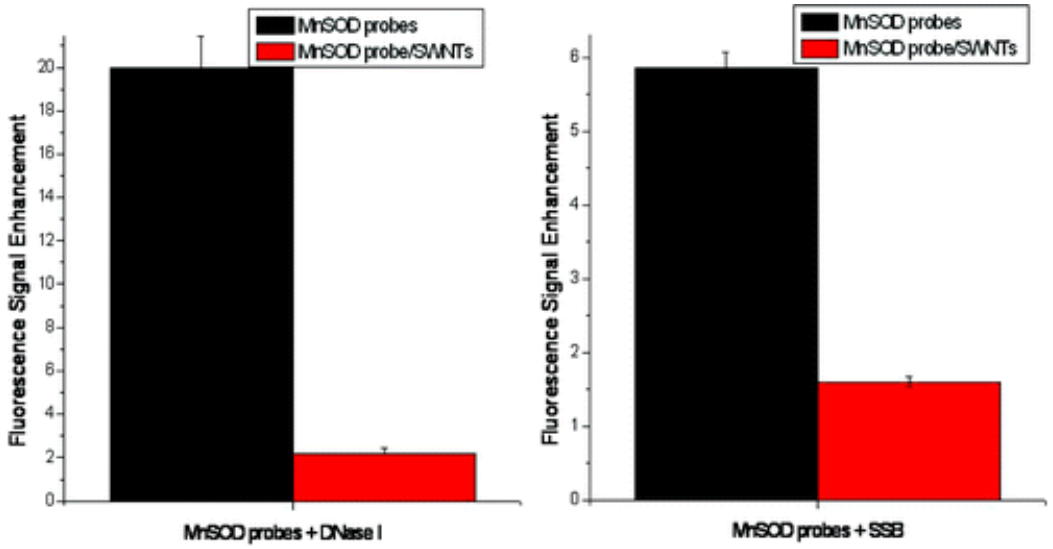

Figure 4-4. (Left) Fluorescence signal enhancements of both free MnSOD probes and MnSOD probe/SWNTs upon the addition of 1U DNase I. (Right) Fluorescence signal enhancements of both probes upon the addition of SSB. Final concentration ratio of probe/SSB = 1:5.

Protection Test in a Cellular Environment

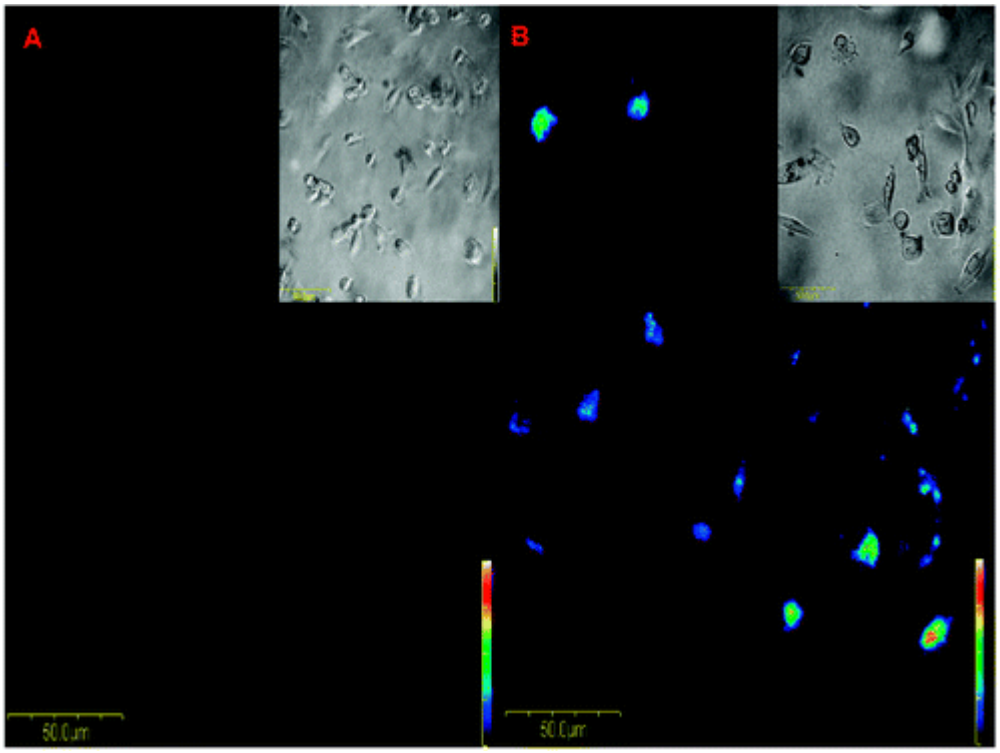

Figure 4-5. Bright field and fluorescent images of MnSOD probes/SWNT complexes inside MDA-MB-231 cells, (A) without LPS stimulation and (B) with LPS stimulation. All the scale bars shown in the graph are 50 μm.

In the context of their promising DNA protective properties, as demonstrated by these two *in vitro* experiments, probe/SWNT complexes show improved biostability when compared to the free probe. However, to further confirm these protection properties, the natural ability of SWNTs to be internalized was used to test the probe/SWNTs in a cellular environment. In this assay, the probe/SWNTs are delivered by simply incubating the complexes with MDA-MB-231 breast carcinoma cells. Under normal culture conditions, this cell line has a low MnSOD expression level; however, when exposed to lipopolysaccharide (LPS), an inflammatory mediator involved in *Escherichia coli* bacterial sepsis, MnSOD mRNA expression levels increase substantially [179,196]. As a result of the resistance of probe/SWNTs to enzymatic cleavage and nonspecific opening, the probe/SWNTs complexes should show lower fluorescence background compared to

the free probes before the cells are stimulated with LPS. Following LPS stimulation, if the probe/SWNTs are still functional after long intracellular incubation times, hybridization with target mRNA sequences will produce a fluorescent signal that can be detected by confocal microscopy.

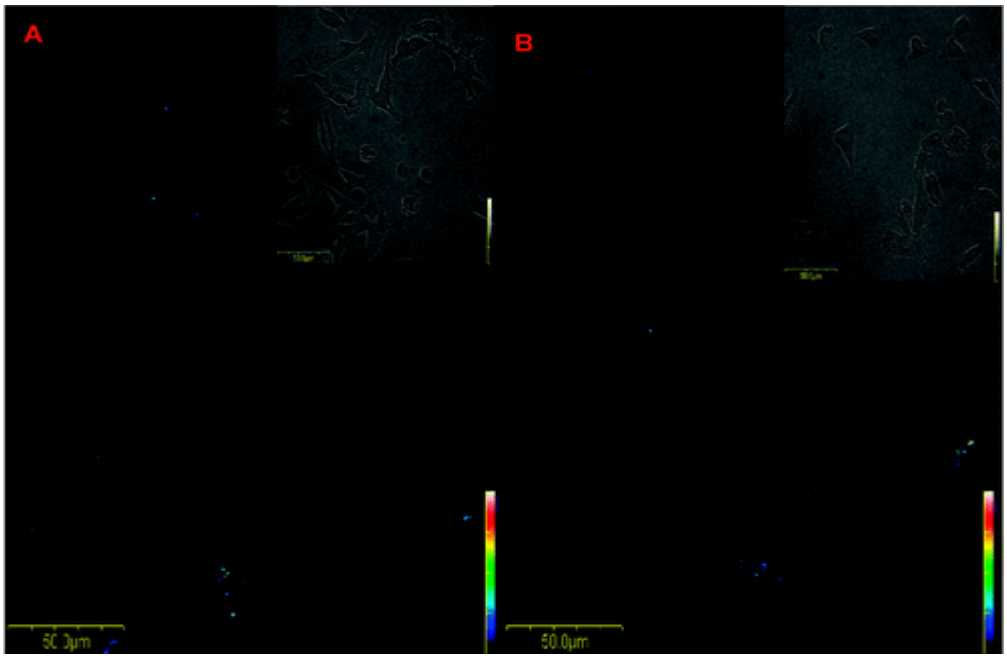

Figure 4-6. Bright field and fluorescent images of free MnSOD probes inside MDA-MB-231 cells, (A) without LPS stimulation and (B) with LPS stimulation. All the scale bars shown in the graph are 50 μm.

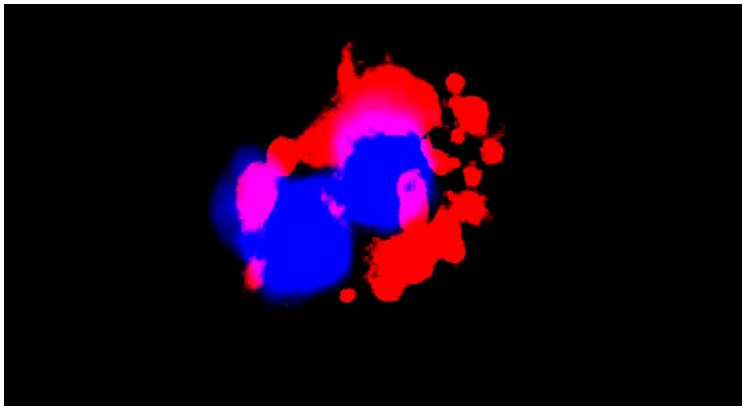

Figure 4-7. Fluorescence image of one single cell labeled by DAPI (or 4`,6-diamidino-2-phenylindole, a nucleus indicator, encoded in blue) and MnSOD MB/SWNTs (encoded in red). It shows MB/SWNTs stay outside the nucleus.

Briefly, 20 μM probes were mixed with 200 mg/L nanotube aqueous solution, sonicated, and centrifuged. The pellet comprising the nanotube impurities and aggregates was discarded, and the supernatant was collected as the probe/SWNTs, which turned out to be soluble. The probe/SWNTs were then incubated with MDA-MB-231 breast carcinoma cells at a final concentration of about 25 mg/L for 12 h. Subsequently, the cells were washed and treated with or without 1 μg/mL LPS for another 4 h before imaging. As shown in Figure 4-5, a high fluorescence signal was observed for most of the cells after LPS stimulation, which indicated the up-regulated MnSOD mRNA expression. Control experiments without LPS stimulation were carried out under the same conditions, and little fluorescence was observed compared to the LPS-stimulated cells. This experiment was repeated, and it was further demonstrated that probe/SWNT complexes produce a few false positive signals. For comparison, free MnSOD probes were incubated with cells under the same conditions, and low fluorescence signal was observed with and without LPS stimulation (Figure 4-6). The background for the free probe without LPS stimulation was higher than that of the complexes without LPS stimulation. This might have been the result of digestion and the nonspecific opening of very few MnSOD probes that were inefficiently self-delivered into the cells after a long incubation time, leading to a false positive signal. It might have also been caused by some probes being trapped between the cells. If these probes had been digested or disrupted, they would have had no ability to detect the different gene expression levels, causing the same fluorescence intensity to be observed with LPS stimulation. To confirm this explanation, another free random DNA probe with no complement inside the cells was tested under the same conditions, and results identical to those of the free MnSOD were obtained, as expected. Thus, the single-walled carbon nanotubes do protect probes from digestion and disruption which ensures that the DNA probes can

successfully distinguish different gene expression levels free from the types of interference examined here.

Possible Mechanisms for the Protection

These two sets of experiments, both in buffer and in cell culture, have demonstrated improved biostability of probe/SWNTs over the free probes. Specifically, the *in vitro* experiments showed that probe/SWNTs have much better resistance to nuclease digestion and nucleic acid binding protein disruption. Furthermore, the intracellular experiments showed that probe/SWNTs complexes are functional, even after a total incubation of 16 h. In contrast, free DNA degrades after only 15–45 min in the cel lular environment [81]. As a consequence of reduced nonspecific opening events, lower background improved the detection sensitivity of probe/SWNT complexes. Therefore, this investigation proves that SWNTs have the ability to protect bound DNA cargos from enzymatic cleavage and DNA binding proteins both during and after delivery into cells.

As noted above, different nanomaterials exhibit various degrees of DNA protection, but the mechanisms of protection are not yet well understood. For example, silica nanoparticles exhibit protection of plasmid DNA. It has been proposed that the positive charges on the silica nanoparticle surface can exclude Mg^{2+} and that the DNA conformational change that results from binding onto this nanoparticle surface prevents digestion [181]. In the case of silica nanotubes, the authors hypothesized that the nanotubes act as a physical shield that protects the loaded materials from environmental damage [187]. To date, no reasoning has been provided to explain the efficacy of gold nanoparticles [94]. The protective properties of SWNTs, on the other hand, may be explained in several ways. First, the probes could be embedded inside small bundles of nanotubes such that the nucleases/proteins cannot physically access the DNA. Second, although the surface of the SWNT has been modified with hydrophilic groups from the

DNA probes, some hydrophobic regions may still remain exposed and cause inhibitory effects on proteins that come into close proximity. Finally, the interaction between DNA and SWNTs [193] may cause the secondary structure of the DNA to be unrecognizable to enzyme binding pockets. Obviously, further investigation is required to address these causal issues to conclusively determine the mechanisms underlying the protective properties of probe/SWNTs complexes.

Other Benefits this SWNT Modification Brings to DNA Molecular Probes

Besides biostability, SWNTs modification to DNA molecular probes brought other benefits for intracellular mRNA monitoring as well. As indicated in Figure 4-5, almosted all the cells showed strong fluorescence signals after four hours' drug stimulation, which indicated that this SWNT modification method provides an efficient high-throughput delivery of MB into the cells. This definitely avoids the need of traditional tedious microinjection method or costy newly developed peptide conjugation.

In addition, DNA probes usually spontaneously accumulate inside the nucleus after injection, which greatly hinders the sensitive detection of intracellular mRNA in the cytoplasm in living cells. Howver, this MB/SWNT method interestingly solved this problem. As demonstrated in Figure 4-7, the fluorescence signals from MB/SWNTs were not co-localized with the signals from DAPI (a traditional nucleus indicator); this indicated that MB/SWNTs prevent the nucleus accumulation, thus they are able to stay in the cytoplasm. The possible reason should be ascribed to the big size of SWNT and rather small pores on the nucleus membrane [191]. Due to the immunity to nucleus accumulation, the interference from nucleus background signal is dramatically decreased, resulting rather sensitive detection of mRNA in the cytoplasm.

Conclusions

In summary, when bound to SWNTs, DNA probes are protected from enzymatic cleavage and interference from nucleic acid binding proteins. These protective properties are particularly

important for applications in which DNA probes are used for intracellular measurements. Our study shows that a SWNT-modified DNA probe, which targets a specific mRNA inside living cells, has increased self-delivery capability and intracellular biostability to nucleus accumulation when compared to free DNA probes. Therefore, this novel material provides significant advantages for basic genomic studies in which DNA probes are used to monitor intracellular levels of molecules and ions. Additionally, for cytoplasmic gene detection by DNA probes, nucleus sequestration is a major cause of reduced sensitivity [197]. The DNA/SWNT complexes, however, stay within the cytoplasm, enabling cytoplasmic mRNAs to be detected and imaged. Furthermore, DNA/SWNT complexes should prove useful as therapeutic agents since they exhibit excellent self-delivery properties that could allow DNA-based drugs to exert their therapeutic presence for longer time before being degraded by cells.

CHAPTER 5
SUMMARY AND FUTURE WORK

Engineering Nucleic Acid Probes/Nanomaterials for Cancer Studies

The high risk of cancer has compelled researchers from various backgrounds to direct their efforts toward cancer research. The major cancer studies include cancer diagnosis, cancer treatment and intracellular biomolecular studies. As ideal building blocks, multifunctional nucleic acids have been investigated in this dissertation as a means of designing various molecular probes and probe-nanomaterial conjugates for cancer studies.

In Chapter Two, in order to enhance the binding capability of otherwise low-affinity aptamers at physiological temperature, an aptamer-micelle was constructed by attaching a lipid tail on the end of the aptamer. Enhanced specific recognition ability is directly built into the nanostructures. Interestingly, the attachment of the lipid tail additionally endows the aptamer-micelles with internalization pathways, thus allowing cell permeability for drug delivery applications. The aptamer-micelle demonstrates several other beneficial properties, including extremely low off-rate once bound to target cells, rapid recognition ablity with enhanced sensitivity, low critical micelle concentration values, no cytotoxicity. As noted above, the potential of dual drug delivery pathways is created by encapsulating the drug molecules inside the aptamer-micelle or by directly conjugating the drug onto the other end of an aptamer via an acid-labile linker. Sensitive and specific trace cell detection in the human whole blood sample indicates the promising application of this aptamer-micelle strategy in cancer diagnosis. Furthermore, we mimicked a tumor site in the blood stream by immobilizing tumor cells onto the surface of a flow channel device. Flushing the aptamer-micelles through the channel demonstrated their selective recognition ability under flow circulation in a human whole blood sample. The aptamer-micelles show great dynamic specificity in flow channel systems mimicing

drug delivery in the blood system. When applying the same lipid tail modification strategy to the other low-affinity aptamers, a similarly enhanced binding capability was observed, indicating that this modification strategy can be a universal method to promote the utilization of aptamers in living systems. Although the exact underlying mechanism is yet to be understood, fluid nature of the micelle was proposed to be a possible explanation to this interesting phenomenon based on our preliminary investigations. Overall, our DNA aptamer-micelle assembly has shown high potential for cancer cell recognition and for *in vivo* drug delivery applications in the blood stream.

In Chapter Three, to develop a molecular tool for long-term real-time intracellular mRNA monitoring inside the living cells, locked nucleic acids (LNAs) were used to engineer novel molecular beacons. A strandard design strategy was proposed and complemented to design several LNA and DNA chimeric probes, which demonstrated excellent nuclease immunity and avoidance of nonspecific DNA binding protein disruption, as well as reasonable hybridization kinetics. Besides buffer system studies, the new beacons were tested with MDA-MB-231 breast cancer cells and used to monitor changes in the expression of MnSOD mRNA upon LPS stimulation for up to 5 hours. After 24 hours inside living cells, the designed MBs were still able to response to their targets, demonstrating a greatly enhanced stability. Considering the fact that DNA-MBs degrade after 15-45 minutes in the cellular environment, the outstanding biostability of the newly designed MBs, while remaining reasonable hybridization kinetics, extends their application to many *in vivo* studies and intracellular monitoring where stability of the molecular probe is needed for a protracted period of time.

Chapter Four investigated the vulnerability of MBs to nuclease digestion and nonspecific disruption. However, when bound to single-walled carbon nanotubes (SWNTs), it was found that DNA probes are protected from enzymatic cleavage and interference from nucleic acid

binding proteins. These protective properties are particularly important for applications in which DNA probes are used for intracellular measurements. With the use of SWNTs, an excellent nanocarrier for a variety of cells, DNA-MBs can enter the cells efficiently in a high-throughput manner. After SWNT modification, the DNA-MBs were found to retain their functional response to the target, either outside or inside the cells. Without the target, the fluorophore from MB was quenched by both the flanked quencher and SWNT. Upon hybridization with its target, the MB modified on the SWNT surface changed its conformation, resulting in the restoration of fluorescence signal. Interestingly, as noted above, SWNTs were demonstrated to provide protection to its DNA-MB cargos from nuclease digestion and nonspecific disruption with DNA binding proteins during cellular delivery. After about 16 hours of incubation with cells, the SWNT/MB complex was still able to detect the stimulated MnSOD mRNA expression upon the LPS stimulation. In addition, because of the large size of SWNTs, SWNT/MB complexes avoid the probes' nucleus accumulation and further enhance their detection sensitivity.

Future Directions

Aptamer-Micelle for Targeted Gene Therapy

Modulation of cancer-related genes has become a popular cancer treatment. To deliver therapeutic agents efficiently across the plasma membrane of the cells *in vivo*, various delivery systems have been developed, including cationic lipids, viral or nonviral vectors, nanoparticles [56], or direct modification of the therapeutic oligonucleotides (e.g., chemical, protein, lipid) [198-200]. However, most of the approaches can only deliver therapeutic agents to the cells nonspecifically. The ideal delivery system should be able to deliver therapeutic agents to target cancer cells in a specific manner; because, in this way, the required dosage and quantity of therapeutic agents for the treatment can be greatly reduced, as well as the cost and the possibility of the side effects.

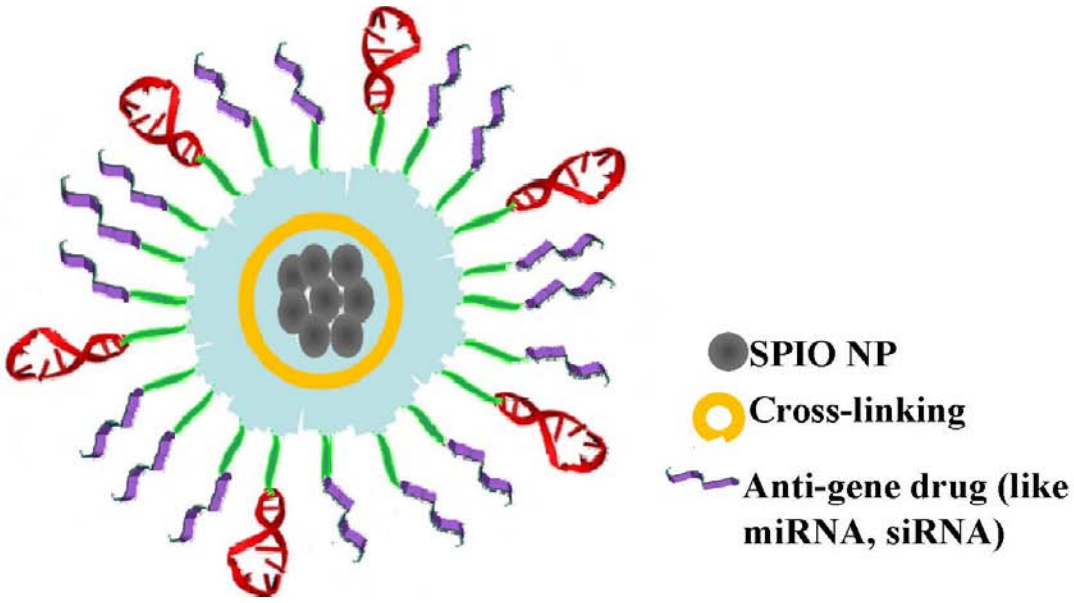

Figure 5-1. Scheme of SPIO NP-doped cross-linked aptamer-micelle for anti-gene drug delivery (including miRNA antogamir and siRNA or antisense).

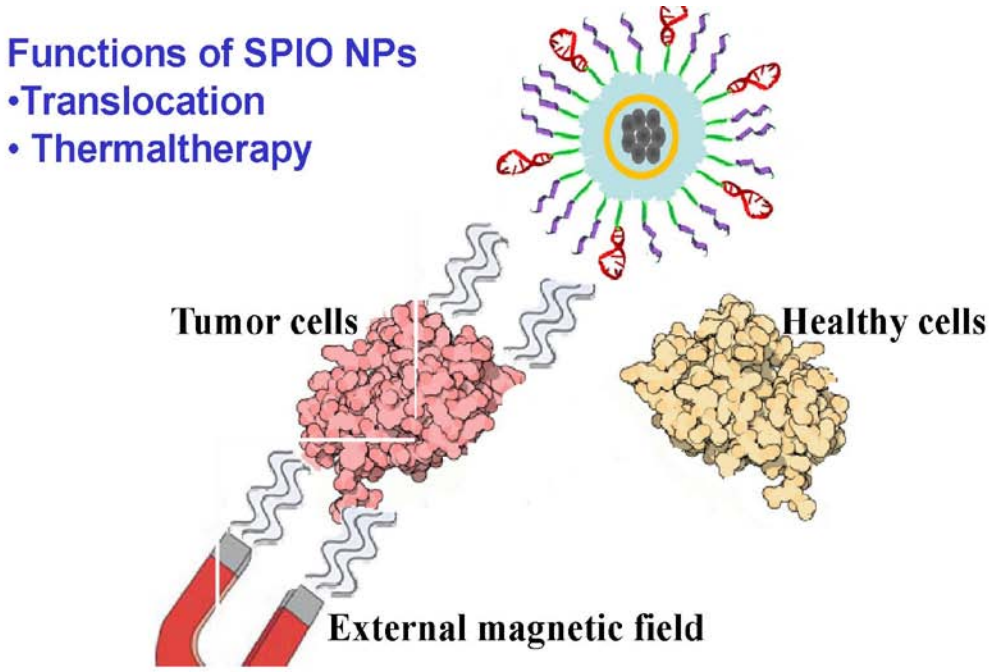

Figure 5-2. Working principle of the SPIO NP-doped cross-linked aptamer-micelle for magnatic narvigated therapy.

To realize targeted gene therapy, a few approaches have been attempted. For example, iron binding protein transferrin has been used to target colloids composed of siRNA and

cyclodextrin-containing polycations and to transfer them to receptor-expressing tumor cells [201]. Antibodies that bind cell-type specific cell surface receptors were fused with protamine and used for tissue-specific delivery of siRNA [202]. More recently, two independent groups have reported an approach that simultaneously executes these two strategies; i.e., using an RNA aptamer (PSMA aptamer) conjugated with siRNA for targeted delivery [203,204]. One group directly applied an aptamer-siRNA chimeric RNA [203], while the other group utilized streptavidin to assemble a biotin-modified aptamer and siRNA complex [204]. These reagents were reported to inhibit tumor growth specifically and mediate tumor regression in a xenograft model of prostate cancer.

The above results demonstrated the promising applications of aptamers in targeted gene therapy. However, the ratios between the therapeutic agent (siRNA) and the targeting ligand (aptamer) in the above two cases were limited to 1 or at most 3. To maximize the therapeutic effect, it is necessary to further increase the loading efficiency of therapeutic agents. To this end, nanotechnology is envisioned to be a promising approach [205].

Chapter Two describes an aptamer-micelle built from an amphiphilic unit (a hydrophilic DNA plus a hydrophobic lipid tail). Results demonstrated that both a homogeneous aptamer-micelle and a heterogeneous aptamer-micelle can be made by mixing two different types of DNA-lipid. By simply replacing one DNA-lipid with a therapeutic oligonucleotide-lipid (such as miRNA antagomir-lipid, siRNA-lipid, antisense-lipid or CpG-lipid), a micelle which is composed of aptamer and therapeutic agents can be made. Based on the results shown in Figure 2-18, even with 9% density of aptamer, the heterogeneous micelle can still bind target cancer cells specifically. This indicates that by this approach, one aptamer sequence can deliver at least 10 therapeutic oligonucleotide sequences specifically into the cells. By simply cross-linking the

micelle [206,207], it is expected that the therapeutic oligonucleotides (TO) integrated into the nanoparticle can be delivered into the specific cancer cells and then released in the cytoplasm to modulate the target mRNA. Furthermore, since a superparamagnetic iron oxide (SPIO) nanoparticle is usually coated with one layer of hydrophobic compounds [208], it would be easy to dope such hydrophobic nanoparticle inside the aptamer-micelle by the precipitation and membrane dialysis method [164] to create an aptamer/therapeutic oligonucleotide micelle (A/TO micelle). It is expected that this SPIO-A/TO micelle would then be a promising targeted therapy vehicle *in vivo*. After injection into the blood stream, the SPIO-A/TO micelle can be navigated to the tumor site facilitated by an external magnetic field [209]. Around the tumor mass, the aptamer then directs the whole particle to enter the specific cancer cells. On one hand, once inside the target cancer cells, the TO can modulate the tumor-related mRNA; on the other hand, by applying an AC magnetic field of sufficient strength and frequency, the encapsulated iron oxide nanoparticles can function as a hyperthermia agent to release heat around the diseased tissue. By this combinational therapy, the therapeutic index of this micelle can be greatly enhanced, while leaving the surrounding healthy tissue intact.

Aptamer-Based Drug Delivery Systems for Selective Deliverer of Drugs to Multidrug-Resistant Cancer Cells

Two main obstacles to successful cancer chemotherapy are selective targeting and multidrug resistance (MDR). Aptamers, one of the most popular molecular recognition ligands, have been utilized in various carriers for delivering chemotherapy drug molecules to target cancer cells specifically [67]. However, until now, no aptamer-based delivery vehicle has been demonstrated to overcome MDR while retaining targeted therapy. Traditional methods used to overcome MDR are still limited to the co-administration of inhibitors of P-glycoprotein [210], which has been reported to be highly associated with the development of MDR in cancer cells.

Here, we hypothesize that an aptamer-based drug delivery system could be used as an alternative approach to overcome MDR, based on the fact that an aptamer-based delivery system can penetrate target cells by receptor-mediated endocytosis, which allows it to bypass the P-glycoprotein. To test the hypothesis, an aptamer-drug conjugate will be synthesized. To investigate whether the nanoparticle construction can further enhance the killing efficiency to drug-resistant cell lines, an aptamer-micelle drug carrier will be synthesized for comparison. In both cases, doxorubicin will be the conjugated drug and an acid labile linkage will be inserted between the drug and the aptamer sequence. The results in Chapter Two demonstrated that the aptamer-micelles displays about 700-fold increase in binding affinity, which indicates the greatly improved drug loading efficiency in the micelle system, thus enhancing the therapeutic index offered by the aptamer-micelle as a drug carrier.

Aptamer-Micelle as a Sensitive Biomarker MRI Sensor

Chapter Two demonstrates how aptamer-micelles allow sensitive cancer detection. Such sensitivity is achieved because just one aptamer recognition event draws the entire micelle particle containing thousands of flouorescence dyes to the target cells and will do so in a highly selective manner. By simply replacing the fluorescence dye with a Gadolilium complex or a ^{19}F-containing molecule [211], aptamer-micelles can function as sensitive MRI sensors. Then, by utilizing automated oligonucleotide synthesis and ready modification, the required replacement will be easily complemented.

SWNT/Aptamer Complex for Targeted Therapy

Chapter Four describes a way to attach nucleic acid molecular beacons onto the surface of SWNT. The attached nucleic acid probe can still respond to its target mRNA, resulting in increased fluorescence signal. By simply replacing the nucleic acid probe with a nucleic acid aptamer, a SWNT/aptamer complex can be made. Again, by virtue of the dedicated design of the

linker inserted between the polyT sequence and aptamer sequence, the aptamer is expected to be able to interact with its target protein, just like molecular beacons discussed in Chapter Four. Therefore, this SWNT/aptamer can become a specific cancer targeting delivery vehicle. SWNTs have been reported to ablate tumors by releasing heat after it absorbs energy from near-infrared (NIR) light [191,212]. Thus, with the assistance of an aptamer, the SWNT/aptamer can be selectively delivered into the target cancer cells. By using similar NIR triggering, the targeted tumor cell should be killed. By simple physical hydrophobic stacking, a chemotherapy drug, doxorubicin, can be loaded onto the SWNT [213]. This combination chemotherapy will potentially increase the killing efficiency while doing no harm to healthy tissue.

LIST OF REFERENCES

1. Jemal A, Siegel R, Ward E, Hao YP, Xu JQ, Thun MJ: **Cancer Statistics, 2009**. *Ca-a Cancer Journal for Clinicians* 2009, **59**:225-249.

2. Zaridze DG: **Molecular epidemiology of cancer**. *Biochemistry-Moscow* 2008, **73**:532-542.

3. Watson JD, Crick FH: **Molecular structure of nucleic acids; a structure for deoxyribose nucleic acid**. *Nature* 1953, **171**:737-738.

4. Zhao XL, Yu YT: **Detection and quantitation of RNA base modifications**. *Rna-a Publication of the Rna Society* 2004, **10**:996-1002.

5. Castanotto D, Rossi JJ: **The promises and pitfalls of RNA-interference-based therapeutics**. *Nature* 2009, **457**:426-433.

6. Chi SW, Zang JB, Mele A, Darnell RB: **Argonaute HITS-CLIP decodes microRNA-mRNA interaction maps**. *Nature* 2009, **460**:479-486.

7. Krieg AM: **Mechanisms and applications of immune stimulatory CpG oligodeoxynucleotides**. *Biochimica Et Biophysica Acta-Gene Structure and Expression* 1999, **1489**:107-116.

8. Krieg AM, Kline JN: **Immune effects and therapeutic applications of CpG motifs in bacterial DNA**. *Immunopharmacology* 2000, **48**:303-305.

9. Sioud M, Iversen PO: **Ribozymes, DNAzymes and small interfering RNAs as therapeutics**. *Current Drug Targets* 2005, **6**:647-653.

10. Schubert S, Kurreck J: **Ribozyme- and deoxyribozyme-strategies for medical applications**. *Current Drug Targets* 2004, **5**:667-681.

11. O'Connell JB, Maggard MA, Ko CY: **Colon cancer survival rates with the new American Joint Committee on cancer sixth edition staging**. *Journal of the National Cancer Institute* 2004, **96**:1420-1425.

12. Eisen MB, Spellman PT, Brown PO, Botstein D: **Cluster analysis and display of genome-wide expression patterns**. *Proceedings of the National Academy of Sciences of the United States of America* 1998, **95**:14863-14868.

13. Hughes TR, Marton MJ, Jones AR, Roberts CJ, Stoughton R, Armour CD, Bennett HA, Coffey E, Dai HY, He YDD, et al.: **Functional discovery via a compendium of expression profiles**. *Cell* 2000, **102**:109-126.

14. Alizadeh AA, Eisen MB, Davis RE, Ma C, Lossos IS, Rosenwald A, Boldrick JG, Sabet H, Tran T, Yu X, et al.: **Distinct types of diffuse large B-cell lymphoma identified by gene expression profiling**. *Nature* 2000, **403**:503-511.

15. Golub TR, Slonim DK, Tamayo P, Huard C, Gaasenbeek M, Mesirov JP, Coller H, Loh ML, Downing JR, Caligiuri MA, et al.: **Molecular classification of cancer: Class discovery and class prediction by gene expression monitoring**. *Science* 1999, **286**:531-537.

16 Sorlie T, Perou CM, Tibshirani R, Aas T, Geisler S, Johnsen H, Hastie T, Eisen MB, van de Rijn M, Jeffrey SS, et al.: **Gene expression patterns of breast carcinomas distinguish tumor subclasses with clinical implications**. *Proceedings of the National Academy of Sciences of the United States of America* 2001, **98**:10869-10874.

17. Garber ME, Troyanskaya OG, Schluens K, Petersen S, Thaesler Z, Pacyna-Gengelbach M, van de Rijn M, Rosen GD, Perou CM, Whyte RI, et al.: **Diversity of gene expression in adenocarcinoma of the lung**. *Proceedings of the National Academy of Sciences of the United States of America* 2001, **98**:13784-13789.

18. Koch I, Slotta-Huspenina J, Hollweckt R, Anastasov N, Hofler H, Quintanilla-Martinez L, Fend F: **Real-time quantitative RT-PCR shows variable, assay-dependent sensitivity to formalin fixation: Implications for direct comparison of transcript levels in paraffin-embedded tissues**. *Diagnostic Molecular Pathology* 2006, **15**:149-156.

19. Tuerk C, Gold L: **Systematic Evolution of Ligands by Exponential Enrichment - Rna Ligands to Bacteriophage-T4 DNA-Polymerase**. *Science* 1990, **249**:505-510.

20. Ellington AD, Szostak JW: **Invitro Selection of RNA Molecules That Bind Specific Ligands**. *Nature* 1990, **346**:818-822.

21. Shangguan D, Li Y, Tang Z, Cao ZC, Chen HW, Mallikaratchy P, Sefah K, Yang CJ, Tan W: **From the Cover: Aptamers evolved from live cells as effective molecular probes for cancer study**. *Proceedings of the National Academy of Sciences of the United States of America* 2006, **103**:11838-11843.

22. Proske D, Blank M, Buhmann R, Resch A: **Aptamers - basic research, drug development, and clinical applications**. *Applied Microbiology and Biotechnology* 2005, **69**:367-374.

23. Missailidis S, Perkins A: **Aptamers as novel radiopharmaceuticals: Their applications and future prospects in diagnosis and therapy**. *Cancer Biotherapy and Radiopharmaceuticals* 2007, **22**:453-468.

24. Perkins AC, Missailidis S: **Radiolabelled aptamers for tumour imaging and therapy**. *Quarterly Journal of Nuclear Medicine and Molecular Imaging* 2007, **51**:292-296.

25. Drolet DW, MoonMcDermott L, Romig TS: **An enzyme-linked oligonucleotide assay**. *Nature Biotechnology* 1996, **14**:1021-1025.

26. Vivekananda J, Kiel JL: **Anti-Francisella tularensis DNA aptamers detect tularemia antigen from different subspecies by aptamer-linked immobilized sorbent assay**. *Laboratory Investigation* 2006, **86**:610-618.

27. Blank M, Weinschenk T, Priemer M, Schluesener H: **Systematic evolution of a DNA aptamer binding to rat brain tumor microvessels - Selective targeting of endothelial regulatory protein pigpen**. *Journal of Biological Chemistry* 2001, **276**:16464-16468.

28. Li W, Yang XH, Wang KM, Tan WH, He Y, Guo QP, Tang HX, Liu JB: **Real-time imaging of protein internalization using aptamer conjugates**. *Analytical Chemistry* 2008, **80**:5002-5008.

29. Bock C, Coleman M, Collins B, Davis J, Foulds G, Gold L, Greef C, Heil J, Heilig JS, Hicke B, et al.: **Photoaptamer arrays applied to multiplexed proteomic analysis**. *Proteomics* 2004, **4**:609-618.

30. Yang CJ, Jockusch S, Vicens M, Turro NJ, Tan WH: **Light-switching excimer probes for rapid protein monitoring in complex biological fluids**. *Proceedings of the National Academy of Sciences of the United States of America* 2005, **102**:17278-17283.

31. Shangguan D, Li Y, Tang ZW, Cao ZHC, Chen HW, Mallikaratchy P, Sefah K, Yang CYJ, Tan WH: **Aptamers evolved from live cells as effective molecular probes for cancer study**. *Proceedings of the National Academy of Sciences of the United States of America* 2006, **103**:11838-11843.

32. Tang ZW, Shangguan D, Wang KM, Shi H, Sefah K, Mallikratchy P, Chen HW, Li Y, Tan WH: **Selection of aptamers for molecular recognition and characterization of cancer cells**. *Analytical Chemistry* 2007, **79**:4900-4907.

33. Sefah K, Tang ZW, Shangguan DH, Chen H, Lopez-Colon D, Li Y, Parekh P, Martin J, Meng L, Phillips JA, et al.: **Molecular recognition of acute myeloid leukemia using aptamers**. *Leukemia* 2009, **23**:235-244.

34. Tang ZW, Parekh P, Turner P, Moyer RW, Tan WH: **Generating Aptamers for Recognition of Virus-Infected Cells**. *Clinical Chemistry* 2009, **55**:813-822.

35. Shangguan DH, Cao ZHC, Li Y, Tan WH: **Aptamers evolved from cultured cancer cells reveal molecular differences of cancer cells in patient samples**. *Clinical Chemistry* 2007, **53**:1153-1155.

36. Huang YF, Chang HT, Tan WH: **Cancer cell targeting using multiple aptamers conjugated on nanorods**. *Analytical Chemistry* 2008, **80**:567-572.

37. Medley CD, Smith JE, Tang Z, Wu Y, Bamrungsap S, Tan WH: **Gold nanoparticle-based colorimetric assay for the direct detection of cancerous cells**. *Analytical Chemistry* 2008, **80**:1067-1072.

38. Herr JK, Smith JE, Medley CD, Shangguan DH, Tan WH: **Aptamer-conjugated nanoparticles for selective collection and detection of cancer cells**. *Analytical Chemistry* 2006, **78**:2918-2924.

39. Phillips JA, Xu Y, Xia Z, Fan ZH, Tan WH: **Enrichment of Cancer Cells Using Aptamers Immobilized on a Microfluidic Channel**. *Analytical Chemistry* 2009, **81**:1033-1039.

40. Nagrath S, Sequist LV, Maheswaran S, Bell DW, Irimia D, Ulkus L, Smith MR, Kwak EL, Digumarthy S, Muzikansky A, et al.: **Isolation of rare circulating tumour cells in cancer patients by microchip technology**. *Nature* 2007, **450**:1235-U1210.

41. Rosenberg SA, Aebersold P, Cornetta K, Kasid A, Morgan RA, Moen R, Karson EM, Lotze MT, Yang JC, Topalian SL, et al.: **Gene-Transfer into Humans - Immunotherapy of Patients with Advanced Melanoma, Using Tumor-Infiltrating Lymphocytes Modified by Retroviral Gene Transduction**. *New England Journal of Medicine* 1990, **323**:570-578.

42. Brannon-Peppas L, Ghosn B, Roy K, Cornetta K: **Encapsulation of nucleic acids and opportunities for cancer treatment**. *Pharmaceutical Research* 2007, **24**:618-627.

43. Gleave ME, Monia BP: **Antisense therapy for cancer**. *Nature Reviews Cancer* 2005, **5**:468-479.

44. El-Aneed A: **Current strategies in cancer gene therapy**. *European Journal of Pharmacology* 2004, **498**:1-8.

45. Nishitani MA, Sakai T, Kanayama HO, Himeno K, Kagawa S: **Cytokine gene therapy for cancer with naked DNA**. *Molecular Urology* 2000, **4**:47-50.

46. Shi FS, Rakhmilevich AL, Heise CP, Oshikawa K, Sondel PM, Yang NS, Mahvi DM: **Intratumoral injection of interleukin-12 plasmid DNA, either naked or in complex with cationic lipid, results in similar tumor regression in a murine model**. *Molecular Cancer Therapeutics* 2002, **1**:949-957.

47. Barajas M, Mazzolini G, Schmitz V, Narvaiza I, Bilbao R, Genove G, Zabala M, Sangro B, Melero I, Qian C: **Gene therapy of orthotopic hepatocellular carcinoma in rats using adenovirus coding for interleukin-12 (IL-12)**. *Journal of Hepatology* 2001, **34**:221-221.

48. Vattemi E, Claudio PP: **Tumor suppressor genes as cancer therapeutics**. *Drug News & Perspectives* 2007, **20**:511-520.

49. Lu C, El-Deiry W: **Targeting p53 for enhanced radio- and chemo-sensitivity**. *Apoptosis* 2009, **14**:597-606.

50. Nemunaitis J, Swisher SG, Timmons T, Connors D, Mack M, Doerksen L, Weill D, Wait J, Lawrence DD, Kemp BL, et al.: **Adenovirus-mediated p53 gene transfer in sequence with cisplatin to tumors of patients with non-small-cell lung cancer**. *Journal of Clinical Oncology* 2000, **18**:609-622.

51. Swisher SG, Roth JA, Komaki R, Gu J, Lee JJ, Hicks M, Ro JY, Hong WK, Merritt JA, Ahrar K, et al.: **Induction of p53-regulated genes and tumor regression in lung cancer patients after intratumoral delivery of adenoviral p53 (INGN 201) and radiation therapy**. *Clinical Cancer Research* 2003, **9**:93-101.

52. Wilson JM: **Gendicine: The first commercial gene therapy product**. *Human Gene Therapy* 2005, **16**:1014-1014.

53. Nakata Y, Kim TK, Shetzline S, Gewirtz AM: **Nucleic acid modulation of gene expression: Approaches for nucleic acid therapeutics against cancer**. *Critical Reviews in Eukaryotic Gene Expression* 2005, **15**:163-182.

54. Stahel RA, Zangemeister-Wittke U: **Antisense oligonucleotides for cancer therapy - an overview**. *Lung Cancer* 2003, **41**:S81-S88.

55. Dass CR, Choong PFM, Khachigian LM: **DNAzyme technology and cancer therapy: cleave and let die**. *Molecular Cancer Therapeutics* 2008, **7**:243-251.

56. Anderson WF: **Human gene therapy**. *Nature* 1998, **392**:25-30.

57. Dollins CM, Nair S, Sullenger BA: **Aptamers in immunotherapy**. *Human Gene Therapy* 2008, **19**:443-450.

58. Lee JH, Canny MD, De Erkenez A, Krilleke D, Ng YS, Shima DT, Pardi A, Jucker F: **A therapeutic aptamer inhibits angiogenesis by specifically targeting the heparin binding domain of VEGF165**. *Proc Natl Acad Sci U S A* 2005, **102**:18902-18907.

59. Fraunfelder FW: **Pegaptanib for wet macular degeneration**. *Drugs Today (Barc)* 2005, **41**:703-709.

60. Bates PJ, Laber DA, Miller DM, Thomas SD, Trent JO: **Discovery and development of the G-rich oligonucleotide AS1411 as a novel treatment for cancer**. *Experimental and Molecular Pathology* 2009, **86**:151-164.

61. Soundararajan S, Chen WW, Spicer EK, Courtenay-Luck N, Fernandes DJ: **The nucleolin targeting aptamer AS1411 destabilizes bcl-2 messenger RNA in human breast cancer cells**. *Cancer Research* 2008, **68**:2358-2365.

62. Choi JH, Chen KH, Han JH, Chaffee AM, Strano MS: **DNA Aptamer-Passivated Nanocrystal Synthesis: A Facile Approach for Nanoparticle-Based Cancer Cell Growth Inhibition**. *Small* 2009, **5**:672-675.

63. Zhao ZL, Xu L, Shi XL, Tan WH, Fang XH, Shangguan DH: **Recognition of subtype non-small cell lung cancer by DNA aptamers selected from living cells**. *Analyst* 2009, **134**:1808-1814.

64. Chen HW, Medley CD, Sefah K, Shangguan D, Tang ZW, Meng L, Smith JE, Tan WH: **Molecular recognition of small-cell lung cancer cells using aptamers**. *Chemmedchem* 2008, **3**:991-1001.

65. oshioka N, Wang L, Kishimoto K, Tsuji T, Hu G-f: **A therapeutic target for prostate cancer based on angiogenin-stimulated angiogenesis and cancer cell proliferation**. *Proceedings of the National Academy of Sciences of the United States of America* 2006, **103**:14519-14524.

66. Hamula CLA, Zhang HQ, Guan LL, Li XF, Le XC: **Selection of aptamers against live bacterial cells**. *Analytical Chemistry* 2008, **80**:7812-7819.

67. Huang YF, Shangguan DH, Liu HP, Phillips JA, Zhang XL, Chen Y, Tan WH: **Molecular Assembly of an Aptamer-Drug Conjugate for Targeted Drug Delivery to Tumor Cells**. *Chembiochem* 2009, **10**:862-868.

68. Ferreira CSM, Cheung MC, Missailidis S, Bisland S, Gariepy J: **Phototoxic aptamers selectively enter and kill epithelial cancer cells**. *Nucleic Acids Research* 2009, **37**:866-876.

69. Mallikaratchy P, Tang ZW, Tan WH: **Cell specific aptamer-photosensitizer conjugates as a molecular tool in photodynamic therapy**. *Chemmedchem* 2008, **3**:425-428.

70. Chen CHB, Dellamaggiore KR, Ouellette CP, Seclano CD, Lizadjohry M, Chernis GA, Gonzales M, Baltasar FE, Fan AL, Myerowitz R, et al.: **Aptamer-based endocytosis of a lysosomal enzyme**. *Proceedings of the National Academy of Sciences of the United States of America* 2008, **105**:15908-15913.

71. Levy-Nissenbaum E, Radovic-Moreno AF, Wang AZ, Langer R, Farokhzad OC: **Nanotechnology and aptamers: applications in drug delivery**. *Trends in Biotechnology* 2008, **26**:442-449.

72. Huang YF, Sefah K, Bamrungsap S, Chang HT, Tan W: **Selective Photothermal Therapy for Mixed Cancer Cells Using Aptamer-Conjugated Nanorods**. *Langmuir* 2008, **24**:11860-11865.

73. Tong GJ, Hsiao SC, Carrico ZM, Francis MB: **Viral Capsid DNA Aptamer Conjugates as Multivalent Cell-Targeting Vehicles**. *Journal of the American Chemical Society* 2009, **131**:11174-11178.

74. Wagner A, Platzgummer M, Kreismayr G, Quendler H, Stiegler G, Ferko B, Vecera G, Vorauer-Uhl K, Prof HK: **GMP production of liposomes - A new industrial approach**. *Journal of Liposome Research* 2006, **16**:311-319.

75. Cao Z, Tong R, Mishra A, Xu W, Wong GC, Cheng J, Lu Y: **Reversible cell-specific drug delivery with aptamer-functionalized liposomes**. *Angew Chem Int Ed Engl* 2009, **48**:6494-6498.

76. Wong ML, Medrano JF: **Real-time PCR for mRNA quantitation**. *Biotechniques* 2005, **39**:75-85.

77. Schena M: **Genome analysis with gene expression microarrays**. *Bioessays* 1996, **18**:427-431.

78. Raval P: **Qualitative and Quantitative-Determination of Messenger-Rna**. *Journal of Pharmacological and Toxicological Methods* 1994, **32**:125-127.

79. McNicol AM, Farquharson MA: **In situ hybridization and its diagnostic applications in pathology**. *Journal of Pathology* 1997, **182**:250-261.

80. Tyagi S, Kramer FR: **Molecular beacons: Probes that fluoresce upon hybridization**. *Nature Biotechnology* 1996, **14**:303-308.

81. Uchiyama H, Hirano K, Kashiwasake-Jibu M, Taira K: **Detection of undegraded oligonucleotides in vivo by fluorescence resonance energy transfer. Nuclease activities in living sea urchin eggs**. *the Journal of Biological Chemistry*, 1996, **271**:380-384.

82. Li JWJ, Fang XH, Schuster SM, Tan WH: **Molecular beacons: A novel approach to detect protein - DNA interactions**. *Angewandte Chemie-International Edition* 2000, **39**:1049-+.

83. Sokol DL, Zhang X, Lu P, Gewirtz AM: **Real time detection of DNA·RNA hybridization in living cells**. *Proceedings of the National Academy of Sciences of the United States of America* 1998, **95**:11538-11543.

84. Peng X-H, Cao Z-H, Xia J-T, Carlson GW, Lewis MM, Wood WC, Yang L: **Real-time Detection of Gene Expression in Cancer Cells Using Molecular Beacon Imaging: New Strategies for Cancer Research**. *Cancer Research* 2005, **65**:1909-1917.

85. Dirks RW, Molenaar C, Tanke HJ: **Methods for visualizing RNA processing and transport pathways in living cells**. *Histochemistry and Cell Biology* 2001, **115**:3-11.

86. Vijayanathan V, Thomas T, Sigal LH, Thomas TJ: **Direct measurement of the association constant of HER2/neu antisense oligonucleotide to its target RNA sequence using a molecular beacon**. *Antisense & Nucleic Acid Drug Development* 2002, **12**:225-233.

87. Fisher TL, Terhorst T, Cao XD, Wagner RW: **Intracellular Disposition and Metabolism of Fluorescently-Labeled Unmodified and Modified Oligonucleotides Microinjected into Mammalian-Cells**. *Nucleic Acids Research* 1993, **21**:3857-3865.

88. Tsourkas A, Behlke MA, Bao G: **Hybridization of 2 '-O-methyl and 2 '-deoxy molecular beacons to RNA and DNA targets**. *Nucleic Acids Research* 2002, **30**:5168-5174.

89. Kuhn H, Demidov VV, Coull JM, Fiandaca MJ, Gildea BD, Frank-Kamenetskii MD: **Hybridization of DNA and PNA molecular beacons to single-stranded and double-stranded DNA targets**. *Journal of the American Chemical Society* 2002, **124**:1097-1103.

90. Braasch DA, Corey DR: **Locked nucleic acid (LNA): fine-tuning the recognition of DNA and RNA**. *Chemical Biology* 2001, **8**:1-7.

91. Molenaar C, Marras SA, Slats JCM, Truffert JC, Lemaitre M, Raap AK, Dirks RW, Tanke HJ: **Linear 2 ' O-Methyl RNA probes for the visualization of RNA in living cells**. *Nucleic Acids Research* 2001, **29**:art. no.-e89.

92. Egholm M, Buchardt O, Nielsen PE, Berg RH: **Peptide Nucleic-Acids (Pna) - Oligonucleotide Analogs with an Achiral Peptide Backbone**. *Journal of the American Chemical Society* 1992, **114**:1895-1897.

93. Wang L, Yang CYJ, Medley CD, Benner SA, Tan WH: **Locked nucleic acid molecular beacons**. *Journal of the American Chemical Society* 2005, **127**:15664-15665.

94. Seferos DS, Giljohann DA, Hill HD, Prigodich AE, Mirkin CA: **Nano-flares: probes for transfection and mRNA detection in living cells**. *Journal of the American Chemical Society* 2007, **129**:15477-15479.

95. Chen AK, Behlke MA, Tsourkas A: **Avoiding false-positive signals with nuclease-vulnerable molecular beacons in single living cells**. *Nucleic Acids Res* 2007, **35**:e105.

96. Santangelo PJ, Nix B, Tsourkas A, Bao G: **Dual FRET molecular beacons for mRNA detection in living cells**. *Nucleic Acids Research* 2004, **32**:-.

97. Sando S, Abe H, Kool ET: **Quenched auto-ligating DNAs: Multicolor identification of nucleic acids at single nucleotide resolution**. *Journal of the American Chemical Society* 2004, **126**:1081-1087.

98. Yang CJ, Lin H, Tan W: **Molecular Assembly of Superquenchers in Signaling Molecular Interactions**. *Journal of the American Chemical Society* 2005, **127**:12772-12773.

99. Kim JH, Morikis D, Ozkan M: **Adaptation of inorganic quantum dots for stable molecular beacons**. *Sensors and Actuators B-Chemical* 2004, **102**:315-319.

100. Chen AK, Behlke MA, Tsourkas A: **Efficient cytosolic delivery of molecular beacon conjugates and flow cytometric analysis of target RNA**. *Nucleic Acids Research* 2008, **36**:-.

101. Medley CD, Drake TJ, Tomasini JM, Rogers RJ, Tan W: **Simultaneous Monitoring of the Expression of Multiple Genes Inside of Single Breast Carcinoma Cells**. *Analytical Chemistry* 2005, **77**:4713-4718.

102. Nitin N, Santangelo PJ, Kim G, Nie SM, Bao G: **Peptide-linked molecular beacons for efficient delivery and rapid mRNA detection in living cells**. *Nucleic Acids Research* 2004, **32**:-.

103. Michelson AM, Todd AR: **Nucleotides .32. Synthesis of a Dithymidine Dinucleotide Containing a 3'-5'-Internucleotidic Linkage**. *Journal of the Chemical Society* 1955:2632-2638.

104. Verma S, Eckstein F: **Modified oligonucleotides: Synthesis and strategy for users**. *Annual Review of Biochemistry* 1998, **67**:99-134.

105. Pon RT: *Protocols for oligonucleotides and analogs: synthesis and properties*, vol 20; 1993.

106. Beaucage SL, Iyer RP: **Advances in the Synthesis of Oligonucleotides by the Phosphoramidite Approach**. *Tetrahedron* 1992, **48**:2223-2311.

107. Beaucage SL, Iyer RP: **The Functionalization of Oligonucleotides Via Phosphoramidite Derivatives**. *Tetrahedron* 1993, **49**:1925-1963.

108. Freier SM, Altmann KH: **The ups and downs of nucleic acid duplex stability: structure-stability studies on chemically-modified DNA:RNA duplexes**. *Nucleic Acids Research* 1997, **25**:4429-4443.

109. Uhlmann E, Peyman A: **Antisense Oligonucleotides - a New Therapeutic Principle**. *Chemical Reviews* 1990, **90**:543-584.

110. Koch T: **Locked nucleic acids: a family of high affinity nucleic acid probes**. *Journal of Physics-Condensed Matter* 2003, **15**:S1861-S1871.

111. Singh SK, Nielsen P, Koshkin AA, Wengel J: **LNA (locked nucleic acids): synthesis and high-affinity nucleic acid recognition**. *Chemical Communications* 1998:455-456.

112. Koshkin AA, Singh SK, Nielsen P, Rajwanshi VK, Kumar R, Meldgaard M, Olsen CE, Wengel J: **LNA (Locked Nucleic Acids): Synthesis of the adenine, cytosine, guanine, 5-methylcytosine, thymine and uracil bicyclonucleoside monomers, oligomerisation, and unprecedented nucleic acid recognition**. *Tetrahedron* 1998, **54**:3607-3630.

113. Kumar R, Singh SK, Koshkin AA, Rajwanshi VK, Meldgaard M, Wengel J: **The first analogues of LNA (Locked Nucleic Acids): Phosphorothioate-LNA and 2 '-thio-LNA**. *Bioorganic & Medicinal Chemistry Letters* 1998, **8**:2219-2222.

114. Singh SK, Kumar R, Wengel J: **Synthesis of Novel Bicyclo[2.2.1] Ribonucleosides: 2'-Amino- and 2'-Thio-LNA Monomeric Nucleosides**. *The Journal of Organic Chemistry* 1998, **63**:6078-6079.

115. Hakansson AE, Wengel J: **The adenine derivative of alpha-L-LNA (alpha-L-ribo configured locked nucleic acid): Synthesis and high-affinity hybridization towards DNA, RNA, LNA and alpha-L-LNA complementary sequences**. *Bioorganic & Medicinal Chemistry Letters* 2001, **11**:935-938.

116. Nielsen P, Wengel J: **A new synthetic approach towards alpha- and beta-LNA (Locked Nucleic Acids)**. *Nucleosides & Nucleotides* 1999, **18**:701-702.

117. Nielsen P, Dalskov JK: **alpha-LNA, locked nucleic acid with alpha-D-configuration**. *Chemical Communications* 2000:1179-1180.

118. Rajwanshi VK, Hakansson AE, Kumar R, Wengel J: **High-affinity nucleic acid recognition using 'LNA' (locked nucleic acid, beta-D-ribo configured LNA), 'xylo-LNA' (beta-D-xylo configured LNA) or 'alpha-L-LNA' (alpha-L-ribo configured LNA)**. *Chemical Communications* 1999:2073-2074.

119. Rajwanshi VK, Kumar R, Kofod-Hansen M, Wengel J: **Synthesis and restricted furanose conformations of three novel bicyclic thymine nucleosides: a xylo-LNA nucleoside, a 3 '-O,5 '-C-methylene-linked nucleoside, and a 2 '-O,5 '-C-methylene-linked nucleoside**. *Journal of the Chemical Society-Perkin Transactions 1* 1999:1407-1414.

120. Rajwanshi VK, Hakansson AE, Dahl BM, Wengel J: **LNA stereoisomers: xylo-LNA (beta-D-xylo configured locked nucleic acid) and alpha-L-LNA (alpha-L-ribo configured locked nucleic acid)**. *Chemical Communications* 1999:1395-1396.

121. Rajwanshi VK, Hakansson AE, Sorensen MD, Pitsch S, Singh SK, Kumar R, Nielsen P, Wengel J: **The eight stereoisomers of LNA (Locked nucleic acid): A remarkable family of strong RNA binding molecules**. *Angewandte Chemie-International Edition* 2000, **39**:1656-+.

122. Petersen M, Wengel J: **LNA: a versatile tool for therapeutics and genomics**. *Trends in Biotechnology* 2003, **21**:74-81.

123. Jepsen JS, Sorensen MD, Wengel J: **Locked nucleic acid: A potent nucleic acid analog in therapeutics and biotechnology**. *Oligonucleotides* 2004, **14**:130-146.

124. Vester B, Wengel J: **LNA (Locked nucleic acid): High-affinity targeting of complementary RNA and DNA**. *Biochemistry* 2004, **43**:13233-13241.

125. Karkare S, Bhatnagar D: **Promising nucleic acid analogs and mimics: characteristic features and applications of PNA, LNA, and morpholino**. *Applied Microbiology and Biotechnology* 2006, **71**:575-586.

126. Obika S, Nanbu D, Hari Y, Morio K, In Y, Ishida T, Imanishi T: **Synthesis of 2'-O,4'-C-methyleneuridine and -cytidine. Novel bicyclic nucleosides having a fixed C-3,-endo sugar puckering**. *Tetrahedron Letters* 1997, **38**:8735-8738.

127. Wahlestedt C, Salmi P, Good L, Kela J, Johnsson T, Hokfelt T, Broberger C, Porreca F, Lai J, Ren K, et al.: **Potent and nontoxic antisense oligonucleotides containing locked nucleic acids**. *Proceedings of the National Academy of Sciences of the United States of America* 2000, **97**:5633-5638.

128. Arzumanov A, Walsh AP, Rajwanshi VK, Kumar R, Wengel J, Gait MJ: **Inhibition of HIV-1 Tat-dependent trans activation by steric block chimeric 2 '-O-methyl/LNA oligoribonucleotides**. *Biochemistry* 2001, **40**:14645-14654.

129. Frieden M, Hansen HF, Koch T: **Nuclease stability of LNA oligonucleotides and LNA-DNA chimeras**. *Nucleosides Nucleotides & Nucleic Acids* 2003, **22**:1041-1043.

130. Kvaerno L, Wengel J: **Investigation of restricted backbone conformations as an explanation for the exceptional thermal stabilities of duplexes involving LNA (locked nucleic acid): synthesis and evaluation of abasic LNA**. *Chemical Communications* 1999:657-658.

131. Petersen M, Nielsen CB, Nielsen KE, Jensen GA, Bondensgaard K, Singh SK, Rajwanshi VK, Koshkin AA, Dahl BM, Wengel J, et al.: **The conformations of locked nucleic acids (LNA)**. *Journal of Molecular Recognition* 2000, **13**:44-53.

132. Frieden M, Orum H: **Locked nucleic acid holds promise in the treatment of cancer**. *Current Pharmaceutical Design* 2008, **14**:1138-1142.

133. Que-Gewirth NS, Sullenger BA: **Gene therapy progress and prospects: RNA aptamers**. *Gene Therapy* 2007, **14**:283-291.

134. Cerchia L, Hamm J, Libri D, Tavitian B, de Franciscis V: **Nucleic acid aptamers in cancer medicine**. *Febs Letters* 2002, **528**:12-16.

135. Fraunfelder FW: **Pegaptanib for wet macular degeneration**. *Drugs of Today* 2005, **41**:703-709.

136. Lou XH, Qian JR, Xiao Y, Viel L, Gerdon AE, Lagally ET, Atzberger P, Tarasow TM, Heeger AJ, Soh HT: **Micromagnetic selection of aptamers in microfluidic channels**. *Proceedings of the National Academy of Sciences of the United States of America* 2009, **106**:2989-2994.

137. Shangguan D, Cao ZH, Meng L, Mallikaratchy P, Sefah K, Wang H, Li Y, Tan WH: **Cell-specific aptamer probes for membrane protein elucidation in cancer cells**. *Journal of Proteome Research* 2008, **7**:2133-2139.

138. Mallikaratchy P, Tang ZW, Kwame S, Meng L, Shangguan DH, Tan WH: **Aptamer directly evolved from live cells recognizes membrane bound immunoglobin heavy mu chain in Burkitt's lymphoma cells**. *Molecular & Cellular Proteomics* 2007, **6**:2230-2238.

139. Bunka DHJ, Stockley PG: **Aptamers come of age - at last**. *Nature Reviews Microbiology* 2006, **4**:588-596.

140. O'Sullivan CK: **Aptasensors - the future of biosensing**. *Analytical and Bioanalytical Chemistry* 2002, **372**:44-48.

141. Nimjee SM, Rusconi CP, Sullenger BA: **Aptamers: An emerging class of therapeutics**. *Annual Review of Medicine* 2005, **56**:555-+.

142. Sokolova V, Epple M: **Inorganic nanoparticles as carriers of nucleic acids into cells**. *Angewandte Chemie-International Edition* 2008, **47**:1382-1395.

143. Seddon AA, Curnow P, Booth PJ: **Membrane proteins, lipids and detergents: not just a soap opera**. *Biochimica Et Biophysica Acta-Biomembranes* 2004, **1666**:105-117.

144. Torchilin VP: **Micellar nanocarriers: Pharmaceutical perspectives**. *Pharmaceutical Research* 2007, **24**:1-16.

145. Sutton D, Nasongkla N, Blanco E, Gao JM: **Functionalized micellar systems for cancer targeted drug delivery**. *Pharmaceutical Research* 2007, **24**:1029-1046.

146. Torchilin VP: **PEG-based micelles as carriers of contrast agents for different imaging modalities**. *Advanced Drug Delivery Reviews* 2002, **54**:235-252.

147. Hait SK, Moulik SP: **Determination of critical micelle concentration (CMC) of nonionic surfactants by donor-acceptor interaction with iodine and correlation of CMC with hydrophile-lipophile balance and other parameters of the surfactants**. *Journal of Surfactants and Detergents* 2001, **4**:303-309.

148. Blute I, Jansson M, Oh SG, Shah DO: **The Molecular Mechanism for Destabilization of Foams by Organic Ions**. *Journal of the American Oil Chemists Society* 1994, **71**:41-46.

149. Gennis RB: *biomembranes: molecular structure and function*: Springer; 1989.

150 Valeur B: *Molecular Fluorescence: Principles and Applications.*: Wiley-VCH Verlag GmbH; 2001.

151. Lakowicz JR: *Principles of Fluorescent Spectroscopy*: Kluwer Academic/Plenum Publishers, New York; 1999.

152. Tyagi S, Bratu DP, Kramer FR: **Multicolor molecular beacons for allele discrimination**. *Nature Biotechnology* 1998, **16**:49-53.

153. Bao Q, Shi Y: **Apoptosome: a platform for the activation of initiator caspases**. *Cell Death and Differentiation* 2007, **14**:56-65.

154. Mikhail AS, Allen C: **Block copolymer micelles for delivery of cancer therapy: Transport at the whole body, tissue and cellular levels**. *Journal of Controlled Release* 2009, **138**:214-223.

155. Ding K, Alemdaroglu FE, Borsch M, Berger R, Herrmann A: **Engineering the structural properties of DNA block copolymer micelles by molecular recognition**. *Angewandte Chemie-International Edition* 2007, **46**:1172-1175.

156. Alemdaroglu FE, Alemdaroglu NC, Langguth P, Herrmann A: **Cellular uptake of DNA block copolymer micelles with different shapes**. *Macromolecular Rapid Communications* 2008, **29**:326-329.

157. Alemdaroglu FE, Ding K, Berger R, Herrmann A: **DNA-templated synthesis in three dimensions: Introducing a micellar scaffold for organic reactions**. *Angewandte Chemie-International Edition* 2006, **45**:4206-4210.

158. Jeong JH, Park TG: **Novel polymer-DNA hybrid polymeric micelles composed of hydrophobic poly(D,L-lactic-co-glycolic acid) and hydrophilic oligonucleotides**. *Bioconjugate Chemistry* 2001, **12**:917-923.

159. Alemdaroglu FE, Alemdaroglu NC, Langguth P, Herrmann A: **DNA block copolymer micelles - A combinatorial tool for cancer Nanotechnology**. *Advanced Materials* 2008, **20**:899-+.

160. Liu JW, Lu Y: **Fast colorimetric sensing of adenosine and cocaine based on a general sensor design involving aptamers and nanoparticles**. *Angewandte Chemie-International Edition* 2006, **45**:90-94.

161. Yang HH, Liu HP, Kang HZ, Tan WH: **Engineering target-responsive hydrogels based on aptamer - Target interactions**. *Journal of the American Chemical Society* 2008, **130**:6320-+.

162. Grabar KC, Freeman RG, Hommer MB, Natan MJ: **Preparation and Characterization of Au Colloid Monolayers**. *Analytical Chemistry* 1995, **67**:735-743.

163. Duffy DC, McDonald JC, Schueller OJA, Whitesides GM: **Rapid prototyping of microfluidic systems in poly(dimethylsiloxane)**. *Analytical Chemistry* 1998, **70**:4974-4984.

164. Chen HT, Kim SW, Li L, Wang SY, Park K, Cheng JX: **Release of hydrophobic molecules from polymer micelles into cell membranes revealed by Forster resonance energy transfer imaging**. *Proceedings of the National Academy of Sciences of the United States of America* 2008, **105**:6596-6601.

165. Dautry-Varsat A, Ciechanover A, Lodish HF: **pH and the recycling of transferrin during receptor-mediated endocytosis**. *Proceedings of the National Academy of Sciences of the United States of America* 1983, **80**:2258-2262.

166. Tsui NBY, Ng EKO, Lo YMD: **Stability of endogenous and added RNA in blood specimens, serum, and plasma**. *Clinical Chemistry* 2002, **48**:1647-1653.

167. Jain RK: **Determinants of Tumor Blood-Flow - a Review**. *Cancer Research* 1988, **48**:2641-2658.

168. Klevens HB: **Solubilization**. *Chemical Reviews* 1950, **47**:1-74.

169. Mukerjee P, Mysels KJ: **A Re-Evaluation of the Spectral Change Method of Determining Critical Micelle Concentration**. *Journal of the American Chemical Society* 1955, **77**:2937-2943.

170. Takeda K, Ohtawa T, Hachiya K, Aoki K: **Kinetics of the Solubilization of Pinacyanol Chloride into a Complex between Bovine Serum-Albumin and Sodium Dodecyl-Sulfate**. *Bulletin of the Chemical Society of Japan* 1987, **60**:1174-1176.

171. Lehninger AL, Nelson DL, Cox MM: *Lehninger principles of biochemistry* edn 4th. New York: W.H. Freeman; 2005.

172. Yao Y, Ghosh K, Epand RF, Epand RM, Ghosh HP: **Membrane fusion activity of vesicular stomatitis virus glycoprotein G is induced by low pH but not by heat or denaturant**. *Virology* 2003, **310**:319-332.

173. Tyagi S, Kramer FR: **Molecular Beacons: Probes that Fluoresce upon Hybridization**. *Nature Biotechnology* 1996, **14**:303-308.

174. Sokol DL, Zhang XL, Lu PZ, Gewitz AM: *Proceedings of the National Academy of Sciences of the United States of America* 1998, **95**:11538-11543.

175 Perlette J, Tan WH: **Real-time monitoring of intracellular mRNA hybridization inside single living cells**. *Analytical Chemistry* 2001, **73**:5544-5550.

176. Bratu DP, Cha BJ, Mhlanga MM, Kramer FR, Tyagi S: **Visualizing the distribution and transport of mRNAs in living cells**. *Proceedings of the National Academy of Sciences of the United States of America* 2003, **100**:13308-13313.

177. Drake TJ, Medley CD, Sen A, Rogers RJ, Tan WH: **Stochasticity of manganese superoxide dismutase mRNA expression in breast carcinoma cells by molecular beacon imaging**. *Chembiochem* 2005, **6**:2041-2047.

178. Yang CJ, Wang L, Wu Y, Kim Y, Medley CD, Lin H, Tan W: **Synthesis and investigation of deoxyribonucleic acid/locked nucleic acid chimeric molecular beacons**. *Nucleic Acids Research* 2007, **35**:4030-4041.

179. Medley CD, Drake TJ, Tomasini JM, Rogers RJ, Tan WH: **Simultaneous monitoring of the expression of multiple genes inside of single breast carcinoma cells**. *Analytical Chemistry* 2005, **77**:4713-4718.

180. Visner GA, Dougall WC, Wilson JM, Burr IA, Nick HS: **Regulation of Manganese Superoxide-Dismutase by Lipopolysaccharide, Interleukin-1, and Tumor Necrosis Factor - Role in the Acute Inflammatory Response**. *Journal of Biological Chemistry* 1990, **265**:2856-2864.

181. He XX, Wang KM, Tan WH, Liu B, Lin X, He CM, Li D, Huang SS, Li J: **Bioconjugated nanoparticles for DNA protection from cleavage**. *Journal of the American Chemical Society* 2003, **125**:7168-7169.

182. Martin CR, Kohli P: **The emerging field of nanotube biotechnology**. *Nature Reviews Drug Discovery* 2003, **2**:29-37.

183. Cui XJ, Yu SH, Li LL, Li K, Yu B: **Fabrication of Ag2SiO3/SiO2 composite nanotubes using a one-step sacrificial templating solution approach**. *Advanced Materials* 2004, **16**:1109-+.

184. Pantarotto D, Briand JP, Prato M, Bianco A: **Translocation of bioactive peptides across cell membranes by carbon nanotubes**. *Chemical Communications* 2004:16-17.

185. Pantarotto D, Singh R, McCarthy D, Erhardt M, Briand JP, Prato M, Kostarelos K, Bianco A: **Functionalized carbon nanotubes for plasmid DNA gene delivery**. *Angewandte Chemie-International Edition* 2004, **43**:5242-5246.

186. Cai D, Mataraza JM, Qin ZH, Huang ZP, Huang JY, Chiles TC, Carnahan D, Kempa K, Ren ZF: **Highly efficient molecular delivery into mammalian cells using carbon nanotube spearing**. *Nature Methods* 2005, **2**:449-454.

187. Chen CC, Liu YC, Wu CH, Yeh CC, Su MT, Wu YC: **Preparation of fluorescent silica nanotubes and their application in gene delivery**. *Advanced Materials* 2005, **17**:404-+.

188. Kwon NH, Beaux MF, Ebert C, Wang L, Lassiter BE, Park YH, Mciiroy DN, Hovde CJ, Bohach GA: **Nanowire-based delivery of Escherichia coli O157 Shiga toxin 1 A subunit into human and bovine cells**. *Nano Letters* 2007, **7**:2718-2723.

189. Hampton T: **Nanowire DNA delivery**. *Jama-Journal of the American Medical Association* 2007, **298**:505-505.

190. Liu Z, Winters M, Holodniy M, Dai HJ: **siRNA delivery into human T cells and primary cells with carbon-nanotube transporters**. *Angewandte Chemie-International Edition* 2007, **46**:2023-2027.

191. Kam NWS, O'Connell M, Wisdom JA, Dai HJ: **Carbon nanotubes as multifunctional biological transporters and near-infrared agents for selective cancer cell destruction**. *Proceedings of the National Academy of Sciences of the United States of America* 2005, **102**:11600-11605.

192. Heller DA, Jeng ES, Yeung TK, Martinez BM, Moll AE, Gastala JB, Strano MS: **Optical detection of DNA conformational polymorphism on single-walled carbon nanotubes**. *Science* 2006, **311**:508-511.

193. Zheng M, Jagota A, Semke ED, Diner BA, Mclean RS, Lustig SR, Richardson RE, Tassi NG: **DNA-assisted dispersion and separation of carbon nanotubes**. *Nature Materials* 2003, **2**:338-342.

194. Yang RH, Jin JY, Chen Y, Shao N, Kang HZ, Xiao Z, Tang ZW, Wu YR, Zhu Z, Tan WH: **Carbon nanotube-quenched fluorescent oligonucleotides: Probes that fluoresce upon hybridization**. *Journal of the American Chemical Society* 2008, **130**:8351-8358.

195. Nakayama-Ratchford N, Bangsaruntip S, Sun X, Welsher K, Dai H: **Noncovalent functionalization of carbon nanotubes by fluorescein-polyethylene glycol: supramolecular conjugates with pH-dependent absorbance and fluorescence**. *Journal of the American Chemical Society* 2007, **129**:2448-2449.

196. Wu YR, Yang CJ, Moroz LL, Tan WH: **Nucleic acid beacons for long-term real-time intracellular monitoring**. *Analytical Chemistry* 2008, **80**:3025-3028.

197. Tyagi S, Alsmadi O: **Imaging native beta-actin mRNA in motile fibroblasts**. *Biophysical Journal* 2004, **87**:4153-4162.

198. Soutschek J, Akinc A, Bramlage B, Charisse K, Constien R, Donoghue M, Elbashir S, Geick A, Hadwiger P, Harborth J, et al.: **Therapeutic silencing of an endogenous gene by systemic administration of modified siRNAs**. *Nature* 2004, **432**:173-178.

199. Takeshita F, Minakuchi Y, Nagahara S, Honma K, Sasaki H, Hirai K, Teratani T, Namatame N, Yamamoto Y, Hanai K, et al.: **Efficient delivery of small interfering RNA to bone-metastatic tumors by using atelocollagen in vivo**. *Proceedings of the National Academy of Sciences of the United States of America* 2005, **102**:12177-12182.

200. Lorenz C, Hadwiger P, John M, Vornlocher HP, Unverzagt C: **Steroid and lipid conjugates of siRNAs to enhance cellular uptake and gene silencing in liver cells**. *Bioorganic & Medicinal Chemistry Letters* 2004, **14**:4975-4977.

201. Hu-Lieskovan S, Heidel JD, Bartlett DW, Davis ME, Triche TJ: **Sequence-specific knockdown of EWS-FLI1 by targeted, nonviral delivery of small interfering RNA inhibits tumor growth in a murine model of metastatic Ewing's sarcoma**. *Cancer Research* 2005, **65**:8984-8992.

202. Song EW, Zhu PC, Lee SK, Chowdhury D, Kussman S, Dykxhoorn DM, Feng Y, Palliser D, Weiner DB, Shankar P, et al.: **Antibody mediated in vivo delivery of small interfering RNAs via cell-surface receptors**. *Nature Biotechnology* 2005, **23**:709-717.

203. McNamara JO, 2nd, Andrechek ER, Wang Y, Viles KD, Rempel RE, Gilboa E, Sullenger BA, Giangrande PH: **Cell type-specific delivery of siRNAs with aptamer-siRNA chimeras**. *Nature Biotechnology* 2006, **24**:1005-1015.

204. Chu TC, Twu KY, Ellington AD, Levy M: **Aptamer mediated siRNA delivery**. *Nucleic Acids Research* 2006, **34**:e73.

205. Rosi NL, Giljohann DA, Thaxton CS, Lytton-Jean AKR, Han MS, Mirkin CA: **Oligonucleotide-modified gold nanoparticles for intracellular gene regulation**. *Science* 2006, **312**:1027-1030.

206. Hao J, Kwissa M, Pulendran B, Murthy N: **Peptide crosslinked micelles: a new strategy for the design and synthesis of peptide vaccines**. *International Journal of Nanomedicine* 2006, **1**:97-103.

207. Koo AN, Lee HJ, Kim SE, Chang JH, Park C, Kim C, Park JH, Lee SC: **Disulfide-cross-linked PEG-poly(amino acid)s copolymer micelles for glutathione-mediated intracellular drug delivery**. *Chemical Communications* 2008:6570-6572.

208. Park J, An KJ, Hwang YS, Park JG, Noh HJ, Kim JY, Park JH, Hwang NM, Hyeon T: **Ultra-large-scale syntheses of monodisperse nanocrystals**. *Nature Materials* 2004, **3**:891-895.

209. Berry CC, Curtis ASG: **Functionalisation of magnetic nanoparticles for applications in biomedicine**. *Journal of Physics D-Applied Physics* 2003, **36**:R198-R206.

210. Baumert C, Hilgeroth A: **Recent Advances in the Development of P-gp Inhibitors**. *Anti-Cancer Agents in Medicinal Chemistry* 2009, **9**:415-436.

211. Mizukami S, Takikawa R, Sugihara F, Hori Y, Tochio H, Walchli M, Shirakawa M, Kikuchi K: **Paramagnetic relaxation-based 19f MRI probe to detect protease activity**. *Journal of the American Chemical Society* 2008, **130**:794-795.

212. Chakravarty P, Marches R, Zimmerman NS, Swafford AD, Bajaj P, Musselman IH, Pantano P, Draper RK, Vitetta ES: **Thermal ablation of tumor cells with antibody-functionalized single-walled carbon nanotubes**. *Proceedings of the National Academy of Sciences of the United States of America* 2008, **105**:8697-8702.

213. Liu Z, Fan AC, Rakhra K, Sherlock S, Goodwin A, Chen XY, Yang QW, Felsher DW, Dai HJ: **Supramolecular Stacking of Doxorubicin on Carbon Nanotubes for In Vivo Cancer Therapy**. *Angewandte Chemie-International Edition* 2009, **48**:7668-7672.

BIOGRAPHICAL SKETCH

Yanrong Wu was born at Fujian Province in China PRC in October, 1978. She joined Huaqiao University in 1997 to study chemistry, and then went to Xiamen University in 2001 to pursue an MS degree in inorganic chemistry under Dr. Lansun Zheng. Inspired by one project related to the origin of life during her master's research, she became strongly interested in life science. Therefore, she moved to University of Florida in the USA and joined Dr. Weihong Tan's group to pursue a PhD degree.